

Effects of Magnetism in Superconducting Hybrid Structures

THÈSE N° 4519 (2009)

PRÉSENTÉE LE 30 OCTOBRE 2009

À LA FACULTÉ SCIENCES DE BASE

CHAIRE DE PHYSIQUE MÉSCOPIQUE ET SYSTÈMES FORTEMENT CORRÉLÉS

PROGRAMME DOCTORAL EN PHYSIQUE

ÉCOLE POLYTECHNIQUE FÉDÉRALE DE LAUSANNE

POUR L'OBTENTION DU GRADE DE DOCTEUR ÈS SCIENCES

PAR

Benoît CROUZY

acceptée sur proposition du jury:

Prof. G. Dietler, président du jury

Prof. D. Ivanov, directeur de thèse

Prof. A. Buzdin, rapporteur

Prof. F. Mila, rapporteur

Prof. M. Sigrist, rapporteur



ÉCOLE POLYTECHNIQUE
FÉDÉRALE DE LAUSANNE

Suisse
2009

Résumé

Cette thèse est consacrée à l'étude du magnétisme dans les jonctions Josephson de type supraconducteur–métal normal/ferroaimant–supraconducteur (SNS ou SFS). Les jonctions SFS offrent en particulier une possibilité unique d'étudier l'interaction entre l'ordre ferromagnétique et la supraconductivité, séparant la source des corrélations supraconductrices du ferromagnétisme, tandis que l'effet orbital d'un champ magnétique dans une jonction SNS résulte dans l'apparition de phénomènes d'interférence entre les courants locaux.

Nous introduisons dans le Chapitre 1 le formalisme adapté à la description de l'effet de proximité et passons en revue la physique des systèmes étudiés dans la thèse.

Dans le Chapitre 2, nous étudions l'effet Josephson entre deux supraconducteurs mis en contact par un ferroaimant (jonction SFS) présentant une structure en domaines non-collinéaires. La présence du champ d'échange [1] entraîne une modulation des corrélations supraconductrices dans le ferroaimant de par la brisure de la symétrie de renversement temporel entre les électrons formant une paire de Cooper [2]. L'apparition d'une différence de phase de π [3] entre les deux électrodes supraconductrices, et par conséquent d'un courant spontané dans un anneau supraconducteur comprenant une jonction SFS résulte de cette modulation. Comme modèle pour notre étude de l'effet de la présence de domaines magnétiques sur la phase π nous considérons une jonction diffusive avec deux domaines le long de la jonction dont l'aimantation est orientée de manière arbitraire. Nous calculons une expression analytique pour le courant en fonction de l'orientation et de la taille des domaines. En variant ces paramètres, la jonction se trouve soit dans la phase 0 (pas de différence de phase entre les électrodes à l'équilibre) soit dans la phase π . La présence de domaines entraîne une réduction de la phase π dans l'espace des paramètres. Pour des domaines de taille égale, la phase π disparaît complètement dès que l'angle entre l'aimantation des domaines excède $\frac{\pi}{2}$. A la fin du chapitre nous commentons sur les implications de nos résultats pour les expériences sur les transitions $0-\pi$ dans les jonctions SFS.

Les réalisations expérimentales de jonctions SFS sont généralement basées sur des couches ferromagnétiques déposées en film. Dans le Chapitre 3, nous étudions l'effet de la présence d'une structure en domaines dans le plan de la jonction. Selon la taille des domaines, comparée à la longueur de cohérence magnétique, nous observons deux comportements différents. Pour des domaines de grande taille, on observe des oscillations entre la phase 0 et la phase π , comme dans une jonction SFS monodomaine. Pour des domaines de petite taille, la jonction se comporte comme une jonction SNS: du fait d'un moyennage

de l'effet du champ, les transitions dans la phase π sont absentes. Nous calculons la taille critique séparant les deux régimes et montrons dans les deux cas comment réduire l'effet des domaines à un taux de spin-flip effectif. Nous discutons enfin de la distribution des courants locaux et montrons que proche des transitions entre phase 0 et π le courant a une direction opposée au milieu des domaines par rapport au voisinage de la paroi de domaine.

Après avoir discuté d'effets paramagnétiques, nous nous concentrons dans le Chapitre 4 sur l'effet orbital d'un champ magnétique extérieur appliqué sur une jonction SNS. Nous montrons que dans le cas d'une longue jonction, il existe une largeur critique (relative à la longueur associée avec le champ magnétique) séparant un régime où le courant critique présente des oscillations amorties en fonction du flux magnétique à travers la jonction d'un régime où le courant décroît de manière monotone. Dans les deux régimes, la décroissance est exponentielle. Pour une jonction large, la période des oscillations est identique à la période des oscillations de Fraunhofer caractérisant le comportement du courant dans une jonction tunnel. On montre finalement que dans cette limite les corrélations supraconductrices et le courant sont concentrés proche des bords du système.

Mots clés : supraconductivité, effet de proximité, ferromagnétisme, effet Josephson, jonctions π , courant critique, domaines magnétiques, effets orbitaux

Abstract

In this thesis we study various effects of magnetism in proximity structures, composed of superconducting electrodes in contact with a normal metal. Magnetism can be present in the system through the Zeeman and the orbital coupling. Proximity structures offer in particular a unique opportunity to study the interplay between ferromagnetism and conventional superconductivity, which can hardly coexist in bulk samples. The orbital effect of an external magnetic field applied to a Josephson junction results in interference effects between local currents.

In Chapter 1, we give an introduction to the main features of the proximity effect and to the theoretical formalism used throughout the thesis.

In Chapter 2 we study the Josephson effect in a superconductor–ferromagnet–superconductor (SFS) junction with ferromagnetic domains of noncollinear magnetization. It is well known [1] that as a consequence of the exchange splitting of the Fermi level [2] the Cooper pair wave function shows damped oscillations in a ferromagnet, leading to the appearance of the so-called “ π state” in SFS junctions [3]. In the π state, the superconducting order parameter is of opposite sign in the two S electrodes of the Josephson junction, and a spontaneous non-dissipative current can appear in a ring containing such a junction. As a model for our study of the influence of magnetic domains on the π state formation, we consider a diffusive junction with two ferromagnetic domains along the junction. We find analytically the critical current as a function of domain lengths and of the angle between the orientations of their magnetizations. Varying those parameters, the junction may undergo transitions between 0 and π phases. We find that the presence of domains reduces the range of junction lengths at which the π phase is observed. For the junction with two domains of the same length, the π phase totally disappears as soon as the misorientation angle exceeds $\frac{\pi}{2}$. We further comment on possible implications of our results for experimentally observable 0– π transitions in SFS junctions.

Experimentally, π junctions are realized as thin films deposited in layers. In Chapter 3, we study therefore the influence of in-plane magnetic domains on the Josephson current. We find that the properties of the junction depend on the size of the domains relative to the magnetic coherence length. In the case of large domains, the junction exhibits transitions to the π state, similarly to a single-domain SFS junction. In the case of small domains, the magnetization effectively averages out, and the junction is always in the zero state, similarly to a superconductor–normal metal–superconductor (SNS) junction. In both those regimes,

the influence of domain walls may be approximately described as an effective spin-flip scattering. We also study the inhomogeneous distribution of the local current density in the junction. Close to the $0-\pi$ transitions, the directions of the critical current may be opposite in the vicinity of the domain wall and in the middle of the domains.

In Chapter 4, we discuss the orbital effects of an external magnetic field in a SNS junction. In the limit of a long junction, we find that the properties of such a system depend on the width of the junction relative to the length associated with the magnetic field. We compute the critical width separating the regime of pure decay (narrow junction) and the regime of damped oscillations (wide junction) of the critical current as a function of the magnetic flux through the junction. We find an exponential damping of the current, different from the well known Fraunhofer limit which corresponds to the limit of a tunnel junction. In the limit of a wide junction, the superconducting pair correlations and the critical current become localized near the border of the junction.

Keywords : superconductivity, proximity effect, ferromagnetism, Josephson effect, π junctions, critical current, magnetic domains, orbital effects

Contents

1 Proximity effect and magnetism	1
1.1 Introduction	1
1.2 Diffusive limit	2
1.3 Andreev reflection	3
1.4 Quasiclassical formalism	4
1.4.1 Model Hamiltonian	4
1.4.2 Gor'kov equations	5
1.4.3 Real-time formulation	9
1.4.4 Scattering on impurities: self-energy	9
1.4.5 Quasiclassical theory	13
1.4.6 Quasiclassical boundary conditions	17
1.5 Features of the proximity effect in the presence of magnetism	18
1.5.1 Interplay between magnetism and superconductivity	18
1.5.2 Closing of the minigap in the presence of magnetic impurities	20
1.5.3 Josephson effect	23
2 SFS junction with two noncollinear ferromagnetic domains	27
2.1 Introduction: π junctions	27
2.2 Model	31
2.3 Domains of different thicknesses in the P and AP configurations	34
2.3.1 Parallel case (P)	34
2.3.2 Antiparallel case (AP)	35
2.4 Arbitrary magnetization misorientation and equal thicknesses	38
2.5 Discussion and experimental aspects	40
3 SFS junction with in-plane ferromagnetic domains	43
3.1 Introduction	43
3.2 Model for the multidomain SFS junction	45
3.3 Critical current	48
3.3.1 Limit of large domains : $a \gg \xi_h$	50
3.3.2 Limit of small domains : $a \ll \xi_h, d, \xi_T$	51

3.3.3	0- π phase diagram	52
3.4	Local current density	53
3.5	Summary	54
4	Orbital effect of a magnetic field	57
4.1	Introduction	57
4.2	SNS junction in a transverse magnetic field	58
4.3	Short junction limit: Fraunhofer interference patterns	61
4.4	Analytical results for a long junction	62
4.4.1	Narrow junction limit	64
4.4.2	Wide junction limit	66
4.5	Josephson current	67
4.6	Applicability of the results	69
4.7	Summary	70
5	Conclusion	73
A	Collision integral in the presence of isotropic spin-flip scattering	75
B	Gap curve close to Γ_{sf}^c	77
C	Zero energy density of states for $\Gamma_{sf} > \Gamma_{sf}^c$	79
D	Solving the linearized Usadel equations	81
E	Josephson current for the SNS junction in a magnetic field	83

Chapter 1

Proximity effect and magnetism

1.1 Introduction

The study of hybrid structures made of superconducting and non-superconducting elements in contact with each other, has started [4] only a few years after the development of the microscopic BCS theory of superconductivity [5]. Recent technical progress has revived the interest in the proximity effect and coherence at mesoscopic scale is theoretically better understood [1, 6, 7]. Technological applications of proximity structures [8] include SQUID Josephson magnetometers, which allow very sensitive magnetic field measurements (fields in the attotesla range can be reached) and photodetectors. The sensitivity of SQUIDS allows to measure the weak magnetic fields generated by the brain activity or to realize the precise displacement sensors used in the detection of gravitational waves [9].

A superconductor S in contact with a normal metal N modifies the behavior of the electrons in the normal region. The electrons in the adjacent normal metal exhibit superconducting properties like the appearance of an energy gap in the density of states, modifications of the conductance or screening of magnetic fields by Meissner currents.

Superconducting pairs can diffuse in a normal metal over mesoscopic lengths from a contact with a superconductor. Mesoscopic systems contain a sufficient number of particles to be studied by statistical methods but still show non-negligible phase coherence effects. The presence of phase coherence makes proximity structures candidates for potential applications to spintronics [10] and to quantum computing [11, 12].

The interplay between ferromagnetism and proximity superconductivity results in physical effects which cannot be observed in bulk superconductors. Singlet superconductivity and ferromagnetism can hardly coexist in bulk compounds: superconductivity favors the arrangement of electrons in pairs with opposite spin while the paramagnetic effect of the ferromagnetic exchange field destroys these pairs by aligning the spins [1]. In supercon-

ductor/ferromagnet SF hybrid structures, the source of superconducting correlations and ferromagnetism are spatially separated. Superconducting pairs can propagate in the ferromagnet from the interface with the superconductor over short distances. The decay length for the superconducting pair correlations in the ferromagnet is of the order of one nanometer due to the typically large ferromagnetic exchange field. Even if superconductivity is strongly suppressed in the ferromagnet, SF hybrid structures present a rich physics. The Cooper pairs acquire in the ferromagnet a momentum due to the splitting of the Fermi level by the exchange field, resulting in a modulation of the pair amplitude. This modulation will in turn lead to oscillations of the density of states in the ferromagnet and of the critical temperature of thin SF bilayers or to the appearance of the so called “ π phase” in SFS Josephson junctions. The last-mentioned effect will be discussed in details in the next chapters.

1.2 Diffusive limit

In this thesis, we will focus on systems satisfying the diffusive (“dirty”) limit condition, i.e., systems for which the motion of the electrons is governed by frequent scattering on impurity atoms, as it is the case for example in alloys. Let us define l_e , the mean free path between two elastic scattering events. In the diffusive limit, we assume that all the length scales relevant to our system are much larger than l_e . The spatial extension associated with diffusive motion occurring over a time interval t is

$$L = \sqrt{Dt} \quad (1.1)$$

where for a three dimensional geometry the diffusion constant D is given by

$$D = \frac{1}{3}v_f l_e. \quad (1.2)$$

It is also possible to associate a characteristic length L_ϵ with an energy ϵ by the relation

$$L_\epsilon = \sqrt{\frac{\hbar D}{\epsilon}}. \quad (1.3)$$

The diffusive limit is experimentally easier to reach than the clean limit, and physical quantities averaged over the realizations of disorder in proximity systems are theoretically often more tractable [13, 14]. Besides, scattering on non-magnetic impurities is harmless for superconductivity resulting from a conventional pairing mechanism. Anderson’s theorem [15] states that for a s-wave (singlet) pairing time-reversal symmetry breaking (for example by applying a magnetic field or by scattering on magnetic impurities) will result in pair breaking. Indeed, the electrons forming a Cooper pair are related by the time reversal operation \hat{T}

$$\hat{T}|\mathbf{k}, \uparrow\rangle = |-\mathbf{k}, \downarrow\rangle \quad (1.4)$$

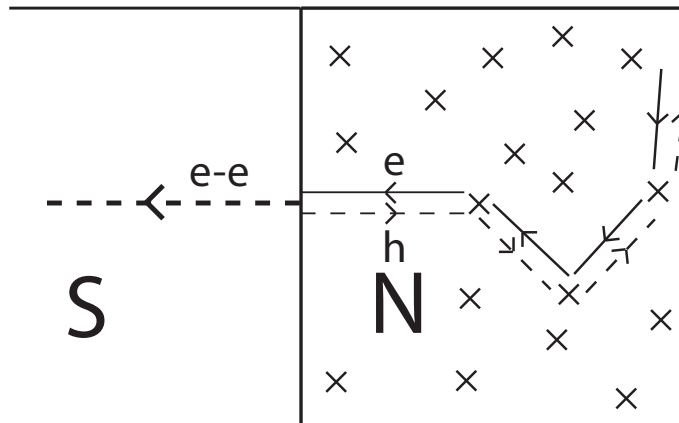


Figure 1.1: Andreev reflection at the SN interface resulting in a non-zero pair amplitude in the N region.

and therefore time reversal symmetry is needed to ensure the existence of available pairing partners. Since elastic scattering preserves \hat{T} , it is not incompatible with the presence of pairs. We will show later that the presence of disorder in the system is even *required* to observe the opening of an energy gap in a proximity superconductor.

1.3 Andreev reflection

The microscopic mechanism resulting in the presence of a finite Cooper pair amplitude in a normal metal in contact with a superconductor is a particular type of reflection at the SN interface [16]. At low energy, the electrons in the N part with an excitation energy ϵ below the superconducting gap Δ cannot cross the interface since no single-particle states are available in the superconductor below the gap. In a simple model of the SN junction, we consider the case where there is no potential barrier at the interface between the two materials: momentum conservation implies that incident electrons cannot be directly reflected either. However, an incident electron can be retro-reflected as a hole with energy $-\epsilon$, opposite spin and the excess charge transmitted as a Cooper pair through the interface. The reflected hole acquires in addition a scattering phase of $\pi/2 - \varphi$ with φ the phase of the superconducting order parameter. The reflection of a hole is equivalent to the absorption of a second electron by the interface. This results in the diffusion of electron-hole pairs (“Andreev pairs”) in the normal metal. These pairs are not due to the presence of an hypothetical interaction in the normal metal but to the contact between the N region (Landau quasiparticles) and the S region (Cooper pairs).

On Fig. 1.1 we draw a pair of Feynman paths contributing to the apparition of a non-zero anomalous amplitude $\langle \psi^\dagger(\mathbf{r})\psi^\dagger(\mathbf{r}) \rangle$ in the N region, i.e., a pair of paths where an

electron is scattered from \mathbf{r} , hits the SN interface and a retro-reflected hole is scattered back at the origin of the trajectory \mathbf{r} . The double average denotes an average over the realizations of disorder in addition to the usual quantum average. The electron-hole pair scattering from the interface is perfect only exactly at the Fermi level. The reflected hole corresponding to an electron with wave vector $\mathbf{k}_e = \mathbf{k}_F + \mathbf{q}$, has a wave vector $\mathbf{k}_h = \mathbf{k}_F - \mathbf{q}$. The resulting wave vector mismatch $2\mathbf{q}$ will lead to an imperfect Andreev pairing, with the dephasing between the correlated incoming electron and reflected hole growing with the distance from the interface and destroying the correlation. For an electron with energy $E_F + \epsilon$, the coherence length of the Andreev pairs L_ϵ is given by relation (1.3). If we consider a sample of length L , this relation gives us the corresponding characteristic correlation energy (Thouless energy)

$$E_{\text{Th}} = \frac{\hbar D}{L^2}. \quad (1.5)$$

This simple description is valid as long as pair breaking effects (scattering on magnetic impurities, for example) or inelastic scattering can be neglected. These types of scattering become important if the spin-flip or the inelastic mean free path are smaller than the length of the N part of the sample L .

1.4 Quasiclassical formalism

1.4.1 Model Hamiltonian

The formulation of the BCS theory in terms of Green functions derived by Gor'kov [17] furnishes efficient tools to study proximity systems: relevant physical quantities can directly be obtained once the electron Green function has been calculated.

We start from the general Hamiltonian describing the proximity systems (SN or SF hybrid junctions) we will consider in the thesis. We take

$$\begin{aligned} \mathcal{H} = \int \sum_{\alpha,\beta} \psi_\alpha^\dagger \left[\left(-\frac{\nabla^2}{2m} - \mu \right) \delta_{\alpha\beta} + \mathbf{h}(\mathbf{r}) \cdot \hat{\boldsymbol{\sigma}} + U_{\alpha\beta}(\mathbf{r}) \right] \psi_\beta \\ + \frac{g(\mathbf{r})}{2} \psi_\beta^\dagger(\mathbf{r}) \psi_\alpha^\dagger(\mathbf{r}) \psi_\alpha(\mathbf{r}) \psi_\beta(\mathbf{r}) d^3 r \end{aligned} \quad (1.6)$$

where the $\psi_\sigma^\dagger(\mathbf{r})$ are the usual field operators and $\hat{\boldsymbol{\sigma}}$ is the vector $(\hat{\sigma}_1, \hat{\sigma}_2, \hat{\sigma}_3)$ with the components given by Pauli matrices. This Hamiltonian includes, in addition to the usual kinetic term, the presence of a ferromagnetic exchange field $\mathbf{h}(\mathbf{r})$ and of an external magnetic field (the Zeeman coupling can be included in the ferromagnetic exchange field), the effect of scattering on impurity atoms through $U_{\alpha\beta}$ and the pairing interaction responsible for superconductivity. A system of units with $\hbar = k_B = \mu_B = 1$ is chosen.

We consider a point-like pairing interaction between the electrons $g(\mathbf{r})\delta(\mathbf{r}-\mathbf{r}')$. The use

of this simple potential to model the complicated pairing mechanism (mediated by phonons in conventional superconductors) is justified in the limit of a weak interaction (“weak-coupling approximation”), when $|g|\nu_0 \ll 1$ [14], with $\nu_0 = \frac{m p_F}{2\pi^2}$ the density of states per one spin projection at the Fermi level in the normal state. The spatial dependence of $g(\mathbf{r})$ allows us to describe systems such as SN junctions: in the normal part, the interaction responsible for the formation of Cooper pairs vanishes. We will treat in the following the pairing interaction in the mean field approximation [18] and reduce the quartic term to a quadratic form. In principle, the corresponding superconducting order parameter $\Delta(\mathbf{r}) = |g(\mathbf{r})|\langle\psi_\downarrow\psi_\uparrow\rangle$ has to be determined self-consistently.

Ferromagnetism is also treated in the mean-field approximation, with the magnetic order parameter $\mathbf{h}(\mathbf{r})$. We consider a metal where ferromagnetism results from the exchange interaction between electrons. We further assume that conduction electrons, which are responsible for the proximity effect, give the main contribution to the exchange energy. To describe the presence of ferromagnetic domains, the exchange field \mathbf{h} can be taken position dependent. The magnetization \mathbf{M} in ferromagnets leads to a correction to the exchange field (due to the presence of the Zeeman term) $\mathbf{h} \rightarrow \mathbf{h} + 4\pi\mathbf{M}$ and to orbital effects in the ferromagnetic layers. However, the correction to the exchange field is typically several orders of magnitude smaller ($\sim 10^{-3}$) than the exchange field itself and orbital effects can usually be neglected since the fields are really weak for the situations considered in this thesis (for more details see the discussion in Ref. [1]).

The external potential $U_{\alpha\beta}(\mathbf{r})$ accounts for the presence of random impurities in the system. Since we want to include in this potential both the contributions from non-magnetic and magnetic impurities, it can in general have a non-trivial spin-structure. In Sec. 1.4.4 we will explain in details how this term can be treated perturbatively. We can decompose the impurity potential in a magnetic and a non-magnetic part (proportional to the unit matrix in spin space $\hat{\sigma}_0$)

$$U_{\alpha\beta}(\mathbf{r}) = V(\mathbf{r})\hat{\sigma}_0 + V'(\mathbf{r})\mathbf{S} \cdot \frac{\hat{\boldsymbol{\sigma}}}{2}. \quad (1.7)$$

The orbital effect of an external magnetic field \mathbf{H} can be included as usual in the gradient term ($\nabla \rightarrow \nabla - \frac{2ie\mathbf{A}}{\hbar}$) and \mathbf{h} comprises both the contributions of the Zeeman coupling with the external magnetic field and the ferromagnetic exchange field.

1.4.2 Gor’kov equations

In order to describe finite temperature properties of the system, we work with imaginary-time Matsubara Green functions [14]

$$G_{\alpha\beta}(\mathbf{r}_1, \tau_1; \mathbf{r}_2, \tau_2) = \left\langle T_\tau \psi_\alpha(\mathbf{r}_1, \tau_1) \psi_\beta^\dagger(\mathbf{r}_2, \tau_2) \right\rangle_{\text{stat}}, \quad (1.8)$$

where the imaginary time is introduced as $t = -i\tau$. Working within the time interval $-1/T < \tau < 1/T$ allows to unambiguously order the operators present in the Gibbs average $\langle \dots \rangle_{\text{stat}}$.

When studying superconducting systems, it is convenient to introduce the matrix Green function in the particle-hole space (Nambu-Gor'kov space)

$$\check{\mathbf{G}}(\mathbf{r}_1, \tau_1; \mathbf{r}_2, \tau_2) = \begin{pmatrix} \mathbf{G}_{\alpha\beta} & \mathbf{F}_{\alpha\beta} \\ -\mathbf{F}_{\alpha\beta}^\dagger & \bar{\mathbf{G}}_{\alpha\beta} \end{pmatrix} \quad (1.9)$$

with the anomalous Green function

$$\mathbf{F}_{\alpha\beta}^{(\dagger)} = \left\langle T_\tau \psi_\alpha^{(\dagger)}(\mathbf{r}_1, \tau_1) \psi_\beta^{(\dagger)}(\mathbf{r}_2, \tau_2) \right\rangle_{\text{stat}} \quad (1.10)$$

and

$$\bar{\mathbf{G}}_{\alpha\beta} = - \left\langle T_\tau \psi_\alpha^\dagger(\mathbf{r}_1, \tau_1) \psi_\beta(\mathbf{r}_2, \tau_2) \right\rangle_{\text{stat}} \quad (1.11)$$

describing the propagation of a hole.

Let us first discuss the simple case of the spin structure of the Green function in the absence of triplet correlations. This is the case when the exchange field \mathbf{h} is zero. We can then write

$$\mathbf{G}_{\alpha\beta}(\mathbf{x}_1, \mathbf{x}_2) = \delta_{\alpha\beta} \mathbf{G}_0(\mathbf{x}_1, \mathbf{x}_2). \quad (1.12)$$

For an s-wave pairing (even parity in the orbital space), the pairing in Cooper pairs can only occur between electrons with opposite spin into a singlet state

$$\Delta_{\alpha\beta} = |g| F_{\alpha\beta}(\mathbf{x}, \mathbf{x}) = -\Delta_{\beta\alpha}. \quad (1.13)$$

Therefore we write

$$\mathbf{F}_{\alpha\beta}(\mathbf{x}_1, \mathbf{x}_2) = i\hat{\sigma}_{\alpha\beta}^{(2)} \mathbf{F}_0(\mathbf{x}_1, \mathbf{x}_2). \quad (1.14)$$

We use the notation $\hat{\sigma}_i$ for the Pauli matrices in the spin space to avoid confusion with the Pauli matrices in the Nambu space which we will denote $\hat{\tau}_i$. We have also introduced the compact notation $\mathbf{x} = (\mathbf{r}, \tau)$.

In experimental observations of superconductivity, the symmetry of the pairing is usually either of s-wave type (conventional pairing) or of d-wave type (unconventional pairing). As an exception we can cite the exotic p-wave superconductivity in Sr2RuO4 [19]. For s-wave and d-wave superconductivity, the paired electrons form a singlet state and p-wave pairing leads to a spin-triplet state. While Anderson's theorem states that s-wave singlet superconductivity is not affected by the presence of disorder, d-wave pairing requires relatively clean samples so that superconductivity can be observed. The sensibility to disorder is strong in the p-wave triplet superconductors: superconductivity exists only in clean Sr2RuO4 samples. In other words, triplet correlations seem not to accommodate the presence of disorder. For triplet correlations, the Pauli principle implies that

$$F_{\sigma\sigma'}(\mathbf{r}, \tau; \mathbf{r}', \tau') = \langle \psi_\sigma(\mathbf{r}, \tau) \psi_{\sigma'}(\mathbf{r}', \tau') \rangle \quad (1.15)$$

is an odd function upon permutation of $\mathbf{r} \leftrightarrow \mathbf{r}'$ at equal times. We introduce \mathbf{k} and ω the momentum and the frequency conjugated to the relative coordinate $\mathbf{r} - \mathbf{r}'$ and time $\tau - \tau'$, respectively. Going to the momentum-frequency representation we have that

$$\sum_{\omega} \langle \psi_{\sigma}(\mathbf{r}, t) \psi_{\sigma'}(\mathbf{r}', t) \rangle_{\mathbf{k}, \omega} \quad (1.16)$$

is either odd in the orbital momentum \mathbf{k} (i.e., the orbital angular momentum L is odd) or zero. The former possibility gives rise to a component sensible to the presence of disorder (like triplet superconductivity in Sr2RuO4). The latter possibility, which can be achieved if the correlation is odd in frequency ω to make the sum vanish, allows triplet correlations to be even in orbital angular momentum. It is therefore possible to have a triplet component, usually denoted “odd triplet component” [6], resistant to the presence of disorder. This triplet component, in contrast to the triplet component in Sr2RuO4, has an s-wave symmetry in diffusive systems. It can therefore accommodate the presence of scattering on non-magnetic impurities.

In ferromagnets, singlet correlations of the type (1.14) are destroyed due to the alignment of spins in the exchange field \mathbf{h} . We will see in Chapter 2 that a part of the odd triplet component does not experience the pair breaking effect from the Zeeman coupling with the exchange field. Usually the exchange field is the strongest source of decoherence in ferromagnets: even in experiments with SFS junctions using weak ferromagnets, we have $\frac{\hbar}{T_c} \gtrsim 100$ (for more details, see the discussion in Chapters 2 and 3). Generating the component resistant to the exchange field should therefore make it possible to observe long range proximity effect in SF systems.

The definition of the Green function (1.9) is the one adopted in [14]. This is a practical definition in the absence of the exchange field \mathbf{h} . Usually, in works focusing on the effect of non-trivial triplet correlations [6, 20] other conventions are adopted. We will follow for now the conventions used in Ref. [6] and redefine the components of the 4x4 matrix Green function as

$$\check{G}_{(n,\alpha),(m,\beta)} = \left\langle T_{\tau} c_{n,\alpha} c_{m,\beta}^{\dagger} \right\rangle_{\text{stat}} \quad (1.17)$$

with $n, m = 1, 2$ the indices operating in particle-hole Nambu space and $\alpha, \beta = \pm 1$ the spin indices. We have introduced new creation and annihilation operators

$$c_{n,s} = \begin{cases} \psi_s & n = 1, \\ \psi_{-s}^{\dagger} & n = 2. \end{cases} \quad (1.18)$$

In terms of the new operators the Hamiltonian (1.6) becomes

$$\mathcal{H} = \frac{1}{2} \int d^3r \sum_{n,n',s,s'} c_{n,s}^{\dagger} \left(-\frac{\nabla^2}{2m} - \mu + V \right) \hat{\tau}_3 \otimes \hat{\sigma}_0 + \hat{\Delta} \otimes \hat{\sigma}_3 + \mathbf{h} \hat{\tau}_3 \hat{\sigma} + V' \mathbf{S} \hat{\tau}_3 \frac{\check{\sigma}}{2} c_{n',s'} \quad (1.19)$$

with as usual $\hat{\tau}_\alpha, \hat{\sigma}_\alpha$ the Pauli matrices operating in Nambu and spin space, respectively. As introduced in (1.7), $V(\mathbf{r})$ and $V'(\mathbf{r})$ account for non-magnetic and magnetic impurities with spin \mathbf{S} (the impurity spin is treated as a classical vector) and we define $\check{\boldsymbol{\sigma}} = (\hat{\sigma}_1, \hat{\sigma}_2, \hat{\tau}_3 \hat{\sigma}_3)$. The order parameter is a matrix in Nambu space

$$\hat{\Delta} = \begin{pmatrix} 0 & \Delta(\mathbf{r}) \\ \Delta^*(\mathbf{r}) & 0 \end{pmatrix}. \quad (1.20)$$

From the microscopic BCS Hamiltonian (1.19), we can compute the equations of motion (“Gor’kov equations”) for the matrix Green function (1.17)

$$\check{\mathcal{G}}^{-1}(x_1) \check{G}(x_1, x_2) = \check{1} \delta(x_1, x_2) \quad (1.21)$$

$$\check{G}(x_1, x_2) \bar{\mathcal{G}}^{-1}(x_2) = \check{1} \delta(x_1, x_2). \quad (1.22)$$

The variables x_i include both imaginary time and space coordinates. The operators $\check{\mathcal{G}}^{-1}$ and $\bar{\mathcal{G}}^{-1}$ are given by

$$\check{\mathcal{G}}^{-1} = \frac{\partial}{\partial \tau} + \check{H} + \check{H}_{\text{imp}} + \check{H}_{\text{ferro}}, \quad (1.23)$$

and

$$\bar{\mathcal{G}}^{-1} = -\frac{\partial}{\partial \tau} + \check{H} + \check{H}_{\text{imp}} + \check{H}_{\text{ferro}}. \quad (1.24)$$

In the absence of impurities and exchange field we have only the term

$$\check{H} = \left(-\frac{\nabla^2}{2m} - \mu \right) \hat{\tau}_3 \otimes \hat{\sigma}_0 + \hat{\Delta} \otimes \hat{\sigma}_3. \quad (1.25)$$

The effect of the impurities is included in the matrix

$$\check{H}_{\text{imp}} = \left(V(\mathbf{r}) + V'(\mathbf{r}) \mathbf{S} \frac{\check{\boldsymbol{\sigma}}}{2} \right) \otimes \hat{\tau}_3. \quad (1.26)$$

Finally, the presence of the ferromagnetic exchange interaction leads to the term

$$\check{H}_{\text{ferro}} = \mathbf{h} \hat{\tau}_3 \check{\boldsymbol{\sigma}}. \quad (1.27)$$

We decompose as in (1.9) the matrix Green function in Nambu space (we introduce a multiplication by $\hat{\tau}_3 \otimes \hat{\sigma}_0$ in order to retrieve \bar{G} as the hole propagator)

$$\check{G}(x_1, x_2) = \hat{\tau}_3 \otimes \hat{\sigma}_0 \begin{pmatrix} G(x_1, x_2) & F(x_1, x_2) \\ -F(x_1, x_2)^\dagger & \bar{G}(x_1, x_2) \end{pmatrix}. \quad (1.28)$$

The equations (1.21) and (1.22) are symmetrical in terms of particle-hole, the function \bar{G} describes the propagation of a hole. In (1.28) we have omitted the spin indices for simplicity but the reader should keep in mind that the Green function \check{G} is a 4x4 matrix (1.17). In the absence of the triplet component ($\mathbf{h} = 0$) we have $G \propto \hat{\sigma}_0$ and $F \propto \hat{\sigma}_3$.

In the following, we will often express the Green function in terms of its Fourier components (momentum-frequency representation). In the frequency space we have

$$\check{G}_{\omega_n}(\mathbf{r}_1, \mathbf{r}_2) = \int_0^{\frac{1}{T}} d\tau e^{i\omega_n \tau} \check{G}(\mathbf{r}_1, \mathbf{r}_2, \tau), \quad (1.29)$$

where $\omega_n = (2n+1)\pi T$ are the Matsubara frequencies and $\tau = \tau_1 - \tau_2$. For the momentum representation of the Green function we cannot assume homogeneity since we want to describe hybrid structures. We write therefore

$$\check{G}(\mathbf{r}_1, \mathbf{r}_2) = \int \frac{d^3 p}{(2\pi)^3} \int \frac{d^3 p'}{(2\pi)^3} \check{G}(\mathbf{p}, \mathbf{p}') e^{i\mathbf{p}\mathbf{r}_1 - i\mathbf{p}'\mathbf{r}_2}. \quad (1.30)$$

1.4.3 Real-time formulation

Until now, we have been working with imaginary time Matsubara Green functions to derive the formalism. We make the link now between the imaginary time formalism and the real time formalism (which allows to get time-dependent properties of the system). The retarded and advanced real time (here $\mathbf{x} = (\mathbf{r}, t)$) Green functions are given by

$$\begin{aligned} \check{G}_{(n,\alpha),(m,\beta)}^R(\mathbf{x}_1, \mathbf{x}_2) &= i \left\langle T_\tau \left[c_{n,\alpha}(\mathbf{x}_1) c_{m,\beta}^\dagger(\mathbf{x}_2) + c_{m,\beta}^\dagger(\mathbf{x}_2) c_{n,\alpha}(\mathbf{x}_1) \right] \right\rangle_{\text{stat}} & t_1 > t_2 \\ \check{G}_{(n,\alpha),(m,\beta)}^R(\mathbf{x}_1, \mathbf{x}_2) &= 0 & t_1 < t_2 \end{aligned}$$

and

$$\begin{aligned} \check{G}_{(n,\alpha),(m,\beta)}^A(\mathbf{x}_1, \mathbf{x}_2) &= -i \left\langle T_\tau \left[c_{n,\alpha}(\mathbf{x}_1) c_{m,\beta}^\dagger(\mathbf{x}_2) + c_{m,\beta}^\dagger(\mathbf{x}_2) c_{n,\alpha}(\mathbf{x}_1) \right] \right\rangle_{\text{stat}} & t_1 < t_2 \\ \check{G}_{(n,\alpha),(m,\beta)}^A(\mathbf{x}_1, \mathbf{x}_2) &= 0 & t_1 > t_2. \end{aligned}$$

Using these definitions and working in the frequency representation (1.29), one can show that the real frequency Green functions $\check{G}_\epsilon^{R(A)}$ are the analytical continuation of the Matsubara Green function \check{G}_{ω_n} from the positive, respectively negative, imaginary axis

$$\check{G}_{\omega_n} = \check{G}_{i\omega_n}^R, \quad \omega_n > 0 \quad (1.31)$$

$$\check{G}_{\omega_n} = \check{G}_{i\omega_n}^A, \quad \omega_n < 0. \quad (1.32)$$

The retarded and advanced Green functions $\check{G}_{\epsilon=i\omega_n}^{R(A)}$ satisfy the same equations (1.21) and (1.22) as the Matsubara Green function (1.17).

1.4.4 Scattering on impurities: self-energy

As mentioned in Sec. 1.2, we will focus in this thesis on systems containing a large amount of random impurities. We explain here how electron scattering on random impurity atoms

can be introduced in the Green function formulation of the BCS theory. The original diagrammatic technique has been derived in [17, 21] and a detailed description of the method can be found in [14, 22]. The theory we develop here can be applied to magnetic or non-magnetic impurities. We make the following assumptions on the type of disorder we consider:

- Scattering is elastic and can be described by an external potential U .
- The scattering potential U is small compared to the Fermi energy E_F (Born approximation).
- The physical properties can be obtained by averaging over the realizations of disorder.

Denoting the position of the impurities \mathbf{r}_a , we decompose the potential U into the sum of the contributions of each impurity

$$U_{\alpha\beta}(\mathbf{r}) = \sum_a u_{\alpha\beta}(\mathbf{r} - \mathbf{r}_a). \quad (1.33)$$

For impurity atoms distributed randomly, we can average over the positions of the impurities substituting

$$\sum_a \rightarrow n_{imp} \int d^3r_a \quad (1.34)$$

with n_{imp} the impurity concentration. Note that for simplicity we have considered only one type of impurity. For impurities carrying a spin \mathbf{S}_a , we further decompose the potential of the impurity into a magnetic and a non-magnetic part

$$u_{\alpha\beta}(\mathbf{r} - \mathbf{r}_a) = v(\mathbf{r} - \mathbf{r}_a)\sigma_0 + v'(\mathbf{r} - \mathbf{r}_a)\mathbf{S}_a \cdot \frac{\hat{\sigma}}{2}. \quad (1.35)$$

Within this framework, it is possible to treat the interaction with the impurities (1.26) perturbatively and to express the Green function \check{G} of the electrons interacting with the random disorder as a Dyson series in powers of the impurity potential U starting from the Green function $\check{G}^{(0)}$ of the clean system. Since we want to study systems like proximity superconductors, we must do the perturbation expansion for a non-homogeneous system. We can distinguish different types of diagrams in the expansion:

- The diagrams of arbitrary order where scattering occurs on different impurities. The contribution of those diagrams can be incorporated into the chemical potential.
- The diagrams of any order with two scattering per impurity atom.
- The diagrams of any order with more than two scattering per atom. It can be shown that the contribution of those diagrams is of higher order in u/E_F than the contribution of the previous type of diagrams and can be safely neglected in the Born approximation.

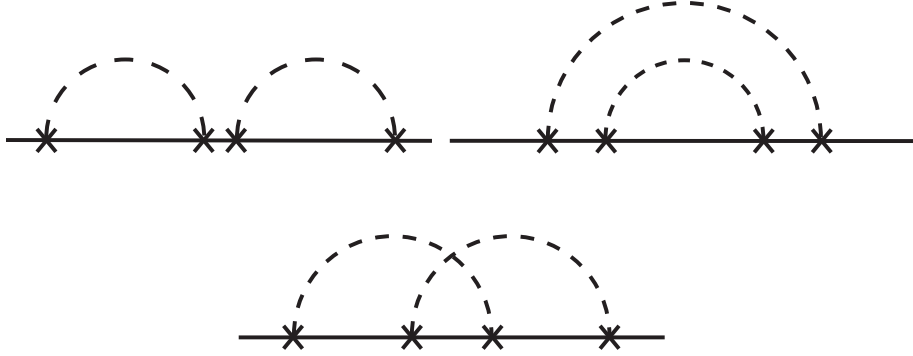


Figure 1.2: Relevant fourth order diagrams of the expansion of the Green function \check{G} in powers of the impurity potential. The solid lines represent $\check{G}_0(\mathbf{p}, \mathbf{p}')$ and the crosses $\check{h}_{\text{imp}}(\mathbf{k})$ (1.38). The dashed lines connect scattering events occurring on the same impurity atom. The upper diagrams are non-crossing diagrams while in the lower diagram the dashed lines cross.

There is only one relevant diagram of order two after averaging over the position of the impurity atoms. In Fig. 1.2 we represent the relevant diagrams of order four. We connect the scattering events occurring on the same atom by a dashed line and distinguish crossing from non-crossing diagrams. It can be shown [22] that the relative contribution of the crossing diagrams compared to non-crossing ones is of the order of $\frac{1}{p_F l_e}$, which is a small factor for metals. We can reduce the summation of all the remaining relevant diagrams (non-crossing with two scattering per impurity atom) to a self-energy $\check{\Sigma}$, and get the Dyson equation for the matrix Green function

$$\check{G}(\mathbf{p}, \mathbf{p}') = \check{G}^{(0)}(\mathbf{p}, \mathbf{p}') + \int \check{G}^{(0)}(\mathbf{p}, \mathbf{p}_1) \check{\Sigma}(\mathbf{p}_1, \mathbf{p}_2) \check{G}(\mathbf{p}_2, \mathbf{p}') d^3 p_1 d^3 p_2, \quad (1.36)$$

where we introduced the self-energy matrix $\check{\Sigma}$ given in the Fourier representation by

$$\check{\Sigma}(\mathbf{p}_1, \mathbf{p}_2) = n_{\text{imp}} \int \frac{d^3 p}{(2\pi)^3} \check{h}_{\text{imp}}(\mathbf{p}_1 - \mathbf{p}) \check{G}(\mathbf{p}, \mathbf{p} - \mathbf{p}_1 + \mathbf{p}_2) \check{h}_{\text{imp}}(\mathbf{p} - \mathbf{p}_1), \quad (1.37)$$

and

$$\check{h}_{\text{imp}} = \left(v(\mathbf{r}) + v'(\mathbf{r}) \mathbf{S} \frac{\check{\sigma}}{2} \right) \otimes \hat{\tau}_3 \quad (1.38)$$

is the single impurity contribution to (1.26). In Fig. 1.3 we represent graphically the series (1.36).

The Dyson equation (1.36) is equivalent to the Gor'kov equation in the momentum representation

$$[(\check{G}_{\text{clean}}^{-1} - \check{\Sigma}) * \check{G}]_{\mathbf{p}, \mathbf{p}'} = (2\pi)^3 \delta(\mathbf{p} - \mathbf{p}') \check{1} \quad (1.39)$$

with

$$[\check{A} * \check{B}]_{\mathbf{p}, \mathbf{p}'} = \int \frac{d^3 p_1}{(2\pi)^3} \check{A}(\mathbf{p}, \mathbf{p}_1) \check{B}(\mathbf{p}_1, \mathbf{p}'). \quad (1.40)$$

$$\overline{\overline{\mathbf{G}}} = \overline{\mathbf{G}^{(0)}} + \overline{\mathbf{G}^{(0)}} \overset{\text{---}}{\underbrace{\hspace{1.5cm}}{\Sigma}} \overline{\mathbf{G}}$$

Figure 1.3: Graphical Dyson equation.

The structure of the self energy matrix depends on type of impurities we consider. The simplest case is the situation where we only have non-magnetic impurities. In this case \check{h}_{imp} commutes with \check{G} in the spin space. We can introduce the scattering cross section $\sigma(\mathbf{p}, \mathbf{p}')$ related to the impurity potential u by the relation (Born approximation)

$$|u(\mathbf{p}_1 - \mathbf{p})|^2 = \frac{2v_F}{\nu_0} \sigma(\mathbf{p}_1 - \mathbf{p}), \quad (1.41)$$

with $\nu_0 = mp_F/2\pi^2$ the density of states per one spin projection in the normal state. In the Born approximation we can write $\sigma(\mathbf{p}_1 - \mathbf{p}) = \sigma(\theta)$ with $\theta = \angle(\mathbf{p}_1, \mathbf{p})$ since all the momenta are in the vicinity of the Fermi surface. Finally we get for the self-energy matrix

$$\check{\Sigma}(\mathbf{p}_1, \mathbf{p}_2) = n_{\text{imp}} \int \frac{d^3p}{(2\pi)^3} \sigma(\theta) \hat{\tau}_3 \check{G}(\mathbf{p}, \mathbf{p} - \mathbf{p}_1 + \mathbf{p}_2) \hat{\tau}_3. \quad (1.42)$$

We can introduce the scattering mean free time τ_e which satisfies

$$\sigma_{\text{tot}} n_{\text{imp}} \underbrace{v_F \tau_e}_{l_e} = 1. \quad (1.43)$$

If we consider the Gor'kov equation (1.39) for a homogeneous material with s-wave singlet pairing Δ and only non-magnetic impurities, one can show that the gap equation for a dirty alloy is the same as the gap equation for a clean superconductor (Anderson's theorem)

$$\frac{\Delta}{|g|} = \nu_0 2\pi T \sum_{n=0}^{n_c} \frac{\Delta}{\sqrt{\omega^2 + |\Delta|^2}}, \quad (1.44)$$

where we have taken a cutoff in the summation over Matsubara frequencies at the Debye frequency.

If we take as a second example the situation where the spin of the impurities is oriented arbitrarily and where there is no correlation between them, we get the disorder averages

$$\overline{\mathbf{S}_a} = 0 \quad \text{and} \quad \overline{\mathbf{S}_a \mathbf{S}_b} = \frac{1}{3} S(S+1) \delta_{ab}. \quad (1.45)$$

This assumption is fully justified only for low concentrations of paramagnetic impurities. If the concentration is high, the interaction between the spins may result in some magnetic ordering and therefore the averaging (1.45) is inapplicable. For simplicity, we restrict

ourselves for now to the situation where we do not have triplet correlations. This is the case in the absence of the exchange field \mathbf{h} . The anomalous Green function (1.28) F is then proportional to $\hat{\sigma}_3$ and G is proportional to $\hat{\sigma}_0$. We have to consider different scattering amplitudes to compute the components of the self-energy matrix (defined in analogy with (1.28))

$$\check{\Sigma} = \hat{\tau}_3 \otimes \hat{\sigma}_0 \begin{pmatrix} \Sigma_1 & \Sigma_2 \\ -\Sigma_2^\dagger & \bar{\Sigma}_1 \end{pmatrix}. \quad (1.46)$$

We get

$$\Sigma_1(\mathbf{p}_1, \mathbf{p}_2) = n_{imp} \int \frac{d^3 p}{(2\pi)^3} |u_1(\theta)|^2 G(\mathbf{p}, \mathbf{p} - \mathbf{p}_1 + \mathbf{p}_2), \quad (1.47)$$

and

$$\Sigma_2(\mathbf{p}_1, \mathbf{p}_2) = n_{imp} \int \frac{d^3 p}{(2\pi)^3} |u_2(\theta)|^2 F(\mathbf{p}, \mathbf{p} - \mathbf{p}_1 + \mathbf{p}_2), \quad (1.48)$$

with $\theta = \angle(\mathbf{p}, \mathbf{p}_1)$. Using relation (1.37), we get

$$|u_1(\theta)|^2 = |v(\theta)|^2 + \frac{1}{4} S(S+1) |v'(\theta)|^2 \quad (1.49)$$

and for the anomalous part

$$|u_2(\theta)|^2 = -|v(\theta)|^2 + \frac{1}{4} S(S+1) |v'(\theta)|^2. \quad (1.50)$$

The corresponding scattering mean free times (1.43) are therefore different for the normal and anomalous parts of the Green function. Generalization to an arbitrary spin structure of the Green function is straightforward.

1.4.5 Quasiclassical theory

In conventional superconductors, the order parameter Δ is much smaller than the Fermi energy ($\frac{\Delta}{E_F} \sim 10^{-3}$). For high temperature superconductors, this ratio is higher but still lies between 10^{-1} and 10^{-2} . The corresponding scale of variation for superconducting properties, i.e., the coherence length ξ_S , is in turn much larger than the Fermi wavelength

$$\frac{1}{p_F \xi_S} \sim \frac{\Delta}{E_F} \ll 1. \quad (1.51)$$

We can take advantage of this situation and simplify the calculation of the Green function. Solving the full Gor'kov equations (1.21) and (1.22) is often not a tractable task: recall for example that the order parameter Δ has to be determined self-consistently from the solution and can therefore in principle show a complicated spatial dependence on the Fermi scale. On the other hand (1.51) implies that superconducting properties are related to the part of the Green function with momenta close to the Fermi surface. The quasiclassical approximation has been developed to use this fact by separating and

integrating out the fast dependence of the Green functions which is related to normal properties of the system and occurs on the Fermi scale. The same method can be developed when working within the quasiparticle wave functions formalism (wave functions solutions of the Bogoliubov de Gennes equations [18]).

To separate the center of mass dependence from the relative coordinates, we introduce the notation

$$\check{G}(\mathbf{p}_1, \mathbf{p}_2) = \check{G}\left(\mathbf{p} + \frac{\mathbf{k}}{2}, \mathbf{p} - \frac{\mathbf{k}}{2}\right). \quad (1.52)$$

Now we define the Green function \tilde{g} integrated over the magnitude of the momentum \mathbf{p}

$$\tilde{g}_{\omega_n}(\hat{\mathbf{p}}, \mathbf{k}) = \hat{\tau}_3 \otimes \hat{\sigma}_0 \int \frac{d\xi_{\mathbf{p}}}{\pi i} \check{G}_{\omega_n}\left(\mathbf{p} + \frac{\mathbf{k}}{2}, \mathbf{p} - \frac{\mathbf{k}}{2}\right). \quad (1.53)$$

The integration is performed over $\xi_p = p^2/2m - \mu$ near the Fermi surface and $\hat{\mathbf{p}}$ is a unit vector in the direction of \mathbf{p} . \tilde{g} will be denoted in the following the ‘‘quasiclassical Green function’’. We have multiplied the green function by $\hat{\tau}_3 \otimes \hat{\sigma}_0$ to account for the particle-hole symmetry $\bar{g} = -g$ of the quasiclassical Green function [14]. The integration over the magnitude of the momentum excludes the fast oscillations of the Green function. In the coordinate representation, we only keep the slow dependence on the center of mass coordinate $\mathbf{r}_1 + \mathbf{r}_2$ which is related to superconducting properties of the system and exclude the Fermi oscillations on the relative coordinate $\mathbf{r}_1 - \mathbf{r}_2$ related to normal properties.

The equation for the quasiclassical Green function can be derived from the Gor’kov equation (1.39). Those equations were originally obtained by Eilenberger [23]. Working in the momentum representation (1.53), we get as a result [14]

$$\mathbf{v}_F \mathbf{k} \tilde{g} - i\omega_n(\tilde{\tau}_3 \tilde{g} - \tilde{g} \tilde{\tau}_3) - \left[(\hat{\tau}_3 \otimes \hat{\sigma}_3 \hat{\Delta} - \mathbf{h} \check{\boldsymbol{\sigma}}) * \tilde{g} \right] + \left[\tilde{g} * (\hat{\tau}_3 \otimes \hat{\sigma}_3 \hat{\Delta} - \mathbf{h} \check{\boldsymbol{\sigma}}) \right] = \check{I} \quad (1.54)$$

with $\check{\boldsymbol{\sigma}}$ and $\hat{\Delta}$ as defined in (1.19). The square bracket denote the usual convolution product in the Fourier representation and the collision integral \check{I} is given by

$$\check{I} = [\hat{\tau}_3 \check{\Sigma} \hat{\tau}_3 * \tilde{g}] - [\tilde{g} * \hat{\tau}_3 \check{\Sigma} \hat{\tau}_3]. \quad (1.55)$$

It is useful to introduce a mixed Fourier-coordinate representation to get rid of the convolution products in the Eilenberger equation (1.54)

$$\tilde{g}_{\omega_n}(\hat{\mathbf{p}}, \mathbf{r}) = \int \frac{d^3 k}{(2\pi)^3} e^{i\mathbf{k}\mathbf{r}} \tilde{g}_{\omega_n}(\hat{\mathbf{p}}, \mathbf{k}). \quad (1.56)$$

Finally, it is important to notice that the quasiclassical Green function $\tilde{g} = \begin{pmatrix} g & f \\ -f^\dagger & \bar{g} \end{pmatrix}$ must satisfy, in addition to (1.54)

$$\tilde{g} \tilde{g} = \check{1}. \quad (1.57)$$

This will impose a constraint on the solution of the Eilenberger equation. The off-diagonal part of this relation is related to the particle-hole symmetry (at equilibrium) of the theory

$$g + \bar{g} = 0, \quad (1.58)$$

and the diagonal part is the so-called normalization condition

$$g^2 - f f^\dagger = \hat{1}. \quad (1.59)$$

Details on the derivation of (1.57) can be found in Ref. [14].

In the diffusive limit ($\frac{1}{\tau_e} \gg T_c, h, E_{\text{Th}}$), it is possible to introduce a further simplification to the Green function formalism. In dirty superconductors, strong scattering produces averaging over momentum directions: the quasiclassical Green function $\tilde{g}(\hat{\mathbf{p}}, \mathbf{r})$ becomes isotropic. We can take advantage of this fact [13] by expanding \tilde{g} in spherical harmonics. Before deriving the equations for the isotropic part of the Green function, we introduce the unitary transformation $U = (1 + i\hat{\tau}_3\hat{\sigma}_3)(1 - i\hat{\sigma}_3)/2$ following the conventions of [20] and define

$$\check{g} = U \tilde{g} U^\dagger. \quad (1.60)$$

This convention will allow us to have a Green function \check{g} proportional to $\hat{\sigma}_0$ in spin-space in the absence of the exchange field.

We denote the isotropic part $\langle \check{g} \rangle$ and the first order correction $\check{\mathbf{g}}$

$$\begin{aligned} \check{g} &\approx \langle \check{g} \rangle + \mathbf{v}_{\mathbf{F}} \check{\mathbf{g}} \\ \langle \check{g} \rangle &= \int \frac{d\Omega_p}{4\pi} \check{g}(\hat{\mathbf{p}}, \mathbf{r}). \end{aligned} \quad (1.61)$$

Averaging the Eilenberger equation (1.54) over the momentum directions, one gets the so called Usadel equations

$$D\hat{\nabla} \left(\langle \check{g} \rangle \hat{\nabla} \langle \check{g} \rangle \right) - \omega [\hat{\tau}_3 \hat{\sigma}_0, \langle \check{g} \rangle] - i [\hat{\tau}_3 (\mathbf{h} \cdot \hat{\boldsymbol{\sigma}}), \langle \check{g} \rangle] - \left[\hat{\Delta} \hat{\sigma}_0, \langle \check{g} \rangle \right] = 0 \quad (1.62)$$

and

$$\check{\mathbf{g}} = -l_e \langle \check{g} \rangle \hat{\nabla} \langle \check{g} \rangle, \quad (1.63)$$

with

$$\hat{\Delta} = \begin{pmatrix} 0 & \Delta e^{i\chi} \\ \Delta e^{-i\chi} & 0 \end{pmatrix}. \quad (1.64)$$

We have included the orbital effect of external magnetic fields through

$$\hat{\nabla} \check{g} = \begin{pmatrix} \nabla g & (\nabla - \frac{2ie}{\hbar} \mathbf{A}) f \\ -(\nabla + \frac{2ie}{\hbar} \mathbf{A}) f^\dagger & -\nabla g \end{pmatrix}. \quad (1.65)$$

The normalization condition (1.57) gives

$$\begin{aligned} \check{g} \check{g} &= \check{1} \\ \Rightarrow \langle \check{g} \rangle \langle \check{g} \rangle &= \check{1} \quad \text{and} \quad \check{\mathbf{g}} \langle \check{g} \rangle + \langle \check{g} \rangle \check{\mathbf{g}} = 0. \end{aligned} \quad (1.66)$$

The equations (1.62) and (1.63) have been derived originally by Usadel in [13]. We presented here their generalization [6] which is adapted to the case of interest in this thesis where the matrix Green function (1.28) can have an arbitrary structure in spin-space due to the presence of the ferromagnetic exchange field \mathbf{h} . The quasiclassical equations can be further generalized to include the description of nonequilibrium situations. One works then with Green functions in the Keldysh representation [24]. Following a procedure similar to the derivation of the equilibrium equations described in this chapter, one obtains equations equivalent to the Eilenberger equation (1.54), the ‘‘Eliashberg equation’’ [25], and to the Usadel equation (1.62).

In the rest of the thesis we will always work in the diffusive limit and therefore use the simple notation \check{g} for the isotropic part of the quasiclassical Green function $\langle \check{g} \rangle$.

The components (in the Nambu space) g and f of the quasiclassical matrix Green function \check{g} are defined in analogy with (1.28)

$$\check{g} = \begin{pmatrix} g_\alpha \hat{\sigma}^\alpha & f_\alpha \hat{\sigma}^\alpha \\ -f_\alpha^\dagger \hat{\sigma}^\alpha & -g_\alpha \hat{\sigma}^\alpha \end{pmatrix}. \quad (1.67)$$

Note that we have made use of the particle-hole symmetry $\bar{g} = -g$ of the quasiclassical Green function at equilibrium [14]. In the spin space, we will in the following denote the component with $\alpha = 0$ ‘‘scalar component’’ and the components with $\alpha = 1, 2, 3$ will constitute the ‘‘vector component’’. We prefer the definition of [20] because it will lead to a Green function in the absence of the exchange field with only the scalar component and in the presence of a uniform exchange field with the vector component collinear to the exchange field.

It is important to notice that the collision integral \check{I} which was introduced with the Eilenberger equation (1.54) vanishes after averaging over momentum direction only if there is no spin-flip or inelastic (electron-phonon) scattering. In Appendix A we compute the contribution of isotropic magnetic disorder to the Usadel equation (1.62) via the collision integral.

From the solution of the Usadel equation (1.62) one can easily get the physical quantities of interest (recall that for simplicity we denote the isotropic part of the Green function \check{g} and drop the $\langle \dots \rangle$ in the following). The current density is given by

$$\mathbf{J} = ie\nu_0 D\pi T \sum_{\omega=-\infty}^{\infty} \frac{1}{2} \text{Tr} \left(\hat{\tau}_3 \hat{\sigma}_0 \check{g} \hat{\nabla} \check{g} \right), \quad (1.68)$$

while the density of states can be obtained from the scalar component $\alpha = 0$ of the normal part of the retarded (1.31) Green function $g^R = g_\alpha^R \sigma^\alpha$

$$\nu(\epsilon, x) = \frac{\nu_0}{8} \text{Tr} \left[\hat{\tau}_3 \hat{\sigma}_0 (\check{g}^R - \check{g}^A) \right] = \nu_0 \Re [g_0^R] \quad (1.69)$$

with $\nu_0 = \frac{m p_F}{2\pi^2}$ the density in the normal state (per one spin projection).

The Usadel formalism often allows to simplify the description of systems where the diffusion occurs in three dimensions by reducing them to a “quasi-one-dimensional” geometry. For examples where such a simplified description can be applied see Sec. 1.5.2 and Sec. 2.

1.4.6 Quasiclassical boundary conditions

The appropriate boundary conditions for the quasiclassical equations (1.54) and (1.62) cannot be derived starting from the quasiclassical theory. Indeed, the presence of an atomic sharp interface between two electrodes requires a description based on the Gor’kov equations (recall that the quasiclassical approximation is valid to describe slow variations of the Green function). The boundary conditions for the Eilenberger equation have been derived by Zaitsev [26]. They impose that the part of the quasiclassical Green function (1.53) $\tilde{g}_{\omega_n}(\hat{\mathbf{p}}, \mathbf{k})$ antisymmetric in $\hat{\mathbf{p}}$ is continuous at the interface between two materials (this condition implies the conservation of the current) while the symmetric part experiences a jump in the case where the interface is not transparent. Those conditions have been simplified in the diffusive limit by Kupriyanov and Lukichev [27]. For an interface without spin-dependent scattering, we get as a result the boundary conditions for the isotropic part of the quasiclassical Green function \check{g}

$$\sigma(-)\check{g}(-)(\mathbf{n} \cdot \hat{\nabla})\check{g}(-) = \sigma(+)\check{g}(+)(\mathbf{n} \cdot \hat{\nabla})\check{g}(+) \quad (1.70)$$

$$\begin{cases} \sigma(\pm)\check{g}(\pm)(\mathbf{n} \cdot \hat{\nabla})\check{g}(\pm) = \frac{G_T}{2} [\check{g}(+), \check{g}(-)] & \text{low transparency} \\ \check{g}(+) = \check{g}(-) & \text{high transparency} \end{cases} \quad (1.71)$$

G_T is the tunnel conductance of the junction (as defined in [28]), \mathbf{n} denotes a normal to the interface, the gradient operator $\hat{\nabla}$ was introduced in (1.65) and σ_{\pm} are the metallic conductance on both sides of the interface. In the limit of a transparent interface, the second boundary condition results in the continuity of the Green function at the interface.

In the thesis we will often simplify the boundary conditions (“rigid boundary conditions”) between a superconductor and a normal metal imposing at the interface between the two materials the Green function of a bulk superconductor

$$\check{g} = \frac{1}{\sqrt{\omega^2 + \Delta^2}} \begin{pmatrix} \omega & \Delta e^{\pm i\chi} \\ -\Delta e^{\mp i\chi} & -\omega \end{pmatrix}_{\text{Nambu}} \otimes \hat{\sigma}_0, \quad (1.72)$$

where Δ is the superconducting order parameter. Formally, we see from (1.70) that rigid boundary conditions are justified for high transparency of the interface, when the condition $\sigma_N \ll \sigma_S$ is fulfilled. This is the case if the normal electrode is much more disordered than the superconducting electrode.

We will apply the boundary conditions described above that were derived in the absence of the exchange field for SN and SF junctions. In principle one would need to take into

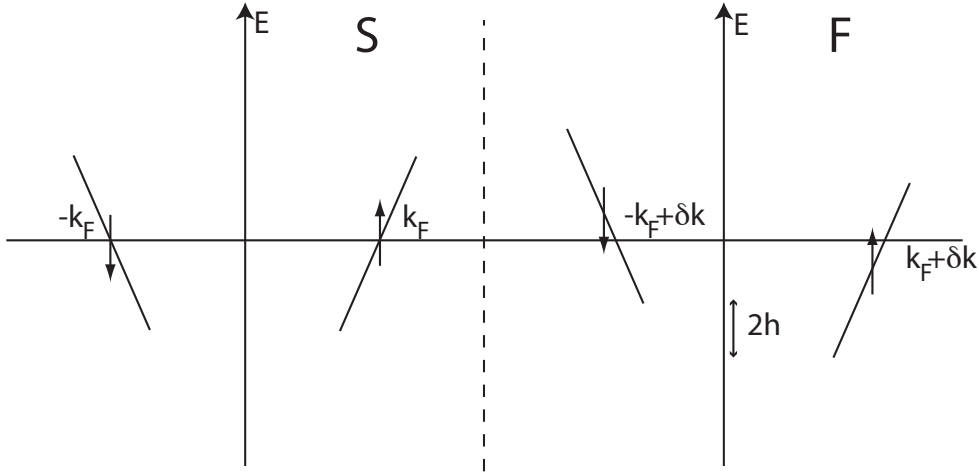


Figure 1.4: Cooper pair in a superconductor S and in a ferromagnet F. In the F region the Cooper pairs acquire a momentum $2\delta k = \frac{2h}{v_F}$ due to the presence of the ferromagnetic exchange field \mathbf{h} .

account the jump of the exchange field at the interface between a superconductor and a ferromagnet. Several works have studied effects related to SF interfaces or magnetically active interfaces [29–31], but, to our knowledge, a general theory of the boundary conditions for SF interfaces is lacking. However, as long as the condition $h \ll E_F$ is satisfied, we can safely apply the conditions (1.70) and (1.71) derived for SN junctions. The typical value of the ferromagnetic exchange field h is of the order of 1000K while the characteristic Fermi temperature for metals is usually two orders of magnitude higher, justifying the use of (1.70) and (1.71) for SF interfaces.

1.5 Features of the proximity effect in the presence of magnetism

1.5.1 Interplay between magnetism and superconductivity

In principle, magnetic and conventional superconducting order are competing orders. There are two mechanisms for the destruction of s-wave superconductivity by magnetism. Firstly, the orbital effect of a magnetic field may destroy the pairs. Secondly, the paramagnetic effect provides another mechanism for the destruction of superconductivity by lifting the degeneracy between the electrons forming Cooper pairs. In general, both mechanisms are present but the importance of their relative contribution to depairing varies. The orbital mechanism plays for example the most important role in the case of an applied external magnetic field in a large sample while the paramagnetic mechanism gives the

main contribution to depairing in systems with magnetic impurities or in the presence of ferromagnetism.

As an illustration of the paramagnetic mechanism one can discuss how scattering on magnetic impurities leads to the destruction of singlet superconductivity. The exchange interaction between the spin of the electrons and the magnetic impurities breaks the time reversal symmetry between the electrons in Cooper pairs and reduces the superconducting correlations. Scattering on magnetic impurities can be described in terms of a spin-flip scattering rate $\Gamma_{\text{sf}} = \frac{1}{2\tau_{\text{sf}}}$ via the collision integral (A.7). In the Born approximation [22, 32] Γ_{sf} is proportional to the impurity concentration. The energy gap E_g in the electron density of states (DoS) of a bulk s-wave superconductor is lowered by spin-flip scattering

$$E_g = \Delta \left[1 - \left(\frac{2\Gamma_{\text{sf}}}{\Delta} \right)^{2/3} \right]^{3/2} \quad (1.73)$$

and closes for the critical concentration of magnetic impurities [21] $\Gamma_{\text{sf}}^{\text{bulk}} = \frac{\Delta}{2}$. Here, the order parameter Δ itself, which has to be determined self-consistently with the anomalous part of the Green function, depends on Γ_{sf} .

As a second illustration, we briefly discuss the coexistence of superconductivity and ferromagnetism in the same material. In bulk compounds, singlet superconductivity cannot accommodate easily the presence of the ferromagnetic exchange field. The inhomogeneous superconducting FFLO state proposed in Refs. [33, 34] can only be observed in a small region of the (h-T) phase diagram of a three-dimensional superconductor [1] and is suppressed in the presence of impurities. This state shall therefore not be relevant for the dirty compounds considered in this thesis. On the contrary, proximity structures can accommodate the presence of both ferromagnetism and superconductivity. In superconductor-ferromagnet junctions (SF), ferromagnetism is separated from the source of superconducting correlations (bulk superconductor). Remarkably, the Cooper pair wave function does not decay monotonically in the ferromagnet when the distance from the SF interface is increased but shows a damped oscillatory behavior. The damping originates in the paramagnetic effect described above while the oscillations result from the momentum acquired by Cooper pairs in the ferromagnet. In Fig. 1.4, we illustrate how the pairs get a momentum in a ferromagnet F. For simplicity we consider a one-dimensional situation. In the F region, the electron with spin up projection (we take the quantization axis along the ferromagnetic exchange field \mathbf{h}) of the spin will have its energy raised by the exchange energy h and its pairing partner will have its energy lowered by the same amount. The corresponding kinetic energy modification leads to a resulting center of mass momentum $2\delta k$ for the Cooper pair. This mechanism is at the origin of a modulation of the order parameter in the ferromagnet.

Finally, for an example of a situation where orbital effects of an external magnetic field are dominant, we refer the reader to Chapter 4.

1.5.2 Closing of the minigap in the presence of magnetic impurities

We introduce in this section an important feature of the proximity effect: the appearance of the minigap in a normal metal connected to a superconductor. As a consequence of Andreev reflection and its interplay with disorder, a gap is opened in the spectrum of the N region (see for example [28, 35–37] and references therein). This minigap does not depend on the position in the junction and is of the order of magnitude of the Thouless energy $E_{\text{Th}} = \frac{\hbar D}{L^2}$, with D the diffusion constant and L the length of the normal wire. Recently, a detailed experimental study was performed by le Sueur *et al.* [38] on the local density of states in Al-Ag-Al SNS junctions showing very good agreement with the predictions of the quasiclassical theory.

It is important to stress that disorder is required to observe a minigap. If we consider for example a clean metallic film in contact with a superconductor, there exist [16, 28] Andreev levels with arbitrarily small energy corresponding to trajectories close to parallel with the SN interface. In the ballistic regime, the density of states is thus zero only exactly at the Fermi level. It can be shown in general that the minigap is a feature of systems with non-integrable classical dynamics [39].

To illustrate the effects of magnetism in proximity structures and as an introduction to the use of quasiclassical methods, we present here a simple analytical study [40] of the minigap in the presence of magnetic impurities. We will first explain how the opening of the minigap can be described within the quasiclassical theory. Then, we will show that the minigap closes when the impurity concentration reaches a critical value and derive a relation similar to (1.73) for the minigap. Understanding the effect of magnetic impurities will also be useful since magnetic domains in ferromagnets can under certain conditions be reduced to an effective spin-flip scattering rate [20, 41, 42].

We consider a finite size normal metal N, of length L connected to a semi-infinite superconducting terminal S by a transparent interface. We assume that electronic motion is diffusive in both the normal and superconducting parts. We restrict our discussion to a quasi one-dimensional geometry/wire or to a thin film and neglect any dependence on transversal coordinates. The origin of the coordinate x is fixed at the SN interface. In the absence of any magnetic anisotropy (exchange field \mathbf{h}), only the scalar (1.67) component of the Green function is present. Introducing the angular parametrization [35] to satisfy the normalization condition (1.66) $g^R = \cos \theta$, $f^R = \sin \theta$ for the normal, respectively the anomalous component of the retarded Green function, the Usadel equation in the N-region, where the pairing interaction vanishes, becomes

$$\frac{D\partial_x^2\theta}{2} + i\epsilon \sin \theta - 2\Gamma_{\text{sf}} \cos \theta \sin \theta = 0. \quad (1.74)$$

The proximity angle θ is a function of the energy ϵ and the position x . The spin-flip scattering rate is given by $\Gamma_{\text{sf}} = \frac{1}{2\tau_{\text{sf}}}$ with τ_{sf} as introduced in (A.7). The electron DoS

(1.69), in units of the normal state bulk value $\nu_0 = \frac{mp_f}{2\pi^2}$, is given in terms of the proximity angle by

$$\frac{\nu(\epsilon, x)}{\nu_0} = \text{Re}[\cos \theta(\epsilon, x)]. \quad (1.75)$$

The boundary conditions for the quasiclassical equations were introduced in Sec. 1.4.6. At the interface with vacuum, the conservation of the quasiparticle current (1.70) yields

$$\partial_x \theta(x = L) = 0. \quad (1.76)$$

We will study these equations analytically using simplified boundary conditions at the SN interface, where we impose the superconducting bulk value at zero energy of the proximity angle

$$\theta(x = 0) = \frac{\pi}{2}. \quad (1.77)$$

This boundary condition is justified for energies much smaller than the superconducting order parameter Δ and if the normal part is much more disordered than the superconducting part (see the discussion of Sec. 1.4.6).

Since the scale of the superconducting order parameter Δ does not appear in the rigid boundary condition (1.77), we will write in the following the energies and the length in units of the only other relevant scale for our system: the Thouless energy E_{Th} , respectively the width of the N-region L .

The boundary conditions (1.76), (1.77) and the calculations presented here for the SN junction can also be applied to describe SNS junctions with no phase difference between the superconducting terminals [43]. It is important to pay attention to the choice of the energy scale E_{Th} . A SNS junction of length unity is equivalent to a SN junction of length $\frac{1}{2}$. Therefore all the energies must be multiplied by a factor four if we consider SNS junctions.

To study the presence of solutions where the electronic DoS (1.75) vanishes we introduce a new notation for the proximity angle θ below the minigap and write $\theta = \frac{\pi}{2} + i\beta$ with β real. The minigap E_g is, by definition, the maximal energy compatible with a real β and can be obtained [43, 44] using a first integral of (1.74)

$$\partial_x \beta = 2\sqrt{f(\beta^1) - f(\beta)}, \quad (1.78)$$

where the superscript 1 denotes the value at $x = 1$ and $f(\beta) = \epsilon \sinh \beta + \Gamma_{\text{sf}} \sinh^2 \beta$. Integrating equation (1.78) over the junction, we get

$$\int_0^{\beta^1} \frac{d\beta}{2\sqrt{f(\beta^1) - f(\beta)}} = 1. \quad (1.79)$$

Without spin-flip, we recover with this relation the well-known value [43] of the minigap $E_g^0 \approx 0.78$. The critical value of the spin-flip at which the minigap in the DoS closes is (see the discussion in Appendix B)

$$\Gamma_{\text{sf}}^c = \frac{\pi^2}{16} \approx 0.62. \quad (1.80)$$

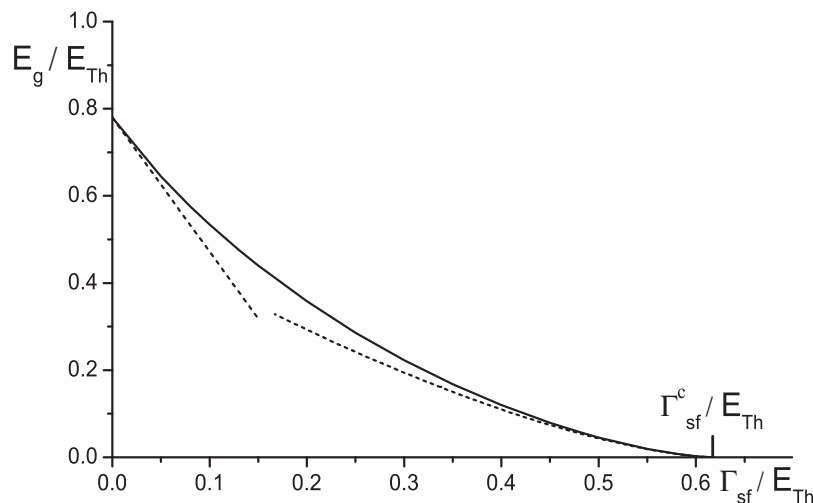


Figure 1.5: Numerical gap curve (solid line): comparison with asymptotic expressions (dashed lines).

For energies $\epsilon < E_g^0$ and $\Gamma_{\text{sf}} = 0$ equation (1.79) is solved for two different values of β^1 . One of these solutions leads to a diverging β^1 when the energy goes to zero and we reject it using a continuity argument. This continuity argument is commonly accepted in the quasiclassical approximation, but the diverging branch may play an important role in the discussion of the presence of a non-zero subgap DoS resulting from mesoscopic fluctuations [45]. Considering a finite spin-flip scattering rate Γ_{sf} , we find that the second branch of the solution no longer diverges at zero energy. If we increase the spin-flip rate up to a critical value the two zero energy solutions merge at Γ_{sf}^c . The critical value can therefore be determined taking the limit $\beta^1 \rightarrow 0$ of the integral in the l.h.s. of equation (1.79) at zero energy.

The complete dependence of the minigap on the spin-flip rate (Fig. 1.5) can be obtained by a simple numerical integration of equation (1.79). But it is possible to derive the asymptotic form of the gap curve for $\Gamma_{\text{sf}} \rightarrow 0$ and for $\Gamma_{\text{sf}} \rightarrow \Gamma_{\text{sf}}^c$.

In the limit of a small spin-flip rate, we can expand the integrand in (1.79) in the small parameter $\frac{\Gamma_{\text{sf}}}{\epsilon}$. Denoting $\hat{\beta}^1 \approx 1.421$ the value of the proximity angle corresponding to the zero spin-flip value of the minigap E_g^0 , we find the resulting correction

$$E_g \approx (E_g^0 - C_1 \Gamma_{\text{sf}}), \quad (1.81)$$

where the coefficient C_1 is given by

$$C_1 = \frac{\int_0^{\hat{\beta}^1} \frac{(\sinh \hat{\beta}^1 + \sinh \beta)}{(\sinh \hat{\beta}^1 - \sinh \beta)^{1/2}} d\beta}{\int_0^{\hat{\beta}^1} \frac{d\beta}{(\sinh \hat{\beta}^1 - \sinh \beta)^{1/2}}} \approx 3.09. \quad (1.82)$$

The minigap decreases linearly with increasing spin-flip scattering rate. From the magnitude of C_1 , we can see that even a small spin-flip rate strongly affects E_g .

To obtain the analytic behavior close to Γ_{sf}^c is more tricky as all $\delta\Gamma_{\text{sf}} = \Gamma_{\text{sf}}^c - \Gamma_{\text{sf}}$, β and $\frac{\epsilon}{\Gamma_{\text{sf}}}$ are small. Following the procedure detailed in Appendix B we obtain the asymptotic dependence of the minigap near the closing point

$$E_g \approx 2 \left[\frac{2\delta\Gamma_{\text{sf}}}{3} \right]^{3/2}. \quad (1.83)$$

In Fig. 1.5, we compare the asymptotics (1.81) and (1.83) with the numerical gap curve. Dimensions are reintroduced in the graphs for clarity.

For $\Gamma_{\text{sf}} > \Gamma_{\text{sf}}^c$ the DoS in the N-region is finite at any energy. In Appendix C we study the zero-energy density of states above the spin-flip scattering rate using the exact zero-energy solution of the Usadel equation (1.74).

To summarize, we have shown how the opening of an energy gap in a long diffusive SN junction with transparent interface can be explained within the quasiclassical theory. As a first illustration to magnetic effects in proximity structures, we have calculated the critical value of the spin-flip scattering rate at which the minigap closes and given the dependence of the minigap on the spin-flip rate. The relevant energy scale for the minigap and the critical spin-flip rate is the Thouless energy, and not the superconducting gap.

1.5.3 Josephson effect

We discuss here the basic features of the Josephson effect and the consequences of the modulation of the order parameter in the ferromagnetic region of a diffusive SFS Josephson junction. We have seen in the previous section that it is necessary to solve the full nonlinear Usadel equations to study the minigap. The study of the Josephson effect can however be performed solving equations linearized around the normal-state solution. The main features, or at least the main features accessible experimentally, of the Josephson current are indeed captured studying weakly coupled superconductors [46, 47]. The limit of weak superconducting correlations corresponds to temperatures close to T_c or to poor electric contact between the electrodes.

The Josephson current flowing between two superconductors is a 2π -periodic function of the phase difference φ between the two S electrodes. It can in general be decomposed into a Fourier series

$$I_J = \sum_{n=1}^{\infty} I_c^{(n)} \sin(n\varphi) + I_c^{(n)} \cos(n\varphi). \quad (1.84)$$

In the case of weak coupling and when both superconductors have the same symmetry,

only the first harmonic is present [7] and we can write the current phase relation in the form

$$I_J = I_c \sin(\varphi + \varphi_0). \quad (1.85)$$

As long as time reversal symmetry is not broken we have $I_c^{(n)} = 0$ to ensure that reversal of the phase difference is equivalent to changing the direction of the current $I_J(-\varphi) = -I_J(\varphi)$ and therefore the dephasing φ_0 in (1.85) is zero.

The free energy of the junction is given by the integral

$$E_J = \frac{\hbar}{2e} \int_0^\varphi J(\chi) d\chi + \text{const.} \quad (1.86)$$

For a sinusoidal current phase relation, this result in

$$E_J = -\frac{\hbar I_c}{2e} \cos(\varphi + \varphi_0) + \text{const.} \quad (1.87)$$

In SNS junctions, the critical current I_c is positive and since time reversal symmetry is preserved we have $\varphi_0 = 0$. This leads to a minimal energy for a phase difference $\varphi = 0$ and a current equals to zero at thermodynamic equilibrium. In the presence of a ferromagnetic exchange field (SFS junction) we can observe a different equilibrium phase difference. In Sec. 1.5.1 we have seen that, in addition to the expected destruction of pairs by the exchange field, we can observe a modulation of the order parameter due to the mechanism described on Fig. 1.4. We will see in the next chapter that in SFS junctions this modulation of the pair amplitude will lead to the possibility of having a dephasing $\varphi_0 = \pm\pi$ in the current phase relation [1, 3] which is equivalent to a negative I_c in (1.85) and (1.87). For negative critical currents, the minimal energy will be for $\varphi = \pi$ (“ π junction”) which will result in the presence of spontaneous non-dissipative currents at equilibrium through a SFS junction with annular geometry, even if for a phase difference of π one gets a zero Josephson current from (1.85). These spontaneous currents result from the gradient of phase in the superconducting part of the ring necessary to ensure a difference of phase of π between the contacts with the F region.

The fact that the minimum of the energy (1.87) is degenerate for a π junction corresponds to two possible directions for the spontaneous current in a ring comprising such a junction. The existence of the double-degenerate ground state makes devices based on π junctions candidates for flux qubits. The two states would constitute the computational basis while the readout and the manipulation of the qubit is achieved by applying an external magnetic flux through the ring. An important difficulty in the implementation of the qubits resides in minimizing the decoherence originating from the interaction with the environment [12].

In the case of low temperatures and good electric contact, the higher harmonics in the current-phase relation (1.84) cannot be neglected anymore. In this situation, an arbitrary

equilibrium phase can in principle be obtained, depending on the sign and relative weight of the harmonics. Such junctions are usually denoted φ junctions in the literature, for a review see Ref. [48]. Although several theoretical works have studied the possibility of realizing such junctions, clear experimental observation has not been yet achieved.

Chapter 2

SFS junction with two noncollinear ferromagnetic domains

2.1 Introduction: π junctions

The interest in proximity structures made of superconducting and ferromagnetic layers (denoted in the following respectively S and F) in contact with each other has been recently renewed due to their potential applications to spintronics [10] and to quantum computing [11, 12]. The interplay between superconductivity (which tends to organize the electron gas in Cooper pairs with opposite spins) and ferromagnetism (which tends to align spins and thus to destroy the Cooper pairs) leads to a variety of surprising physical effects (for a review, see Sec. 1.5 and Ref. [1]). We study in this chapter the influence of magnetic domains on the appearance of the π phase.

We have seen in Sec. 1.5.1 that as a consequence of the exchange splitting of the Fermi level [2], the Cooper pair wave function exhibits damped oscillations in a ferromagnet. We show in the following how one can explain the appearance of the so-called “ π state” in diffusive SFS Josephson junctions [3] within the framework of the quasiclassical theory. In the π state, the superconducting order parameter is of opposite sign in the two S electrodes of the junction, and thus a macroscopic superconducting phase difference of π appears in the thermodynamic equilibrium. This phase difference should lead to spontaneous non-dissipative currents in a Josephson junction with annular geometry [49, 50]. As shown in Sec. 1.5.3, a possible signature for the appearance of the π state is a cancellation of the Josephson critical current (1.85) followed by a reversal of its sign as a function of the junction length or the temperature [1]. A negative critical current will give a minimal Josephson energy (1.87) for a phase difference of π between the superconducting electrodes. The recent observations of critical-current oscillations in experiments [51–54] have demonstrated such 0 – π transitions as a function of the ferromagnet thickness and temperature.

As explained in the previous chapter, the appropriate formalism to deal with mesoscopic S/F junctions has been derived by Eilenberger [23]. The equations of motion for the quasiclassical Green function (averaged over the fast Fermi oscillations) can be further simplified in the diffusive regime, i.e., when the motion of the electrons is governed by frequent scattering on impurity atoms: the Green functions can then be averaged over the momentum directions. This averaging is justified as long as the elastic mean free path l_e is much smaller than the relevant length scales of the system, namely the size of the layers, the superconducting coherence length, given in the diffusive limit by $\xi_S = \sqrt{D/2\pi T_c}$, and the length characterizing the Cooper pair wave function decay in the ferromagnet $\xi_h = \sqrt{D/h}$. Here and in the following, D denotes the diffusion constant, T_c the superconducting critical temperature, h the magnitude of the exchange field, and the system of units with $\hbar = k_B = \mu_B = 1$ is chosen. The diffusive limit is reached in most of the experimental realizations of SF heterostructures. In this limit, the Green functions can be combined in a 4×4 matrix in the Nambu \otimes spin space, and this matrix obeys the Usadel equation (1.62). SFS Josephson junctions with homogeneous magnetization have been studied in detail within this framework [1].

We shall not derive at this point in details how the appearance of the π coupling in SFS junctions can be explained within the quasiclassical formalism. We refer for this the reader to Sec. 2.3.1 where the critical current for a SFS junction with a homogeneous ferromagnet is computed. The critical current I_c shows a damped oscillatory dependence on the F-layer thickness (this was first pointed out in Refs. [55] and [56]). Close to T_c or in case of poor electric contact between the S and F electrodes we can linearize the Usadel equations in the deviation from the normal state solution. For linearized equations and rigid boundary conditions (see the discussion in Sec. 1.4.6), we get as a result a sinusoidal current-phase relation

$$I_J = I_c \sin \varphi, \quad (2.1)$$

where φ is the superconducting phase difference across the junction and the critical current is given by

$$I_c = e\nu_0 DS\pi T \sum_{\omega, \sigma=\pm} \frac{\Delta^2}{\omega^2} \left[\frac{\lambda_\sigma}{\sinh(\lambda_\sigma d_F)} \right] \quad (2.2)$$

with

$$\lambda_\pm = \left[2 \frac{|\omega| \mp i h \operatorname{sgn}(\omega)}{D} \right]^{1/2} \quad (2.3)$$

d_F is the thickness of the F layer and S the section of the layer. From (2.2) we see that the critical current can change its sign when either the temperature, recall that the Matsubara frequencies are given by $\omega = (2n + 1)\pi T$, or d_F are varied. The observation of temperature induced $0 - \pi$ transitions [52] has constituted the first experimental evidence for the existence of the π phase. Later works have also studied oscillations induced by a variation of the F-layer thickness, see for example [54] and Fig. 2.1. The combined observation of temperature and thickness induced transitions allows to improve the fitting

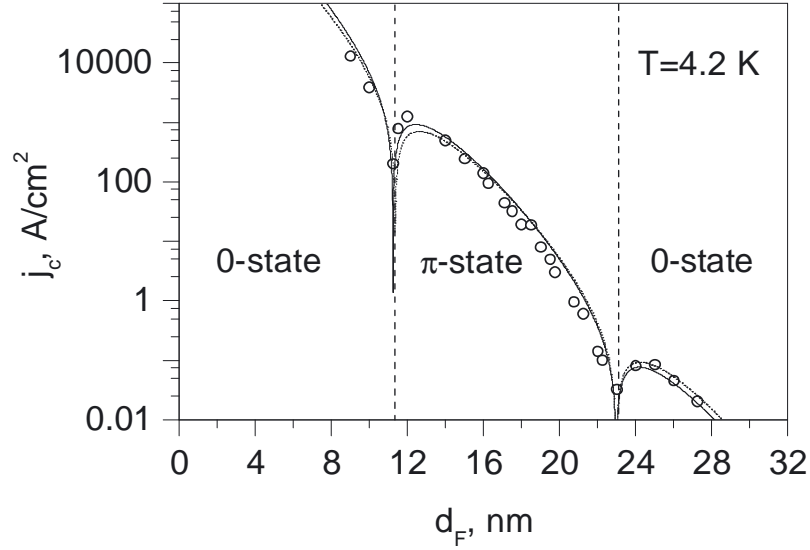


Figure 2.1: Oscillations of the critical current density j_c as a function of the ferromagnetic layer thickness d_F in a $Nb - Cu_{0.47}Ni_{0.53} - Nb$ SFS junction. The two lines represent theoretical fits based on the Usadel equation made with and without taking the high field limit. Adapted from [54].

of the experimental data with the theoretical model. However, due to the large number of adjustable parameters in the model there remain different possible ways of understanding the data at hand. The exchange field itself is determined from the fit based on the Usadel equations. The strength and the type of spin-flip scattering also plays an important role. Uniaxial spin-flip scattering is usually considered in SF structures due to the presence of the strong magnetic anisotropy resulting from the ferromagnetic exchange field but little is known about its precise origin. In [57], for example, experimental data is fitted equally well using different types (uniaxial and isotropic) of spin-flip scattering on top of the uniform exchange field. Other relevant parameters include the transparency of the interfaces and the elastic mean free path l_e which is related to the diffusion constant D .

In the high field limit $h \gg T_c$, we have $\lambda_{\pm} \approx \frac{1 \mp i}{\sqrt{D/h}}$ and we can perform the summation over Matsubara frequencies in (2.2) analytically. In this limit, the critical current will show a damped oscillatory dependence on d_F with same oscillation and decay length given by $\xi_h = \sqrt{D/h}$. The problem is that for strong ferromagnets this length is very short resulting in a very fast decay of the current. The early experimental works on π junctions have made use of diluted ferromagnetic alloys to get measurable currents. Even for the diluted ferromagnet $Nb - Cu_{0.47}Ni_{0.53} - Nb$ used in [54], the exchange field has been estimated to be of the order of 850K and the ratio $h/T_c \approx 100$. For pure Nickel, its value is about four times larger [58, 59] resulting in very short decay and oscillation lengths (of the order of one nanometer).

Understanding the effect of a nonhomogeneous magnetization is of crucial interest for obtaining a good quantitative description for the critical-current oscillations in SFS junctions. Indeed, it is known that real ferromagnetic compounds usually have a complex domain structure. Strong ferromagnets (such as Ni or Fe) consist of domains with homogeneous magnetization pointing in different directions whereas the magnetic structure of the weak ferromagnets (Cu-Ni and Pd-Ni alloys) used in the experiments reported in Refs. [51–54, 60] is still unresolved. Theoretical fits of the data yield the addition of considerable spin-flip scattering rates to the model and the presence of a substantial magnetically dead layer at the SF interfaces. In [54] the data is fitted with a spin-flip scattering rate larger than the exchange field $1/\tau_{\text{sf}} \approx 1.33 h$. It is conjectured that the strong spin-flip scattering could originate from the presence of clusters in the alloy where the concentration of Nickel is higher. Recently Veshchunov *et al.* [61] have shown that thin films made of $Nb - Cu_{0.47}Ni_{0.53} - Nb$ (the weak ferromagnet used in [54]) contains magnetic domains with a size of the order of 100 nm. However, the resolution of the experiment does not allow to exclude the existence of smaller inhomogeneities: the decoration method applied in [61] was realized with particles of ten nanometers average size. Furthermore, incorporating the film in a SFS junction may reduce the size of ferromagnetic domains as suggested in [62].

In a recent work by Bannykh *et al.* [58] on $0-\pi$ oscillations in SFS junctions with a strong ferromagnetic interlayer (pure Nickel), it has been suggested that the magnetic structure of the ferromagnet may strongly depend on the size of the layer. Junctions thinner than the dead layer thickness $d_F < d_{\text{dead}} \approx 2 \text{ nm}$ are believed not to show any magnetic ordering. In this region the decay of the critical current as a function of d_F is slow (decay length given by the thermal length $\xi_T = \sqrt{D/2\pi T}$). For $d_{\text{dead}} < d_F < d_c$ the faster decay of the critical current and the observation of a 0 to π transition is connected to the appearance of the ferromagnetic exchange field. When the junction becomes thicker than $d_c \approx 3.5 \text{ nm}$ a net magnetization appears in the F layer. The presence of this net magnetization leads to shifted Fraunhofer patterns in the dependence of I_c on the flux of an external magnetic field through the junction. It is therefore believed that for thin junctions the ferromagnetic layer contains random domains whose magnetizations average out while for larger junctions a magnetic anisotropy appears. For more details on magnetic interference patterns in Josephson junctions we refer to Chapter 4.

The problem of SFS junctions with inhomogeneous magnetization has been theoretically previously addressed for spiral magnetizations [63] and in the case of domains with antiparallel (AP) magnetizations [64, 65]. In the latter case, the critical-current oscillations (and thus the π state) are suppressed in the symmetric case where the F layer consists of two domains of the same size. This can be explained by a compensation between the phases acquired by the Andreev reflected electrons and holes, of opposite spins, in the two domains [64].

In the present chapter, we extend that analysis to the case of a SFF'S junction close to

T_c , with the two magnetic domains F and F' of arbitrary length and relative orientation of the magnetizations. To emphasize the effect of the misorientation angle between the magnetizations of the two domains, we choose to minimize the number of parameters in the model. The interfaces are then chosen to be perfectly transparent, and spin-flip scattering is neglected in both S and F layers. Furthermore, we assume that the diffusive limit is fully reached, that is we do not take into account corrections due to a finite mean free path (note that for strong ferromagnets the magnetic coherence length ξ_h may become comparable to l_e).

The main result of our calculation is that, in the symmetric case where the two domains have equal thicknesses, we obtain a progressive reduction of the π -state region of the phase diagram as the misorientation angle increases. Surprisingly, the π state completely disappears as soon as the misorientation angle θ exceeds $\frac{\pi}{2}$.

The chapter is organized as follows. In Sec. 2.2 we solve the linearized Usadel equations and give the general expression for the Josephson current. In Sec. 2.3 we discuss the simplest cases of parallel and antiparallel relative orientation of magnetizations with different domain sizes d_1 and d_2 . We obtain analytically the full phase diagram in d_1 - d_2 coordinates. In agreement with Ref. [64], the π state is absent in the symmetric case $d_1 = d_2$ for domains with antiparallel magnetizations. In the asymmetric case, the critical current oscillates as d_2 is varied while keeping d_1 constant. For sufficiently thick layers ($d_{1,2} \gg \xi_h$), the critical-current oscillations behave like in a single domain of thickness $|d_1 - d_2| + (\pi/4)\xi_h$. In Sec. 2.4, we discuss the case of an arbitrary misorientation angle in the symmetric configuration $d_1 = d_2 = d$. In the limit when the exchange field is much larger than T_c , we derive analytically the 0 - π phase diagram of the junction depending on the junction length d and on the misorientation angle θ . We show that the π state disappears completely for $\theta > \frac{\pi}{2}$. In the last Sec. 2.5, we discuss possible implications of our findings for experimentally observed 0 - π transitions in SFS junctions.

2.2 Model

We study a diffusive SFF'S Josephson junction with semi-infinite (that is, of thickness much larger than ξ_S) superconducting electrodes, as shown in Fig. 2.2. The phase difference between the S layers is denoted $\varphi = 2\chi$, the thicknesses of the two ferromagnetic domains d_1 and d_2 . In the following we consider a quasi-one-dimensional geometry where the physical quantities do not depend on the in-plane coordinates. For simplicity, we assume that the SF and FF' interfaces are transparent. We further assume that the temperature is close to T_c so that $\Delta \ll T$, and this allows us to linearize the Usadel equations.

In the case of superconductor-ferromagnet systems, the proximity effect involves both the singlet and the triplet components of the Green's functions (1.67). The Usadel equation

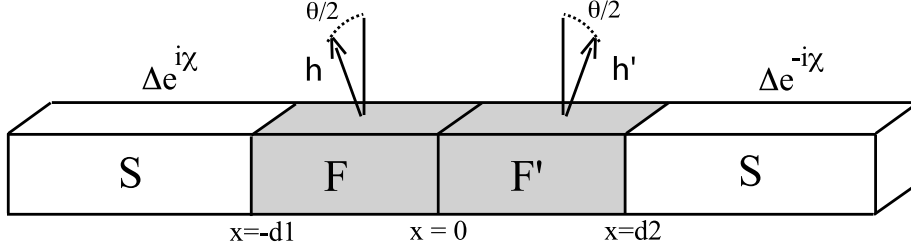


Figure 2.2: SFF'-S junction with noncollinear magnetization.

(1.62) in the ferromagnetic layers takes the form (we follow here and in the next chapters the conventions used in Ref. [20])

$$D\nabla(\check{g}\nabla\check{g}) - \omega[\hat{\tau}_3\hat{\sigma}_0, \check{g}] - i[\hat{\tau}_3(\mathbf{h} \cdot \hat{\boldsymbol{\sigma}}), \check{g}] = 0. \quad (2.4)$$

The Green function \check{g} is a matrix in the Nambu \otimes spin space, $\hat{\tau}_\alpha$ and $\hat{\sigma}_\alpha$ denote the Pauli matrices respectively in Nambu (particle-hole) and spin space, $\omega = (2n + 1)\pi T$ are the Matsubara frequencies, and \mathbf{h} is the exchange field in the ferromagnet. The Usadel equation is supplemented with the normalization condition for the quasiclassical Green function

$$\check{g}^2 = \check{\mathbf{1}} = \hat{\tau}_0\hat{\sigma}_0. \quad (2.5)$$

For simplicity, we assume that the superconductors are much less disordered than the ferromagnets, and then we can impose, as discussed in Sec. 1.4.6, the rigid boundary conditions at the S/F interfaces

$$\check{g} = \frac{1}{\sqrt{\omega^2 + \Delta^2}} \begin{pmatrix} \omega & \Delta e^{\pm i\chi} \\ -\Delta e^{\mp i\chi} & -\omega \end{pmatrix}_{\text{Nambu}} \otimes \hat{\sigma}_0, \quad (2.6)$$

where Δ denotes the superconducting order parameter and the different signs refer respectively to the boundary conditions at $x = -d_1$ and $x = d_2$.

Close to the critical temperature T_c , the superconducting correlations in the F region are weak [1], and we can linearize the Usadel equations (2.4) and (2.5) around the normal solution $\check{g} = \hat{\tau}_3\hat{\sigma}_0\text{sgn}(\omega)$. The Green function then takes the form

$$\check{g} = \begin{pmatrix} \sigma_0\text{sgn}(\omega) & f_\alpha\sigma^\alpha \\ -f_\alpha^\dagger\sigma^\alpha & -\sigma_0\text{sgn}(\omega) \end{pmatrix}, \quad (2.7)$$

where the scalar f_0 (respectively f_0^\dagger) and vector \mathbf{f} (respectively \mathbf{f}^\dagger) components of the anomalous Green functions obey the linear equations

$$\begin{aligned} \frac{\partial^2 f_\pm^{(\dagger)}}{\partial x^2} - [\lambda_\pm]^2 f_\pm^{(\dagger)} &= 0 \\ \frac{\partial^2 f_\perp^{(\dagger)}}{\partial x^2} - [\lambda_\perp]^2 f_\perp^{(\dagger)} &= 0 \end{aligned} \quad (2.8)$$

with

$$\lambda_{\pm} = \left[2 \frac{|\omega| \mp ih \operatorname{sgn}(\omega)}{D} \right]^{1/2}, \quad \lambda_{\perp} = \left[2 \frac{|\omega|}{D} \right]^{1/2}. \quad (2.9)$$

The projections of the anomalous Green function on the direction of the exchange field (“parallel” components) are defined as $f_{\pm}^{(\dagger)}(x) = f_0^{(\dagger)} \pm \mathbf{f}^{(\dagger)} \cdot \mathbf{e}_h$ where \mathbf{e}_h is the unit vector in the direction of the field. The “perpendicular” component $f_{\perp}^{(\dagger)}$ refers to the axis orthogonal to the exchange field. Generally, this component is a two-dimensional vector. In our system, however, \mathbf{f} lies in the plane spanned by the magnetizations in the two domains, and therefore $f_{\perp}^{(\dagger)}$ has only one component.

It follows from Eqs. (2.8) that the decay of the “parallel” and the “perpendicular” components is governed by two very different length scales. The parallel component decays on the length scale ξ_h , while the perpendicular component is insensitive to the exchange field and decays on the typically much larger scale $\xi_S = \xi_h \sqrt{\frac{h}{2\pi T_c}}$ (experimentally, h may be more than 100 times larger than T_c , see, e.g., Ref. [54]).

In the absence of the exchange field, f_{σ} and f_{σ}^{\dagger} components are related by complex conjugation. The exchange field h breaks this symmetry, and the relation between f_{σ} and f_{σ}^{\dagger} becomes

$$f_{\sigma}^{\dagger}(\chi) = f_{\sigma}(-\chi). \quad (2.10)$$

The solutions to the equations (2.8) in each of the ferromagnetic layers are given by

$$f_{\pm, \perp}^j(x) = A_{\pm, \perp}^j \sinh \lambda_{\pm, \perp} x + B_{\pm, \perp}^j \cosh \lambda_{\pm, \perp} x, \quad (2.11)$$

where the 12 coefficients $A_{\pm, \perp}^j$ and $B_{\pm, \perp}^j$ ($j = 1, 2$ denotes the layer index) must be determined using the boundary conditions at each interface. Note that it is enough to solve the equations for the functions f_{σ}^j : the functions $f_{\sigma}^{j\dagger}$ can be then obtained from the symmetry relation (2.10).

As we assume transparent S/F interfaces and rigid boundary conditions, we impose (linearizing (2.6))

$$\begin{aligned} f_{\pm}^1(x = -d_1) &= \frac{\Delta}{\omega} e^{i\chi}, \\ f_{\pm}^2(x = d_2) &= \frac{\Delta}{\omega} e^{-i\chi}, \\ f_{\perp}^1(x = -d_1) &= f_{\perp}^2(x = d_2) = 0. \end{aligned} \quad (2.12)$$

At the (perfectly transparent) FF' interface, the standard Kupriyanov-Lukichev boundary conditions (1.70) and (1.71) provide the continuity relations

$$\begin{aligned} f_{\alpha}^1(x = 0) &= f_{\alpha}^2(x = 0) \\ \frac{\partial f_{\alpha}^1}{\partial x} \Big|_{x=0} &= \frac{\partial f_{\alpha}^2}{\partial x} \Big|_{x=0} \end{aligned} \quad (2.13)$$

(here α takes values from 0 to 3 and refers to a fixed coordinate system). Note that, in the general case, since the ferromagnetic exchange fields do not have the same orientation in the two F-layers, the latter conditions do not lead to the continuity of the reduced functions $f_{\pm,\perp}^j$ and their derivative, except in the parallel case.

The last step will be to compute the Josephson current density using the formula (1.68)

$$I_J = ie\nu_0 DS\pi T \sum_{\omega=-\infty}^{\infty} \frac{1}{2} \text{Tr} (\hat{\tau}_3 \hat{\sigma}_0 \check{g} \partial_x \check{g}), \quad (2.14)$$

where S is the cross section of the junction, ν_0 is the density of states in the normal metal phase (per one spin direction), and the trace has to be taken over Nambu and spin indices. The current can be explicitly rewritten for the linearized \check{g}

$$I_J = -ie\nu_0 DS\pi T \sum_{\omega=-\infty}^{\infty} \sum_{\sigma=\pm} \frac{1}{2} (f_{\sigma} \partial_x f_{\sigma}^{\dagger} - f_{\sigma}^{\dagger} \partial_x f_{\sigma}) + f_{\perp} \partial_x f_{\perp}^{\dagger} - f_{\perp}^{\dagger} \partial_x f_{\perp}. \quad (2.15)$$

Using the coefficients introduced in equations (2.11), the Josephson current (2.15) reads

$$I_J = ie\nu_0 DS\pi T \sum_{\omega,\sigma=\pm} \frac{\lambda_{\sigma}}{2} [A_{\sigma}(\chi)B_{\sigma}(-\chi) - B_{\sigma}(\chi)A_{\sigma}(-\chi)] \\ + \lambda_{\perp} [A_{\perp}(\chi)B_{\perp}(-\chi) - B_{\perp}(\chi)A_{\perp}(-\chi)]. \quad (2.16)$$

Since the coefficients A_{σ}^j and B_{σ}^j are solutions to the linear system of equations (2.12) and (2.13), they are linear combinations of $e^{i\chi}$ and $e^{-i\chi}$. The expression (2.16) is explicitly antisymmetric with respect to $\chi \mapsto -\chi$, it therefore always produces the sinusoidal current-phase relation (2.1). Finally, the expression (2.16) does not contain the domain index j : it can be calculated in any of the two domains, and the results must coincide due to the conservation of the supercurrent in the Usadel equations.

In the following sections, this formalism is used to study the influence of a magnetic domain structure on the Josephson current.

2.3 Domains of different thicknesses in the P and AP configurations

2.3.1 Parallel case (P)

In the most trivial case $\theta = 0$, the equations can be solved easily with $A_{\perp}^j = B_{\perp}^j = 0$. We naturally retrieve the expression reported in Ref. [1] for a single-domain SFS trilayer (of thickness $d_1 + d_2$),

$$I_c^P = e\nu_0 DS\pi T \sum_{\omega,\sigma=\pm} \frac{\Delta^2}{\omega^2} \left[\frac{\lambda_{\sigma}}{\sinh \lambda_{\sigma}(d_1 + d_2)} \right]. \quad (2.17)$$

The exact summation over the Matsubara frequencies ω can be done numerically. However, in many experimental situations, the exchange field is much larger than T_c . In this limit, we can assume $h \gg \omega$ which implies $\lambda_{\pm} = \frac{1 \mp i}{\xi_h}$. The summation over Matsubara frequencies reduces then to

$$\sum_{\omega} \frac{1}{\omega^2} = \frac{1}{4T^2} \quad (2.18)$$

and the critical current is given by the simple expression

$$I_c^P = I_0 \text{Re} \left[\frac{1+i}{\sinh \left[(1+i) \left(\frac{d_1+d_2}{\xi_h} \right) \right]} \right] \quad (2.19)$$

with

$$I_0 = \frac{e\nu_0 DS \pi \Delta^2}{2\xi_h T}. \quad (2.20)$$

From Eq. (2.19) it is clear that the critical current oscillates as a function of the junction length, with a pseudo-period of the order of ξ_h . When the critical current becomes negative, the SFS hybrid structure is in the π state.

The high field limit expression is often sufficient to describe experimental data, as can be seen from the almost identical theoretical fits in Fig. 2.1 made with and without taking this limit.

2.3.2 Antiparallel case (AP)

In the antiparallel configuration $\theta = \pi$, the exchange field has the opposite direction in the two domains. In this case we again find $A_{\perp}^j = B_{\perp}^j = 0$, and the critical current can be easily derived,

$$I_c^{AP} = I_0 \xi_h T^2 \sum_{\omega, \sigma = \pm} \frac{1}{\omega^2} \left[\frac{2\lambda_{\sigma} \lambda_{-\sigma}}{\lambda_{\sigma} \sinh \lambda_{-\sigma} d_2 \cosh \lambda_{\sigma} d_1 + \lambda_{-\sigma} \cosh \lambda_{-\sigma} d_2 \sinh \lambda_{\sigma} d_1} \right]. \quad (2.21)$$

In the limit of the large exchange field $h \gg T_c$, the summation over the Matsubara frequencies (2.18) results in

$$I_c^{AP} = I_0 \text{Re} \left[\frac{2}{\sin(d_+ + id_-) + \sinh(d_+ - id_-)} \right] \quad (2.22)$$

with

$$d_+ = (d_1 + d_2)/\xi_h \quad (2.23)$$

$$d_- = (d_1 - d_2)/\xi_h. \quad (2.24)$$

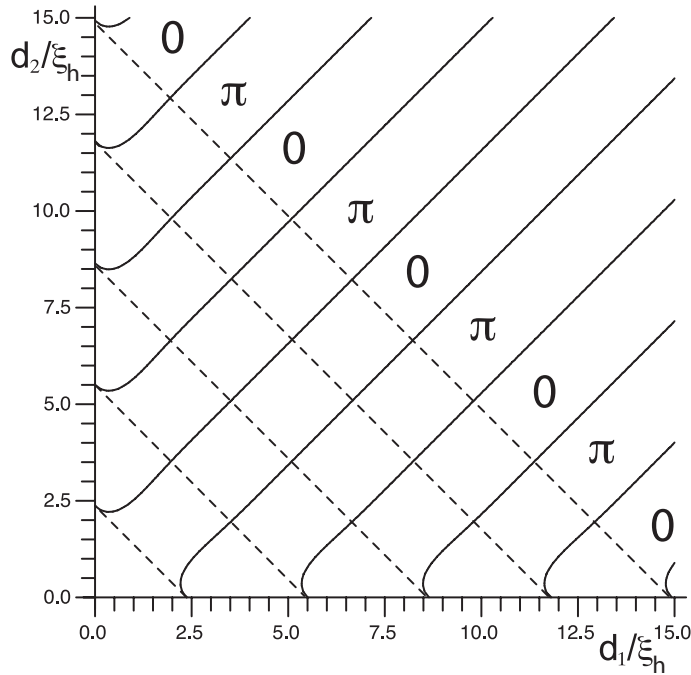


Figure 2.3: Quasiperiodic 0 to π transitions for antiparallel (solid lines) and parallel (dashed lines) magnetization. On the graph, the indications 0 and π refer to the antiparallel case. In the parallel case, the transitions occur along lines with $d_1 + d_2 = \text{const}$, starting from the zero state.

For plotting the 0- π phase diagram in d_1 - d_2 coordinates we use the condition of the vanishing critical current. From the equations (2.19) and (2.22), the critical current vanishes if

$$\sin d_+ \cosh d_+ + \sinh d_+ \cos d_+ = 0 \quad (2.25)$$

in the parallel case, and if

$$\sin d_+ \cosh d_- + \sinh d_+ \cos d_- = 0 \quad (2.26)$$

in the antiparallel case. The resulting phase diagram is plotted in Fig. 2.3.

For $d_1 = d_2 = d$ (symmetric case), we obtain that the critical current is positive for any d : identical F layers in the AP configuration cannot produce the π state (a similar conclusion was drawn in Ref. [64] for ballistic junctions and for diffusive junctions at low temperature). For $d_1 \neq d_2$, the SFF'S junction can be either in the usual 0 state or in the π state depending on the difference between d_1 and d_2 (see Fig. 2.3). For large d_1 and d_2 , the periodic dependence of the phase transitions on the layer thicknesses approximately corresponds to a single-layer SFS junction of the thickness $|d_1 - d_2| + (\pi/4)\xi_h$. This result is similar to the case of the clean SFF'S junction where the phase compensation arising from the two antiparallel domains is observed [64].

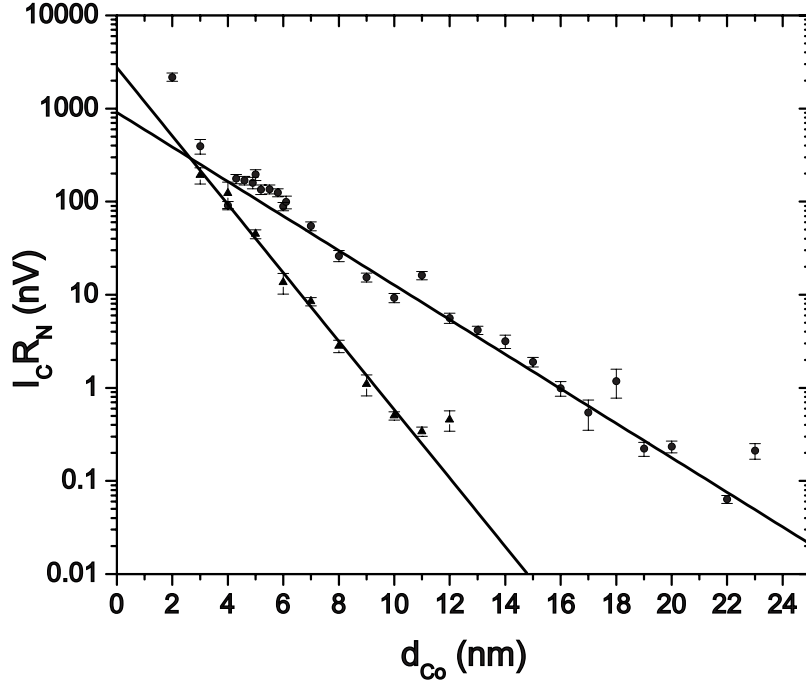


Figure 2.4: Critical current multiplied by the normal-state resistance as a function of the total thickness of the ferromagnetic layer for a Nb/Co/Ru/Co/Nb junction with antiparallel magnetization of the ferromagnetic Cobalt layers. For the upper set of points an additional Copper layer is added at the SF interfaces to achieve a larger $I_c R_N$ product. Adapted from [66].

Another interesting feature of the phase diagram in Fig. 2.3 is the “reentrant” behavior of the phase transition at a very small thickness of one of the layers. If the SFS junction is tuned to a $0-\pi$ transition point, and one adds a thin layer F' of antiparallel magnetization, then a small region of the “opposite” phase (corresponding to increasing the F thickness) appears, before the $F-F'$ compensation mechanism stabilizes the phase corresponding to reducing the F thickness.

Recently, SFF'S junctions (Nb/Co/Ru/Co/Nb) with antiparallel magnetization and identical dimensions of the F layers have been studied experimentally by Khasawneh *et al.* [66]. The antiparallel orientation of the magnetization in the ferromagnetic Cobalt layers results from an antiferromagnetic coupling mediated by the additional thin Ruthenium layer. As can be seen on Fig. 2.4, their data is consistent with a monotonic exponential decay of the critical current as a function of the thickness of the ferromagnetic layer.

In this section, we have seen that the π state disappears in the antiparallel orientation for geometrically identical F -layers. However, we do not observe an enhancement of the critical current (compared to the zero field current) in the AP configuration such as reported in Refs. [65, 67]. This is in agreement with the claim of Ref. [65] that this enhancement is

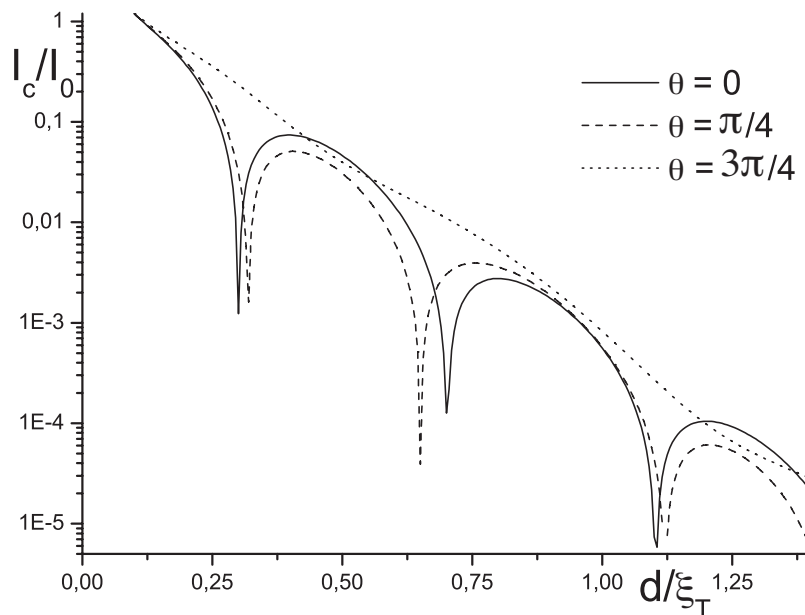


Figure 2.5: Critical current dependence on the size of the junction for $\theta = 0, \pi/4$ and $3\pi/4$. We take $h/T = 100$ which corresponds to a realistic value for a diluted ferromagnet, as reported in Ref. [54] and $\xi_T = \sqrt{D/2\pi T}$.

present only at low temperatures.

In the next section, we demonstrate that the suppression of the π state occurs continuously as we change the misorientation angle.

2.4 Arbitrary magnetization misorientation and equal thicknesses

In the previous section, we have plotted the phase diagram for arbitrary layer thicknesses d_1 and d_2 in the cases of parallel and antiparallel magnetization. In principle, one can extend this phase diagram to arbitrary misorientation angles θ . Such a calculation amounts to solving a set of linear equations (2.12) and (2.13) for the 12 parameters defined in Eq. (2.11). This calculation is straightforward, but cumbersome, and we consider only the simplest situation with equal layer thicknesses $d_1 = d_2 = d$.

For equal layer thicknesses, the 0 - π transitions are present at $\theta = 0$ and absent at $\theta = \pi$. We will see below that with increasing the misorientation angle θ the amplitude of the critical-current oscillations (as a function of d) decreases, and the π phase progressively shrinks. At a certain “critical” angle θ_c , the π phase disappears completely for any value of d . We find that the critical value is $\theta_c = \frac{\pi}{2}$, surprisingly independent of the strength of

the exchange field.

The details of the calculation of the critical current are presented in Appendix D. In the general case, the current can be written in the form of a Matsubara sum such as given in Eq. (D.2). In Fig. 2.5, we plot the current as a function of the domain thickness for different angles performing the summation over Matsubara frequencies numerically using realistic values for the temperature and the exchange field. We find that the domain structure reduces the π -state regions compared to the $\theta = 0$ parallel case as well as the amplitude of the current in this state. To the contrary, the 0-state regions are extended and the current amplitude is increased in this state. This result may be simply understood as a continuous interpolation between a sign-changing I_c in the single-domain case and an always-positive I_c in the antiparallel case.

Considering the high-exchange-field limit introduced in Sec. 2.3, namely $h \gg T_c$, and assuming further $d \ll \xi_S$ (which is a reasonable assumption for the first several $0-\pi$ transitions in the high-field limit), we have $\lambda_\perp \ll \lambda_\pm$ and $\lambda_\perp d \ll 1$ so that one can expand Eq. (D.2) in powers of λ_\perp . To the lowest order of expansion, the sum over Matsubara frequencies is done and we obtain

$$I_c(\theta) = \frac{8dI_0}{\xi_h} \frac{(Q_+ + P_+ \tan^2 \frac{\theta}{2})(P_+ + Q_+ \tan^2 \frac{\theta}{2}) - (1 - \tan^4 \frac{\theta}{2})P_- Q_-}{(P_+^2 - P_-^2 + \tan^2 \frac{\theta}{2}(P_+ Q_+ + P_- Q_-))} \times \frac{1}{(Q_+^2 - Q_-^2 + \tan^2 \frac{\theta}{2}(P_+ Q_+ + P_- Q_-))}, \quad (2.27)$$

where P_\pm and Q_\pm are simple functions of the ratio d/ξ_h ,

$$P_\pm = 2 \frac{d}{\xi_h} \left(\cosh(1+i) \frac{d}{\xi_h} \pm \cosh(1-i) \frac{d}{\xi_h} \right) \\ Q_\pm = (1+i) \sinh(1-i) \frac{d}{\xi_h} \pm (1-i) \sinh(1+i) \frac{d}{\xi_h}. \quad (2.28)$$

From the general formula (2.27), one can retrieve the expressions (2.19) and (2.22) for the Josephson current in the (symmetric $d_1 = d_2$) parallel and antiparallel cases by setting respectively $\theta = 0$ and $\theta = \pi$. Within the approximation of a high exchange field, the critical current (2.27) is a ratio of second degree polynomials in the variable $\tan^2 \frac{\theta}{2}$. The critical current cancels if

$$\tan^4 \frac{\theta}{2} (P_+ Q_+ + P_- Q_-) + \tan^2 \frac{\theta}{2} (P_+^2 + Q_+^2) + (P_+ Q_+ - P_- Q_-) = 0. \quad (2.29)$$

This equation allows one to compute the full SFF'S phase diagram in the $d-\theta$ coordinates (Fig. 2.6). We observe that Eq. (2.29) cannot be satisfied for any thickness as soon as θ exceeds $\frac{\pi}{2}$. As the misorientation angle θ decreases below $\frac{\pi}{2}$, the region of the π state in the phase diagram Fig. 2.6 increases, and it becomes maximal at $\theta = 0$ (i.e., in the parallel configuration).

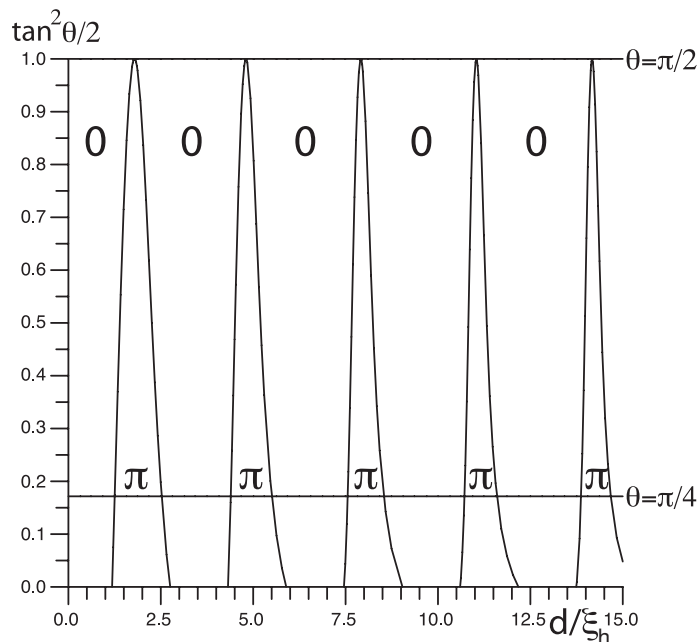


Figure 2.6: d - θ phase diagram in the limit of a large exchange field. The dependence on d is almost (but not exactly) periodic.

Away from the high-exchange-field limit, we can find the value of θ_c numerically using the exact formula, Eq. (D.2). Remarkably, our calculations show that the critical value $\theta_c = \frac{\pi}{2}$ remains independent of the strength of the field h .

2.5 Discussion and experimental aspects

The main conclusion of the present work is that a domain structure in the SFS junction reduces the region in the phase space occupied by the π state. We have demonstrated this reduction with the example of the two domains placed along the junction. However we expect that this qualitative conclusion survives for more general configurations of domains. In view of this reasoning, we suggest that a domain structure in the junction can contribute to the shift in the 0 - π transition sequence reported in Ref. [54] and attributed to a “dead layer” in the ferromagnet. If such a domain structure slightly reduces the region of the π phase in favor of the zero phase, this would shift the positions of the two first 0 - π - 0 transitions in a manner similar to the effect of a “dead layer” (see, e.g., our $\theta = \pi/4$ plot in Fig. 2.5). To distinguish between the two scenarios, one would need to observe at least three consecutive 0 - π transitions and/or develop a more realistic theory of the effect of domains in SFS junctions. In addition, no quantitative theory can presently describe the appearance of the “dead layer” at the SF interfaces.

Many of our results are based on the high-exchange-field approximation assuming $\xi_S/\xi_h = \sqrt{h/(2\pi T_c)} \gg 1$. This is a reasonable approximation for the type of samples reported in Ref. [54]: the exchange field in the CuNi ferromagnetic alloys has been estimated at 850 K, whereas the critical temperature of Nb is of the order of 9 K. Thus, the ratio ξ_S/ξ_h is of the order of 4. Note that the high-field limit is consistent with the diffusive limit condition $h\tau_e \ll 1$ with τ_e the elastic mean free time (see the discussion of Sec. 1.4.4 for details). The parameters of the experiments [54] yield the estimation $h\tau_e \approx 0.1$.

In our treatment we have neglected the finite transparency of the interfaces, the finite mean free path of electrons, the spin-flip and spin-orbit scattering. Of course, those effects may be incorporated in the formalism of Usadel equations in the usual way (see, e.g., Refs. [68–70]). We expect that they do not change the qualitative conclusion about the reduction of the π state by the domain structure. This has been confirmed by a subsequent numerical work on the same setup [71]. It appears that to observe a significant deviation from the critical misorientation angle $\theta_c = \pi/2$ one needs to go to low temperatures *and* low exchange field. The latter condition being experimentally not accessible even when working with diluted ferromagnetic alloys. With regards to introducing finite interface transparencies and spin-flip scattering, the authors of [71] remark that they did not find any indication that our results [72] may change in any significant way. However, a realistic quantitative theory of SFS junctions may need to take those effects into account, in addition to a more realistic domain configuration in the ferromagnet.

Finally, it is interesting to remark that we do not observe any long range Josephson effect in the system we consider. As remarked by Houzet and Buzdin in [73], it is necessary to have two sources of triplet component (noncollinear magnetization) to generate the component of the current decaying at the same rate as the current in a SNS junction, for which the characteristic decay length is given by $\xi_T = \sqrt{D/2\pi T}$ (this length is obtained taking $h \rightarrow 0$ in (2.17)). The authors of [73] propose therefore a junction with three domains to generate long range triplet correlations.

Chapter 3

SFS junction with in-plane ferromagnetic domains

3.1 Introduction

The physics of single-domain SFS junctions (including the effect of spin-flip [74–76] and spin-orbit scattering [2, 70, 77]) is now well understood. However, as we have seen in the previous chapter, in some experiments the $0\text{--}\pi$ transition points may deviate from standard predictions [54, 78] or even be absent [79, 80]. There is no consensus on the interpretation of such deviations. They may be attributed either to the presence of a magnetically dead layer at the interface between the superconductor and the ferromagnet [54, 59], or to a domain structure or inhomogeneities in the ferromagnetic layer. The domain structure crucially depends on the nature of the ferromagnet: strong ferromagnets consist of well-defined magnetic domains whose spatial extension may be reduced by the proximity effect [81–84]. In weakly ferromagnetic alloys, on the other hand, the magnetization may fluctuate on short length scales without forming domains [85].

Theoretically, SFS junctions with inhomogeneous magnetization have been studied recently in different setups, see for example [63, 64, 68, 72, 86–89]. However, in most works (except in Refs. [86–89]) only domains along the junction were studied (quasi-one-dimensional geometry), while we believe that in the experimental realizations of SFS junctions with thin F layers the domain structure is also likely to form in the plane of the F film.

Motivated by the experimental progress on π junctions, we study a model of a diffusive SFS junction with in-plane domains (so that the domain walls are orthogonal to the S and F layers, see Fig. 3.1). This geometry has been studied previously by Volkov and Anishchanka within the macroscopic approach of London equations [87]. Our model is different from

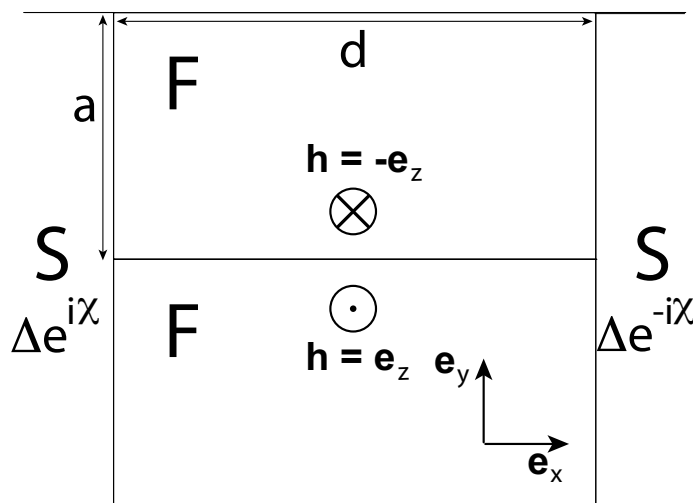


Figure 3.1: SFS junction with in-plane magnetic domains.

the one studied in Ref. [86]: in that work, the Neel domain walls are considered, and the junction is brought to the regime with only the long-range triplet component contributing to the Josephson current. In our model, the domain walls are taken to be sharp, and no long-range triplet component appears for domains with antiparallel magnetization.

The domain structure introduces an additional length scale: the domain size a . As one can expect, we find that the effect of inhomogeneous magnetization depends strongly on the relative magnitude of a and ξ_h . In the limit of small domains, $a \ll \xi_h$, the exchange field effectively averages out, and the critical current of a single nonmagnetic SNS junction is retrieved. In the opposite limit of large domains $a \gg \xi_h$, the influence of domain walls is localized to their vicinity and produces only a small correction to the current of a single-domain SFS junction. Between those limits, the supercurrent shows either a damped oscillatory behavior as a function of the junction thickness (for large domains $a > a_c \approx 0.83 \xi_h$), or a monotonic exponential decay (for smaller domains $a < a_c$). In the former case, the multidomain junction may be compared to a single-domain SFS trilayer with spin-flip scattering [70] and a renormalized exchange field, whereas in the latter case the junction behaves like a SNS junction with spin-flip scattering. The effective parameters are determined analytically in both limits of small and large domains. When considering the dependence of the critical current on the junction thickness, one finds that in SNS junctions the presence of spin-flip scattering reduces the decay length, as can be expected from the suppression of the proximity effect by magnetic scattering (see also Sec. 1.5.2). In SFS junctions, spin-flip scattering leads to an *increased* oscillation period of the critical current in addition to the faster decay. The decay and oscillation length which are the same in monodomain SFS junctions (2.17) become therefore different in the presence of magnetic scattering.

We also study the inhomogeneous distribution of the current density and conjecture that at low temperatures such SFS junctions with domains may realize the intermediate φ phase proposed by Buzdin [90].

The chapter is organized as follows. In Sec. 3.2 we compute the superconducting Green functions and the Josephson-current density for the multidomain SFS junction. Sec. 3.3 is devoted to the analysis of the total Josephson current. In Sec. 3.4 we discuss the spatial distribution of the current density. Finally, in Sec. 3.5 we summarize our conclusions.

3.2 Model for the multidomain SFS junction

As in the previous chapter, we assume that the ferromagnetic layer is strongly disordered, and the motion of electrons is diffusive. In this regime, the quasiclassical Green functions (averaged over the fast Fermi oscillations and the momentum directions) are given by the solutions to the Usadel equations (1.62). To simplify the calculations, we further assume that the junction is close to the superconducting critical temperature T_c . In this case, the superconducting correlations are weak so that the Usadel equations can be linearized, and the current-phase relation is sinusoidal

$$J = I_c \sin \varphi, \quad (3.1)$$

where $\varphi = 2\chi$ is the superconducting phase difference across the junction and I_c is the critical current. The sign of I_c determines if the junction is in the zero phase or in the π phase.

In this chapter, we consider a SFS junction with in-plane ferromagnetic domains of opposite magnetization. We introduce a coordinate system with the F layer in the yz plane (Fig. 3.1). The x axis is directed along the junction, and the SF interfaces correspond to the coordinates $x = 0, d$. The domain walls are taken to be normal to the y axis. The origin of the y axis is chosen at the interface between two domains. The system is invariant under translation along the z axis. Our further calculations will be equally applicable to either the system with two domains of width a (see Fig. 3.1) or the $2a$ -periodic multidomain case (the same setup periodically repeated in the y direction).

The (nonlinear) Usadel equation (1.62) in the ferromagnetic layer takes the form

$$D\nabla(\check{g}\nabla\check{g}) - \omega[\hat{\tau}_3\hat{\sigma}_0, \check{g}] - i[\hat{\tau}_3(\mathbf{h}\cdot\hat{\boldsymbol{\sigma}}), \check{g}] = 0. \quad (3.2)$$

where D denotes the diffusion constant and as usual the system of units with $\hbar = k_B = \mu_B = 1$ is chosen. The Green function \check{g} is a matrix in the Nambu \otimes spin space, $\hat{\tau}_\alpha$ and $\hat{\sigma}_\alpha$ denote the Pauli matrices respectively in Nambu (particle-hole) and spin space, $\omega = (2n + 1)\pi T$ are the Matsubara frequencies and \mathbf{h} is the exchange field in the ferromagnet.

The Usadel equation is supplemented with the normalization condition for the quasiclassical Green function

$$\check{g}^2 = \check{1} = \hat{\tau}_0 \hat{\sigma}_0. \quad (3.3)$$

The boundary conditions for the quasiclassical Green functions have been discussed in Sec. 1.4.6. Those conditions were initially derived for superconductor-normal metal interfaces but are still valid [1] in the presence of an exchange field h , provided $h \ll E_F$. For simplicity, we assume that the superconductors are much less disordered than the ferromagnet, and then we can impose the rigid boundary conditions at the SF interfaces,

$$\check{g} = \frac{1}{\sqrt{\omega^2 + \Delta^2}} \left(\begin{array}{cc} \omega & \Delta e^{\pm i\chi} \\ -\Delta e^{\mp i\chi} & -\omega \end{array} \right)_{\text{Nambu}} \otimes \hat{\sigma}_0, \quad (3.4)$$

where Δ denotes the superconducting order parameter, and the different signs refer respectively to the boundary conditions at $x = 0$ and $x = d$. At the boundary between ferromagnetic domains, we impose the continuity of the Green functions and of their derivatives (transparent interface). In fact, one obtains those transparent boundary conditions as long as the jump in the exchange field h is much smaller than E_F , and provided there is no mismatch between structural and electronic parameters of the domains.

Close to the critical temperature T_c , we linearize the Usadel equations (3.2), (3.3) around the solution for the normal metal state $\check{g} = \hat{\tau}_3 \hat{\sigma}_0 \text{sgn}(\omega)$. The linearized Green function then takes the form

$$\check{g} = \left(\begin{array}{cc} \sigma_0 \text{sgn}(\omega) & f_\alpha \sigma^\alpha \\ -f_\alpha^\dagger \sigma^\alpha & -\sigma_0 \text{sgn}(\omega) \end{array} \right), \quad (3.5)$$

where the scalar f_0 (respectively f_0^\dagger) and vector \mathbf{f} (respectively \mathbf{f}^\dagger) components of the anomalous Green functions obey the linear equations

$$\left(\frac{\partial^2}{\partial x^2} + \frac{\partial^2}{\partial y^2} \right) f_\pm^{1(\dagger)} - \lambda_\pm^2 f_\pm^{1(\dagger)} = 0, \quad (3.6)$$

with

$$\lambda_\pm = \left[2 \frac{|\omega| \mp ih \text{sgn}(\omega)}{D} \right]^{1/2}. \quad (3.7)$$

The projections of the anomalous Green function along the direction of the exchange field (“parallel” components) are defined as $f_\pm^{(\dagger)}(x, y) = f_0^{(\dagger)} \pm \mathbf{f}^{(\dagger)} \cdot \mathbf{e}_z$ (we assume that the ferromagnetic exchange field \mathbf{h} is aligned in the direction \mathbf{e}_z , see Fig. 3.1). Note that there is no perpendicular “long-range triplet” [91] component of the vector part of the Green function, since the magnetizations of the domains are collinear. We have used the invariance under translation along the z direction. The superscript 1 refers to domains with field along \mathbf{e}_z and in the following we will use the superscript 2 for domains with the field along $-\mathbf{e}_z$. Similar equations hold for $f_\pm^{2(\dagger)}$ with $\lambda_\pm \leftrightarrow \lambda_\mp$.

It is convenient to write the solutions to those equations in the form

$$f_{\pm}^{(\dagger)1,2}(x, y) = f_{\pm\text{Bulk}}^{(\dagger)1,2}(x) + \delta_{\pm}^{(\dagger)1,2}(x, y) \quad (3.8)$$

where $f_{\pm\text{Bulk}}^{1,2}$ are the solutions of Eq. (3.6) for a single-domain SFS junction with the magnetization along \mathbf{e}_z (respectively $-\mathbf{e}_z$). Since the equations (3.6) are linear, the correction $\delta(x, y)$ is also a solution to the same equations with the boundary conditions

$$\partial_y \delta_{\pm}^{1,2}(x, y = \mp a) = 0, \quad (3.9)$$

$$\delta_{\pm}^{1,2}(x = \{0, d\}, y) = 0, \quad (3.10)$$

$$\delta_{\pm}^1(x, y = 0) - \delta_{\pm}^2(x, y = 0) = \Delta f_{\pm\text{Bulk}}(x), \quad (3.11)$$

$$[\partial_y] \delta_{\pm}^1(x, y = 0) - [\partial_y] \delta_{\pm}^2(x, y = 0) = 0. \quad (3.12)$$

Here $\Delta f_{\pm\text{Bulk}} = f_{\pm\text{Bulk}}^2(x) - f_{\pm\text{Bulk}}^1(x)$ is the difference of the bulk Green functions in the two domains. For the two-domain junction, the first condition imposes zero current at the interface with vacuum, the second condition ensures the continuity of the Green functions at the SF interfaces. Finally, the last two conditions reflect the continuity of the Green function and its derivatives at the interface between the two domains. It can be easily shown from symmetry considerations that this set of boundary conditions can also be applied to a periodic multidomain SFS junction with domains of width $2a$.

The condition (3.10) allows us to express $\delta_{\pm}^{1,2}$ in the form of the Fourier series

$$\delta_{\pm}^{1,2} = \sum_{n=1}^{\infty} \sin\left(\frac{\pi n}{d}x\right) A_{n\pm}^{1,2}(y). \quad (3.13)$$

For each n we solve

$$\partial_y^2 A_{n\pm}^1 = \gamma_{n\pm}^2 A_{n\pm}^1 \quad (3.14)$$

with

$$\gamma_{n\pm} = \sqrt{\left(\frac{\pi n}{d}\right)^2 + \lambda_{\pm}^2}. \quad (3.15)$$

To obtain the equation for $A_{n\pm}^2$ one needs to substitute $\gamma_{n\pm} \leftrightarrow \gamma_{n\mp}$. We can solve those equations for each Fourier component n with the boundary conditions provided by (3.9), (3.11) and (3.12). The solution is given by

$$\begin{aligned} \delta_{\pm}^1 &= \frac{\Delta}{|\omega|} \sum_{n=1}^{\infty} \sin\left(\frac{\pi n x}{d}\right) \frac{2\pi n \cosh \gamma_{n\pm}(y+a)}{d^2 \cosh \gamma_{n\pm} a} \frac{\gamma_{n\mp} \tanh \gamma_{n\mp} a}{\gamma_{n\mp} \tanh \gamma_{n\mp} a + \gamma_{n\pm} \tanh \gamma_{n\pm} a} \\ &\times \left(\frac{1}{\gamma_{n\mp}^2} - \frac{1}{\gamma_{n\pm}^2}\right) (e^{ix} - (-1)^n e^{-ix}). \end{aligned} \quad (3.16)$$

In the second domain, the correction δ_{\pm}^2 is given by the same formula with the replacement of y, γ_{\pm} by $-y, \gamma_{\mp}$. The bulk Green functions are given by [72]

$$f_{\pm\text{Bulk}}^1 = \frac{\Delta}{|\omega|} \left[\frac{\sinh \lambda_{\pm} x}{\sinh \lambda_{\pm} d} e^{-ix} + \frac{\sinh \lambda_{\pm} (d-x)}{\sinh \lambda_{\pm} d} e^{ix} \right], \quad (3.17)$$

and $f_{\pm\text{Bulk}}^2 = f_{\mp\text{Bulk}}^1$. Finally, note that f_{Bulk}^\dagger and δ^\dagger are given by the same expressions (3.16), (3.17) with the replacement of χ by $-\chi$.

The last step will be to compute the Josephson current density using the formula (1.68)

$$\mathbf{J} = ie\nu_0 D\pi T \sum_{\omega=-\infty}^{\infty} \frac{1}{2} \text{Tr}(\hat{\tau}_3 \hat{\sigma}_0 \check{g} \nabla \check{g}), \quad (3.18)$$

where ν_0 is the density of states in the normal metal phase (per one spin projection) and the trace has to be taken over the Nambu and spin indices. The current density can be explicitly rewritten for the linearized \check{g}

$$\mathbf{J} = -ie\nu_0 D\pi T \sum_{\omega=-\infty}^{\infty} \left[\sum_{\sigma=\pm} \frac{1}{2} (f_\sigma \nabla f_\sigma^\dagger - f_\sigma^\dagger \nabla f_\sigma) \right]. \quad (3.19)$$

The symmetry of translation along the z direction implies that the current remains in the xy plane. Using the expression for the Green functions (3.16) and (3.17), we can obtain a general expression for the current density (which is too cumbersome to be reproduced here). This expression involves two contributions. The first one is produced exclusively by the bulk Green functions (3.17) and corresponds to a homogeneous ferromagnetic interlayer. The second contribution is due to the correction (3.16) and reflects the influence of the domain structure. The current resulting from this contribution is not uniform in space. The characteristic decay scale of the correction as a function of the distance from the domain interface is given by $\Re\left(\frac{1}{\gamma_{n\pm}}\right) \sim \min(\xi_T, \xi_h, d)$, where $\xi_T = \sqrt{D/2\pi T}$ and $\xi_h = \sqrt{D/h}$ are the thermal and magnetic coherence lengths, respectively. Far from the interface between the domains ($y \gg \min(\xi_T, \xi_h, d)$), the correction (3.16) vanishes and we recover locally the single-domain SFS current. Thus we expect the properties of the junction to be very different in the two limits of small [$a \ll \min(\xi_T, \xi_h, d)$] and large [$a \gg \min(\xi_T, \xi_h, d)$] domains.

3.3 Critical current

Experimentally, in SFS hybrid junctions the measurable quantity is the total current flowing through the junction, that is along the x -axis. Since $\nabla \cdot \mathbf{J} = 0$, the total current is conserved along the x direction. We can therefore compute it at $x = 0$, and we find

$$\begin{aligned} \frac{J_c}{I_0} &= \Re \left[\sum_{\omega>0} \frac{\Delta^2}{\omega^2} \frac{\lambda_+ d}{\sinh \lambda_+ d} \right] \\ &+ \frac{16\pi^2}{ad^2 \xi_h^4} \sum_{\omega>0} \frac{\Delta^2}{\omega^2} \sum_{n=1}^{\infty} \left[\frac{(-1)^{n-1} n^2}{(\gamma_{n+} \gamma_{n-})^3} \frac{1}{\gamma_{n-} \coth \gamma_{n+} a + \gamma_{n+} \coth \gamma_{n-} a} \right] \end{aligned} \quad (3.20)$$

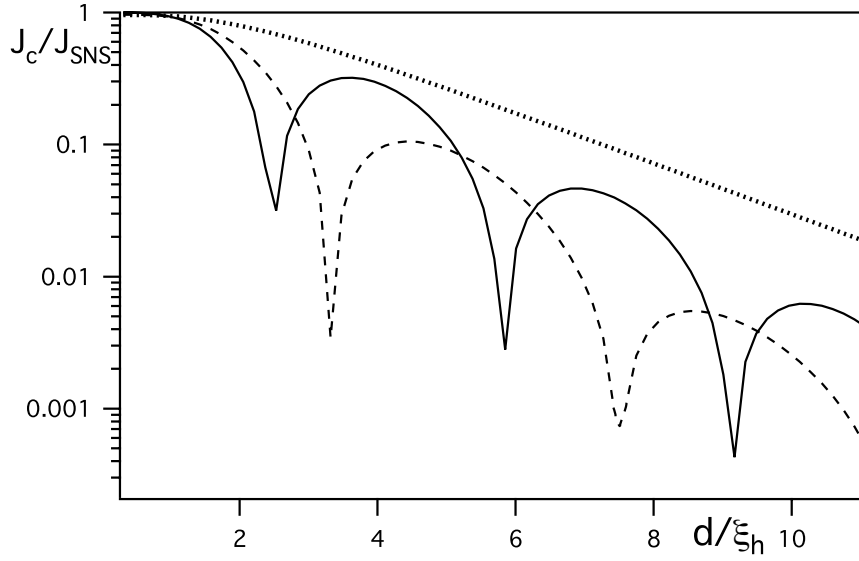


Figure 3.2: Critical current J_c/J_{SNS} vs. junction length d/ξ_h for $a = 0.6 \cdot \xi_h$ (dotted line), $1.6 \cdot \xi_h$ (dashed line) and ∞ (solid line). Here J_{SNS} is the critical current of the junction in the absence of the exchange field. We take $\frac{\hbar}{T} = 100$.

with

$$I_0 = \frac{4e\nu_0 DS\pi T}{d}, \quad (3.21)$$

and S the area of the junction. The first term is the critical current for a single-domain SFS junction with a damped oscillatory dependence on the F-layer thickness (for a review, see the discussion of the previous chapter in Sec. 2.3.1). It can be either positive (zero state of the junction) or negative (π state). The second term reflects the influence of the domain structure. The critical current (3.20) depends on the three dimensionless parameters: a/ξ_h , d/ξ_h , and ξ_T/ξ_h . For some values of the parameters, the critical current (3.20) computed numerically is plotted in Fig. 3.2. Depending on the values of the parameters, it shows either an exponential decay or an exponential decay with oscillations, as a function of d .

Note that, as discussed in the previous chapter, in most experimental situations $\xi_T \gg \xi_h$ because the ferromagnetic exchange energy exceeds by far the superconducting critical temperature. In the following we will refer to this situation as the high-field limit. In this limit, the summation over ω in Eq. (3.20) can be performed analytically [$\sum_{\omega>0} \Delta^2/\omega^2 = \Delta^2/(8T^2)$], and the deviation δJ_c from the critical current of a single-domain SFS junction [the second term in Eq. (3.20)] is expressed in terms of the reduced variables $n^* = \frac{d\sqrt{2}}{\pi\xi_h}$ and $a^* = \frac{\pi a}{d}$:

$$\frac{\delta J_c}{I_0} = -\frac{\Delta^2}{2T^2} \frac{n^{*4}}{a^*} \sum_{n=1}^{\infty} \frac{(-1)^n n^2}{(n^4 + n^{*4})^{3/2}} \times \frac{1}{\Re \left[\sqrt{n^2 + in^{*2}} \coth \left(a^* \sqrt{n^2 - in^{*2}} \right) \right]}. \quad (3.22)$$

In the limit of large d , the asymptotic behavior of this expression may be estimated as an integral (in the variable $z = n/n^*$)

$$\frac{\delta J_c}{I_0} = -\frac{\Delta^2}{2T^2 a^*} \int_{-\infty}^{\infty} dz \frac{e^{i\pi n^* z} z^2}{(z^4 + 1)^{3/2}} \times \frac{1}{\left[\sqrt{z^2 + i} \coth \left(a^* n^* \sqrt{z^2 - i} \right) + \sqrt{z^2 - i} \coth \left(a^* n^* \sqrt{z^2 + i} \right) \right]}, \quad (3.23)$$

which is, in turn, determined to the exponential precision by the singular points of the integrand in the complex plane. Remarkably, the contribution from the poles at $(\pm i)^{1/2}$ cancels exactly the first term (single-domain contribution) of Eq. (3.20). For sufficiently large d , to the exponential precision, the critical current is then given by

$$J_c \propto e^{-\lambda d}, \quad \lambda = -\frac{i\sqrt{2}z_0}{\xi_h}, \quad (3.24)$$

where z_0 is the singular point of the integrand with the smallest positive imaginary part. Note that z_0 is now a function of one dimensionless parameter $\alpha = a^* n^* = \sqrt{2}a/\xi_h$.

By analogy with a single-domain SFS junction with spin-flip scattering, the real and imaginary parts of λ^2 may be interpreted as an effective magnetic field and an effective spin-flip rate¹,

$$\lambda^2 = -\frac{2i}{\left[\xi_h^{(\text{eff})} \right]^2} + \frac{4\Gamma_{sf}^{(\text{eff})}}{D}, \quad \xi_h^{(\text{eff})} = \sqrt{\frac{D}{h^{(\text{eff})}}}. \quad (3.25)$$

Therefore the effective field and spin-flip rate can be found as

$$h^{(\text{eff})} = h\Im(z_0^2), \quad \Gamma_{sf}^{(\text{eff})} = -\frac{h}{2}\Re(z_0^2). \quad (3.26)$$

In the following, we discuss the limits of large and small domain sizes.

3.3.1 Limit of large domains : $a \gg \xi_h$

We consider the limit of large domains, $a \gg \xi_h$, with the assumption of the strong exchange field, $\xi_T \gg \xi_h$. In this regime, the damped oscillations of the critical current at large d are

¹We define the spin-flip scattering rate by $\Gamma_{sf} = 1/(2\tau_{sf})$, as in Sec. 1.5.2 and Refs. [20, 40, 92]

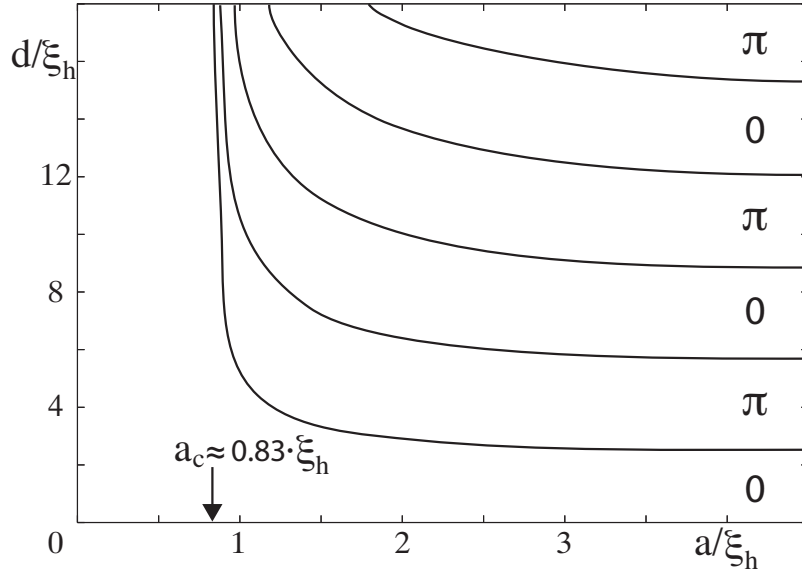


Figure 3.3: Phase diagram of the junction in the high-exchange-field limit. Here a represents the width of the domains and d is the length of the junction.

determined by the solutions to the equation

$$\sqrt{z^2 + i} \coth(\alpha \sqrt{z^2 - i}) + \sqrt{z^2 - i} \coth(\alpha \sqrt{z^2 + i}) = 0 \quad (3.27)$$

with the smallest positive imaginary part. At $\alpha = \sqrt{2}a/\xi_h \gg 1$, one of the arguments of $\coth(\alpha \sqrt{z^2 \pm i})$ must be close to $\pm i\pi/2$. Expanding around this point, we obtain $z_0^2 = i - \frac{\pi^2}{4\alpha^2} + \frac{(1-i)\pi^2}{4\alpha^3} + \dots$. This translates into the reduced effective field

$$h^{(\text{eff})} \approx h \left[1 - \frac{\pi^2}{8\sqrt{2}} \left(\frac{\xi_h}{a} \right)^3 \right] \quad (3.28)$$

and the effective spin-flip rate

$$\Gamma_{sf}^{(\text{eff})} \approx \frac{\pi^2}{16} \left(\frac{\xi_h}{a} \right)^2 h = \frac{\pi^2 D}{16a^2}. \quad (3.29)$$

Thus, to the leading order in (ξ_h/a) , the effect of domain walls reduces to an effective spin-flip rate, which increases the period of 0 – π transitions as a function of d and simultaneously decreases the overall decay length of the critical current (see Fig. 3.2, dashed line, for an illustration).

3.3.2 Limit of small domains : $a \ll \xi_h, d, \xi_T$

In the limit of small domains $a \ll \xi_h, d, \xi_T$, we can calculate a perturbative correction to the critical current by expanding (3.20) in a . To the lowest order in a , we obtain (without

assuming the high-field limit),

$$\frac{J_c}{I_0} = \frac{J_{SNS}}{I_0} - \frac{2a^2 d^2}{3\xi_h^4} \sum_{\omega>0} \frac{\Delta^2}{\omega^2} \left[\frac{\lambda_0 d \cosh \lambda_0 d - \sinh \lambda_0 d}{\lambda_0 d \sinh^2 \lambda_0 d} \right], \quad (3.30)$$

where $\lambda_0^2 = \frac{\lambda_+^2 + \lambda_-^2}{2} = \frac{2|\omega|}{D}$ does not contain the exchange energy h , and $J_{SNS} = J_c(h=0)$. This expression reveals that in the limit $a \rightarrow 0$ the multidomain SFS junction behaves like a SNS junction: the exchange field is averaged out when the domain width is small. Note also that the correction arising from a finite domain width is always negative: the amplitude of the current is decreased compared to the SNS case.

A more accurate approximation may be obtained in the high-field limit $\xi_T \gg \xi_h$ by the asymptotic estimate of the oscillating sum described earlier in this section. To the second order in a , the solution to the equation (3.27) is given by $z_0 = -\frac{\alpha^2}{3}$, which translates into

$$h^{(\text{eff})} = 0, \quad \Gamma_{sf}^{(\text{eff})} \approx \frac{1}{3} \left(\frac{a}{\xi_h} \right)^2 h = \frac{h^2 a^2}{3D} \quad (3.31)$$

This expression for $\Gamma_{sf}^{(\text{eff})}$ agrees with the general estimate for the effective spin-flip rate obtained by Ivanov and Fominov [20] for SF structures with inhomogeneous magnetization.

Note that for sufficiently small a , the equation (3.27) has a solution with real z_0^2 corresponding to a pure decay (without oscillations) of the critical current. The dependence of the critical current on d is then purely decaying, without $0-\pi$ oscillations (Fig. 3.2, dotted line).

3.3.3 $0-\pi$ phase diagram

Between the two regimes of small and large domains, there is a phase transition as a function of a/ξ_h corresponding to a bifurcation of the real solution z_0^2 to Eq. (3.27) at smaller a to complex solutions at larger a . For a/ξ_h smaller than the critical value, the critical current decays as a function of d without oscillations (always in the 0 phase). For a/ξ_h larger than the critical value, the dependence on d is damped oscillatory, qualitatively similar to a single-domain SFS junction.

Numerically, we find the critical value $a_c/\xi_h \approx 0.83$. The full $0-\pi$ phase diagram in the high-field limit is plotted in Fig. 3.3. Periodic $0-\pi$ transitions (as a function of d) above a_c/ξ_h and zero phase below a_c/ξ_h illustrate our discussion. The absence of the $0-\pi$ transitions in the case of small domains may explain why in some experimental SFS junctions the π state is absent [79, 80].

For completeness, in Fig. 3.4 we also plot the locus of solutions z_0^2 to Eq. (3.27) in the complex plane for all values of α (in the units $\Gamma_{sf}^{(\text{eff})}/h$ and $h^{(\text{eff})}/h$). The corresponding

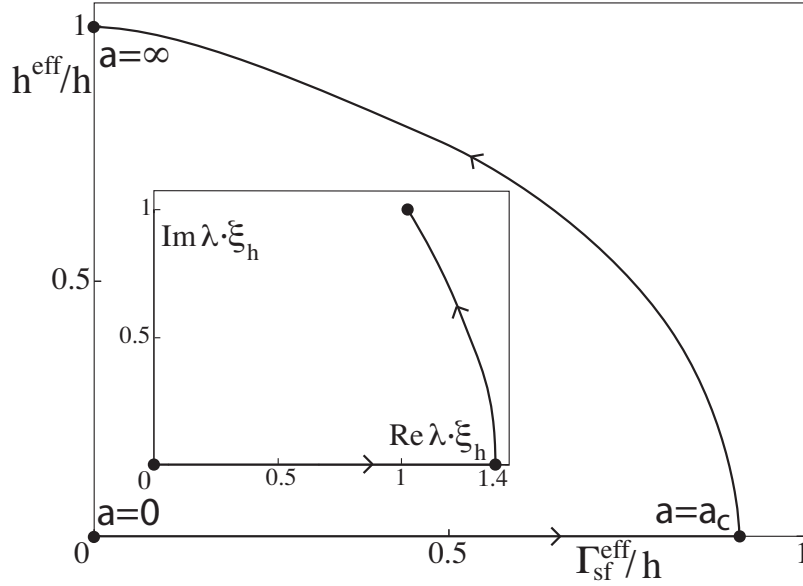


Figure 3.4: The effective spin-flip scattering rate $\Gamma_{sf}^{(eff)}$ and the effective exchange field $h^{(eff)}$. The curve starts at $a = 0$ and ends at $a = \infty$. The inset shows the real part (decay length) and the imaginary part (rate of oscillations) of λ in Eq. (3.24).

real and imaginary parts of λ determining the d dependence of the critical current (3.24) are plotted in the inset.

3.4 Local current density

Since the system does not have a translational symmetry along the y direction, the Josephson current forms a nontrivial pattern in the x - y plane. In Fig. 3.5 we present plots of the current density (proportional to $\sin \varphi$) at two different points of the phase diagram: in the zero phase and in the π phase.

Those inhomogeneous patterns may be qualitatively understood on the basis of interpreting the domain walls as producing an effective spin-flip scattering. Different regions of the ferromagnet may be attributed different effective spin-flip rates, depending on their distance from the domain wall. The effective spin-flip processes renormalize the decay coefficient λ in (3.24) and, therefore, different parts of the junction experience 0 - π transitions at different values of d . This can be clearly seen in Fig. 3.6 depicting the current density near a 0 - π transition. While the neighborhood of the domain wall is in the 0 phase, the region near the free boundaries (at $y = \pm a$) are in the π phase. This situation resembles a model studied by Buzdin *et al.* [90]: a system of alternating zero and π junctions. In that work, an intermediate equilibrium phase difference was predicted, depending on the ratio

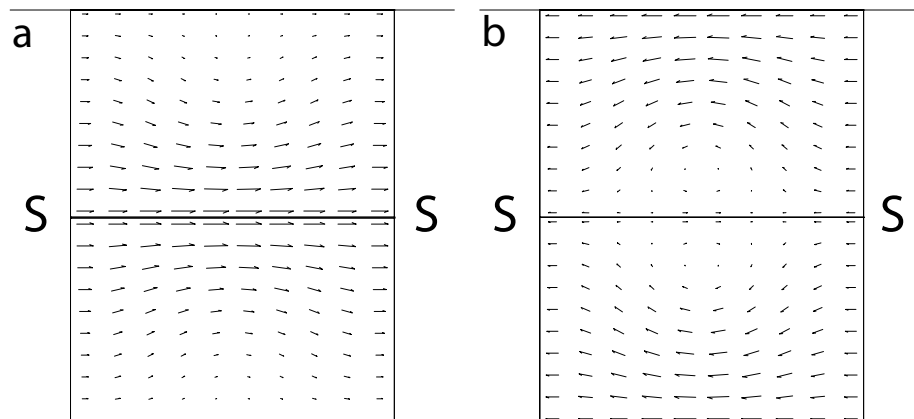


Figure 3.5: Josephson-current density in the two-domain SFS junction in the zero and π phases. The domain size is $a = 1.6 \xi_h \ll \xi_T$, and d is taken to be below (left) and above (right) the first $0-\pi$ transition.

between the junction widths and the magnetic coherence length. Even though our model cannot lead to such a φ -junction (we consider linearized Usadel equations and therefore obtain a purely sinusoidal current-phase relation with only two possible equilibrium phases 0 or π), at low temperatures such a SFS system with domains could possibly produce a φ -state.

3.5 Summary

In this chapter we consider a Josephson SFS junction consisting of domains with opposite magnetization connected “in parallel”. As a function of the junction thickness, the critical current may exhibit either a decaying oscillating or a purely decaying behavior, depending on the domain width. The effect of domain walls in this geometry may be approximated as an effective spin-flip scattering, together with a renormalization of the effective magnetic field. This behavior is different from that in SFF’S junctions with the domains connected “in series” studied in Chapter 2 and Ref. [72]. In that SFF’S setup, the domain structure lead to a gradual reduction of the π phase (at a non-parallel configuration of the two domains), so that the relative fraction of the zero phase increases as a function of the mismatch in the magnetization directions. In the present chapter, however, we do not consider the case of an arbitrary angle between the two magnetizations, because of the complexity of the problem.

It is justified to ask oneself to what extend our conclusions [42] depend on the particular choice of the realization of the in-plane domains. In a recent work by Champel *et al.* [88] a similar study was performed for a different type of domain structure. It is shown that

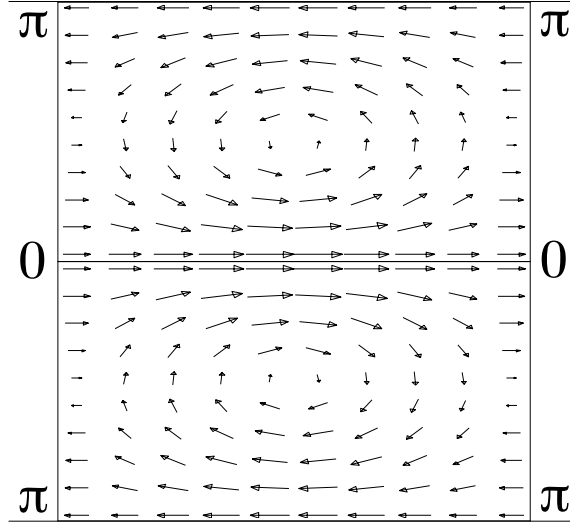


Figure 3.6: Current lines close to the $0\text{--}\pi$ transition. The domain size is $a = 1.6 \xi_h \ll \xi_T$, and d is taken to be close to the first $0\text{--}\pi$ transition. Part of the junction is in the zero phase and part in the π phase.

for a ferromagnet with cycloidal spiral modulation of the magnetization in the plane of the ferromagnetic layer, one gets a phase diagram of the same form as Fig. 3.3 and effective decay and oscillations rates comparable with Fig. 3.4. In Ref. [88] the inverse wave vector of the spiral order is the relevant parameter and plays the same role as the size of the domains a in our work. It appears therefore that our conclusions do not rely crucially on the form of the in-plane domains.

We expect that in a realistic geometry of domains both effects of the spin-flip scattering and of the reduction of the π phase take place simultaneously, and our findings presented in this chapter and in the previous chapter (published in Refs. [72] and [42]) may help to qualitatively describe the $0\text{--}\pi$ phase diagram of real SFS junctions with inhomogeneous ferromagnetic interlayers.

Chapter 4

Orbital effect of a magnetic field

4.1 Introduction

After having discussed in the previous chapters the physics resulting from the interplay between ferromagnetism and superconductivity in proximity structures, we turn here to the effect of an external magnetic field in a Josephson junction. We can distinguish between the orbital and the Zeeman effect of the magnetic field. Some studies have focused on the Zeeman effect of the magnetic field in proximity systems (see for example Ref. [93]) or, since the Zeeman term in the Usadel equations is formally equivalent to the ferromagnetic exchange field, considered the possibility to obtain a π junction by applying a field [94].

In this chapter we address the orbital effect of an external magnetic field in a diffusive superconductor-normal metal-superconductor (SNS) Josephson junction. As we saw in the previous chapters, one-dimensional models can often successfully be applied to describe the proximity effect in the diffusive regime. However, including orbital effects in the formalism forbids reducing the system to one dimension. As a result, the proximity effect in the presence of the orbital effect of the magnetic field has been studied until now essentially numerically or in simple limits (wide and short junction or narrow junction) for diffusive hybrid structures [95, 96] and in the clean limit [97].

It is well established that in the limit of a thin (tunnel) junction the Josephson current changes sign along the transverse direction when an external magnetic field is applied and that the total current exhibits a Fraunhofer-like dependence on the magnetic flux through the junction [46] due to the interference between the local currents. Observation of this type of dependence has been extensively used experimentally to confirm the Josephson nature of the coupling between superconductors. More recently, shifted Fraunhofer patterns have also served as an indicator for the presence of a net magnetization when a ferromagnetic interlayer is used [58, 60]. It has been then shown both experimentally [98] and theoretically

[95, 96] that in proximity structures, discrepancies from the usual Fraunhofer patterns can be present. In particular, the authors of Refs. [95, 96] have discussed numerically how the damped oscillatory behavior (Fraunhofer like) characterizing wide and short junctions is replaced by a monotonic exponential decay in narrow junctions. They have also identified the length scale over which the transition between the two regimes takes place.

Motivated by this recent activity and by the rarity of analytical results on the Usadel equation for non one-dimensional geometries, we revisit the problem of the diffusive SNS junction in an external magnetic field. We consider the limit of a long junction and linearized Usadel equations to obtain analytical results for a two dimensional problem. We show that for a narrow junction, the Josephson critical current decays exponentially as a function of the flux through the junction. We find the transition point (the critical width of the junction) where this monotonic decay is replaced by damped oscillations of the critical current. Finally, in the limit of a wide junction, we find damped oscillations with the same period as in the Fraunhofer limit but an exponential decay instead of the purely algebraic decay characterizing Fraunhofer patterns. In this regime, the superconducting correlations become localized in a small region close to the border of the junction. The method we develop does not rely crucially on the choice of particular boundary conditions for the interface between the superconductor and the normal metal: it can be applied either to the situation where the SN interfaces are transparent or to systems with finite interface transparency.

The chapter is organized as follows. In Sec. 4.2 we describe the SNS Josephson junction we consider and introduce the formalism used throughout the chapter. We discuss then (Sec. 4.3) the basic mechanism of formation of Fraunhofer-like interference patterns in short SNS junctions. We compute (Sec. 4.4) the superconducting Green function and the Josephson current (Sec. 4.5) for long SNS junctions in a transverse field. In Sec. 4.6 we discuss the applicability conditions of our method and finally in Sec. 4.7 we summarize our conclusions.

4.2 SNS junction in a transverse magnetic field

We consider a SNS junction in a transverse magnetic field. We introduce a coordinate system with the N layer in the yz plane (Fig. 4.1). The x axis is directed along the junction, and the SN interfaces correspond to the coordinates $x = 0, L_x$. The origin of the y axis is chosen in the middle of the N layer and we denote the width L_y . The system is invariant under translation along the z axis. We take a uniform magnetic field \mathbf{H} directed along the z axis and neglect the screening of the magnetic field by the Josephson currents. This assumption is justified in most experimental situations with sufficiently weak critical currents, see, e.g., Refs. [94–96] for estimates. Namely, we must require that the junction

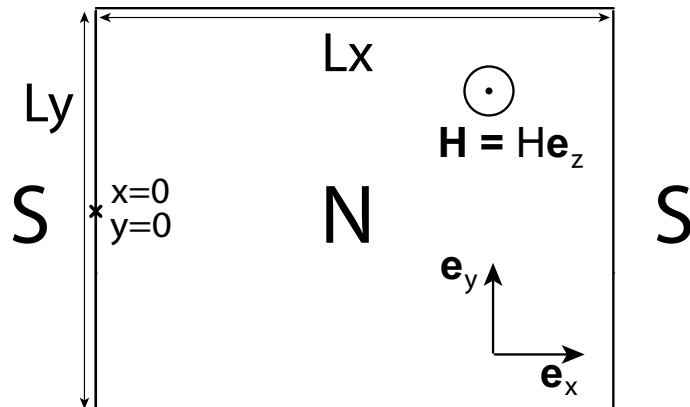


Figure 4.1: SNS junction in a transverse magnetic field.

is narrow compared to the Josephson penetration depth [47]

$$L_y \ll \lambda_J = \sqrt{\frac{\phi_0}{2\pi j_c L_x}}, \quad (4.1)$$

with j_c the critical current density and $\phi_0 = h/2e$ the superconducting flux quantum.

For simplicity, we further consider that the London length is short compared to the length of the junction L_x and neglect the penetration of the magnetic field in the superconducting electrodes. An exact treatment would require to add twice the London length to L_x in order to get the total flux through the junction [47].

We assume that the normal layer is strongly disordered and the motion of electrons is diffusive. In this regime, the quasiclassical Green functions (averaged over the fast Fermi oscillations and the momentum directions) are given by the solutions to the Usadel equations (1.62).

The (nonlinear) Usadel equation in the normal layer takes the form

$$\hbar D \hat{\nabla} \left(\check{g} \hat{\nabla} \check{g} \right) - \omega [\hat{\tau}_3, \check{g}] = 0. \quad (4.2)$$

$D = v_F l_e / 3$ is the diffusion constant with l_e the elastic mean free path and $\omega = (2n + 1) \pi k_B T$ is the Matsubara frequency. We have taken Eq. (1.62) in the absence of the vector component (1.67): the singlet version of the Usadel equation is sufficient since we consider only the orbital coupling to the external magnetic field. The Green function

$$\check{g} = \begin{pmatrix} G & F \\ -F^\dagger & -G \end{pmatrix} \quad (4.3)$$

is therefore a matrix in the Nambu (particle-hole) space, and $\hat{\tau}_\alpha$ denote the Pauli matrices in this space. The gradient operator $\hat{\nabla}$ contains the vector potential \mathbf{A} in order to describe

the orbital effect of the field

$$\hat{\nabla}\check{g} = \begin{pmatrix} \nabla G & (\nabla - \frac{2ie}{\hbar}\mathbf{A})F \\ -(\nabla + \frac{2ie}{\hbar}\mathbf{A})F^\dagger & -\nabla G \end{pmatrix}. \quad (4.4)$$

We neglect the Zeeman splitting which, in the case of the transverse magnetic field, has a typically much smaller effect than the vector-potential term, provided the quasiclassical condition $k_F l_e \gg 1$ is satisfied. The Zeeman term may be added as the contribution $\pm i\mu\mathbf{H}$ to the Matsubara frequency in the Usadel equation (4.2). On the other hand, the characteristic dimensions of the junction for observing the orbital effects discussed here are of the order of the magnetic length [93, 96]

$$\xi_H = \sqrt{\frac{\phi_0}{H}}. \quad (4.5)$$

One can check that, for $L_x \sim \xi_H$, the Zeeman splitting is much smaller than the Thouless energy $E_{\text{Th}} = \hbar D/L_x^2$ (using the quasiclassical assumption $k_F l_e \gg 1$) and thus may be neglected for most purposes.

The Usadel equation is supplemented with the normalization condition for the quasiclassical Green function

$$\check{g}^2 = \check{1}. \quad (4.6)$$

For simplicity, we assume for the moment that the proximity effect is weak (close to the critical temperature of the superconductor) and that the boundary conditions at the interface with the superconductor are rigid. Recall that this is the case for the transparent interface, if the normal region is much more disordered than the superconductor, as discussed in Sec. 1.4.6. We will see in Sec. 4.6 that these assumptions are not crucial and can be relaxed.

Then the Green function can be linearized around the normal-metal solution as

$$\check{g} = \begin{pmatrix} \text{sgn}(\omega) & F \\ -F^\dagger & -\text{sgn}(\omega) \end{pmatrix}, \quad (4.7)$$

and, choosing the gauge $\mathbf{A} = -yH\mathbf{e}_x$, the linearized Usadel equation (4.2) takes the form [95, 96]

$$\left[(\nabla_x + 2i\pi y)^2 + \nabla_y^2 - \frac{2|\omega|\xi_H^2}{\hbar D} \right] F(x, y) = 0. \quad (4.8)$$

Here we have rescaled both coordinates x and y in the units of the magnetic length ξ_H (4.5).

This equation is supplemented by the boundary conditions at the interface with the superconductor and at the open interface,

$$F(x = \{0, L_x\}, y) = F_{\text{B}} e^{\pm ix}, \quad (4.9)$$

$$\nabla_y F(x, y = \pm L_y/2) = 0. \quad (4.10)$$

The boundary condition (4.9) is the rigid one, with F_B being the bulk value of the anomalous Green function in the superconductor (close to the superconducting transition temperature, $F_B = \Delta/|\omega|$). The phase difference across the junction is thus denoted 2χ . Condition (4.10) expresses the vanishing of the current through the interface with vacuum.

The second anomalous component $F^\dagger(x, y)$ can be obtained solving the Usadel equation (4.8) with the boundary conditions (4.9) and (4.10) after the substitution $(\chi, H) \leftrightarrow (-\chi, -H)$. It is therefore the complex conjugate of $F(x, y)$.

The current density can be calculated from the solution of the Usadel equation using (1.68)

$$\mathbf{J} = 2\pi i e \nu_0 D T \sum_{n=0}^{\infty} \left[F^\dagger \nabla F - F \nabla F^\dagger - \frac{4ie\mathbf{A}}{\hbar} F F^\dagger \right] \quad (4.11)$$

where ν_0 is the density of states in the normal metal phase (per one spin projection). The symmetry of translation along the z direction implies that the current remains in the xy plane. The sum is taken over the Matsubara frequencies ω .

4.3 Short junction limit: Fraunhofer interference patterns

Introducing the variables $\tilde{x} \in [0, 1]$ and $\tilde{y} \in [-1/2, 1/2]$, we can rewrite the Usadel equation (4.8) in the form

$$\left[(\nabla_{\tilde{x}} + 2i\pi\phi\tilde{y})^2 + \left(\frac{L_x}{L_y} \right)^2 \nabla_{\tilde{y}}^2 - \frac{2|\omega|\xi_H^2}{E_{\text{Th}}} \right] F(\tilde{x}, \tilde{y}) = 0. \quad (4.12)$$

with $E_{\text{Th}} = \frac{\hbar D}{L_x^2}$ and $\phi = L_y L_x$ (recall that the lengths L_x and L_y are given in the units of ξ_H). In the limit, $L_x \ll \xi_H \ll L_y$ we can neglect the gradient term along the y direction. The Usadel equation (4.12) is then reduced to a one-dimensional problem which can be easily solved for the boundary condition (4.9)

$$F(\tilde{x}, \tilde{y}) = \frac{F_B e^{2i\pi\phi\tilde{y}(\tilde{x}-1)}}{\sinh W} \left[e^{-i\chi} \sinh [W\tilde{x}] - e^{i\chi+2i\pi\phi\tilde{y}} \sinh [W(\tilde{x}-1)] \right]. \quad (4.13)$$

with $W = \sqrt{2|\omega|\xi_H^2/E_{\text{Th}}}$. Note that it is not sufficient to require the condition $L_x, \xi_H \ll L_y$ as claimed in Ref. [96]. Indeed, from the solution (4.13) we see that with $L_x \sim \xi_H$ the gradient term along the y direction in (4.12) can give a non-negligible contribution.

Using the expression of the current (4.11) we can easily compute the total current through the junction. As usual, we get a sinusoidal current phase relation,

$$J_{\text{tot}} = I_c \sin 2\chi. \quad (4.14)$$

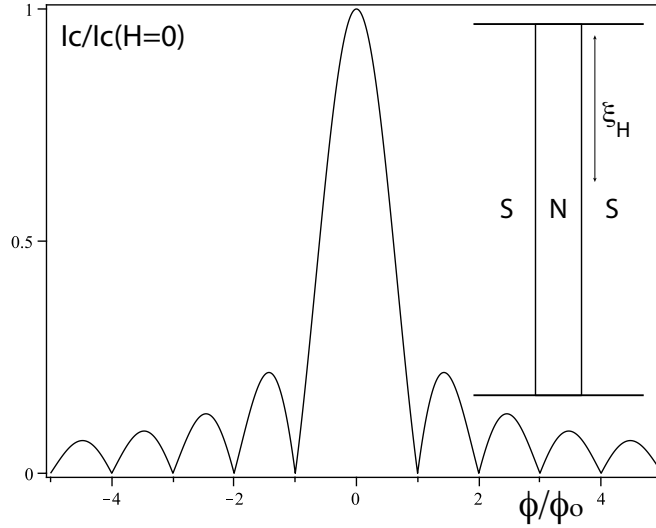


Figure 4.2: Critical current $I_c/(I_c(H = 0))$ as a function of the magnetic flux through a SNS junction for $L_x \ll \xi_H \ll L_y$.

The critical current is given by

$$I_c = I_0 \frac{\sin(\pi\phi/\phi_0)}{\pi\phi/\phi_0} \quad (4.15)$$

with $I_0 = I_c(H = 0)$ the critical current in a SNS junction at zero field and we have reintroduced physical units. As expected, we recover the same Fraunhofer patterns (see Fig. 4.2) as in a tunnel junction [46, 47].

4.4 Analytical results for a long junction

We are interested in solving the Usadel equation (4.8) in the middle of the long junction: $L_x \gg \xi_H$. This will allow us to retain only the mode with the slowest decay along the x direction from a spectral decomposition of the solution. To simplify our treatment, we assume that the temperature is sufficiently low, compared to the junction length: $\xi_T \gg L_x$, where the thermal length scale is defined as $\xi_T = \sqrt{\hbar D/2\pi T}$. This assumption allows us to neglect the ω term in the Usadel equation (4.8). We will comment on this assumption in Sec. 4.6.

First, notice that in the limit of the long junction (when the junction length L_x is much larger than the characteristic length of the decay of the anomalous Green function F) we can approximate the solution of (4.8) as a superposition [44] of the two Green functions for the semi-infinite SN problem

$$F(x, y) \approx F_\infty(x, y)e^{i\chi} + F_\infty(L_x - x, -y)e^{-i\chi} \quad (4.16)$$

where $F_\infty(x, y)$ is the solution for the SN problem with the semi-infinite normal layer. It obeys the same equation (4.8) with the same boundary condition (4.10) and with the second boundary condition (4.9) replaced by $F_\infty(x = 0, y) = F_B$ and $F_\infty(x \rightarrow \infty, y) = 0$. Note the mirror operation $y \leftrightarrow -y$ between the two terms in the right-hand side of (4.16).

It will be convenient to use the Fourier decomposition along the x direction by extending the semi-infinite problem to the whole real axis,

$$\left[(\nabla_x + 2i\pi y)^2 + \nabla_y^2 \right] F_\infty(x, y) = f(y) \delta(x), \quad (4.17)$$

where the right-hand side accounts for the jump in the derivative of the function at $x = 0$. Taking the Fourier transform, we can rewrite this equation in the integral form

$$F_\infty(x, y) = \int \frac{dk}{2\pi} e^{ikx} \left[\nabla_y^2 - (k + 2\pi y)^2 \right]^{-1} f(y). \quad (4.18)$$

The function $f(y)$ is fixed self-consistently by the boundary condition $F_\infty(x = 0, y) = F_B$.

At positive x , we can close the integration contour in the upper half-plane, and the poles of the integrand are given by the zero modes of the operator

$$A = \nabla_y^2 - (k + 2\pi y)^2 \quad (4.19)$$

(this operator acts on the functions $\psi(y)$ on the interval $-L_y/2 < y < L_y/2$ with the boundary conditions $\psi'(\pm L_y/2) = 0$). In the long-junction limit, the solution in the middle of the junction is determined by the zero mode with the smallest positive imaginary part of k .

The general solution to the second-order differential equation $A\psi = 0$ can be written in terms of a linear combination of two modified Bessel functions [99],

$$\psi = \sqrt{k + 2\pi y} \left(C_1 I_{1/4} \left[\frac{(k + 2\pi y)^2}{4\pi} \right] + C_2 K_{1/4} \left[\frac{(k + 2\pi y)^2}{4\pi} \right] \right). \quad (4.20)$$

The boundary conditions at $y = \pm L_y/2$ fix the ratio C_1/C_2 and limit the possible values of k to a discrete set. We get from the condition at $y = -L_y/2$

$$\frac{C_1}{C_2} = \frac{K_{3/4} \left[\frac{(k - \pi L_y)^2}{4\pi} \right]}{I_{-3/4} \left[\frac{(k - \pi L_y)^2}{4\pi} \right]}. \quad (4.21)$$

In Fig. 4.3, we plot the value of k with the smallest positive imaginary part as the width of the junction L_y increases from zero to infinity solving the boundary condition at $y = L_y/2$. In the limit $L_y \rightarrow 0$, the $2\pi y$ correction in the operator (4.19) may be neglected, and the spectrum is composed of the non-degenerate eigenvalues $k = in\pi/L_y$ (the “leading” eigenvalue with the smallest imaginary part in the limit $L_y \rightarrow 0$ is thus zero). At a small finite L_y , the leading eigenvalue also becomes finite, but remains purely

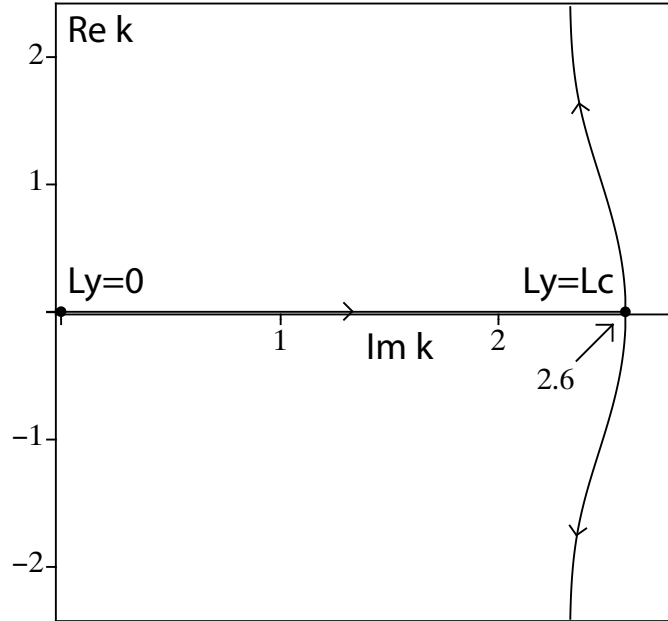


Figure 4.3: Effective wave number k , the lengths are given in units of ξ_H . A purely imaginary k indicates a monotonic decay.

imaginary. This follows from the combined symmetry of the complex conjugation and the reflection $y \mapsto -y$, which relates the eigenvalues k and $-k^*$. Since the leading eigenvalue is nondegenerate in the limit $L_y \rightarrow 0$, by continuity it must remain purely imaginary for sufficiently small L_y .¹

At larger L_y , two imaginary eigenvalues may collide and bifurcate to a pair of complex-conjugate eigenvalues. This happens at $L_y = L_c \approx 0.82$ (see Fig. 4.3). For $L_y > L_c$, we must take into account the contributions of the two modes (corresponding to the wave vectors k and $-k^*$) since they decay with the same rate (given by the imaginary part of k). In the discussion of the wide-junction limit (Sec. 4.4.2), we will show that those modes correspond to solutions localized close to the two edges of the junction $y = \pm L_y/2$ (for $L_y \gg 1$). The critical length L_c separates the regime where the superconducting anomalous Green function $F(x, y)$ decays along the x direction without oscillations (narrow junction, purely imaginary k) and the regime where the decay of the Green function is damped oscillatory (wide junction, complex k with both real and imaginary parts).

4.4.1 Narrow junction limit

For $L_y \ll 1$ (in the units of ξ_H) we expand the exact solution (4.20) in powers of L_y and find the wave number k solving the equation for the boundary condition (4.10) at $y = L_y/2$.

¹We thank M. Skvortsov for pointing to us this symmetry.

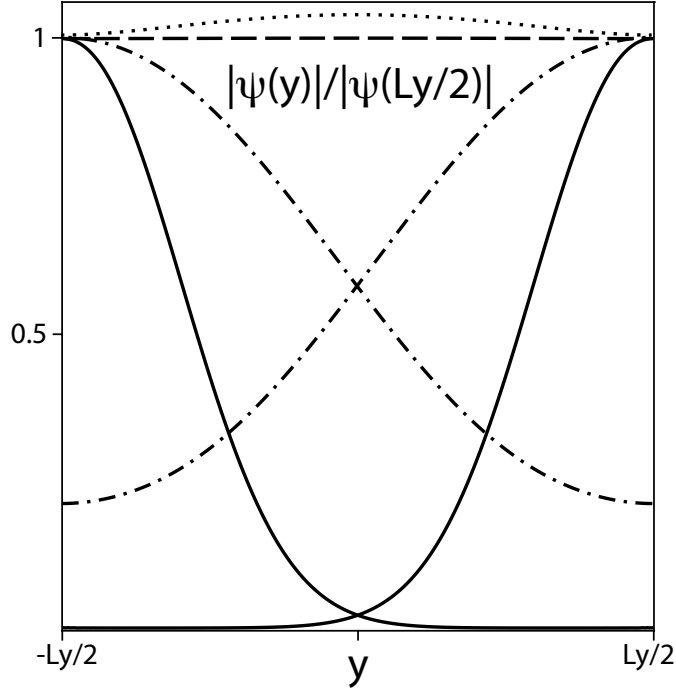


Figure 4.4: Superconducting pair correlations $|\psi|$ normalized to their value at the border of the junction for $L_y = 0.25\xi_H$ (dash), $0.75\xi_H$ (dot), ξ_H (dash dot) and $2.5\xi_H$ (solid).

This yields the expansion

$$k = \frac{i\pi}{\sqrt{3}}L_y \left(1 + \frac{4\pi^2}{63}L_y^4 + \frac{932\pi^4}{218295}L_y^8 + \frac{7976\pi^6}{13752585}L_y^{12} + \dots \right) \quad (4.22)$$

To the lowest order in L_y , the solution to the Usadel equation does not depend on y . In this limit, one can simply average the y^2 term in the Usadel equation (4.8) and arrive at a pair-breaking term [40, 95, 96, 98]

$$\frac{\hbar D}{2}\nabla_x^2 F(x) = (|\omega| + 2\Gamma)F(x). \quad (4.23)$$

with

$$\Gamma = -\frac{\hbar D k^2}{4} = \frac{D e^2 H^2 L_y^2}{12\hbar}. \quad (4.24)$$

This result obviously reproduces the first term in (4.22). For wider junctions, the dependence of the anomalous Green function $F(x, y)$ along the y direction cannot be neglected anymore, but as long as L_y remains smaller than L_c , the function $F(x, y)$ exhibits a monotonic exponential decay along the x direction.

4.4.2 Wide junction limit

In the limit of a wide junction $L_y \gg 1$ (as usual, in the units of ξ_H), the solution is determined by the two complex conjugate wave numbers k and $-k^*$. We show below that the asymptotic behavior of k (in the units of ξ_H^{-1}) is

$$k = \pi L_y + k_{\text{res}} \quad (4.25)$$

where k_{res} is the constant term in the expansion in L_y^{-1} .

Indeed, in the wide junction limit, each of the two zero modes (solutions to $A\psi = 0$) is localized near one of the two edges of the junction and decays quasiclassically towards the other edge. The solution localized near $y = -L_y/2$ should therefore have the quasiclassical wave vector in the operator (4.19) vanishing in that region, which immediately gives the leading asymptotics $k \approx \pi L_y$ (the solution localized at the opposite edge has $k \approx -\pi L_y$).

To get the subleading term k_{res} , we consider one of those zero modes (say, the one localized near $y = -L_y/2$). This zero mode decays quasiclassically towards the opposite edge of the junction, and with an exponential precision we can replace the boundary condition at $y = L_y/2$ by the decaying condition at infinity, $\psi(y \rightarrow \infty) = 0$. This selects a solution from (4.20) of the form

$$\psi = \sqrt{k + 2\pi y} K_{1/4} \left[\frac{(k + 2\pi y)^2}{4\pi} \right]. \quad (4.26)$$

Imposing now the boundary condition $\psi'(-L_y/2) = 0$ implies an equation on k_{res} :

$$K_{3/4} \left[\frac{(k_{\text{res}})^2}{4\pi} \right] = 0. \quad (4.27)$$

A numerical solution to this equation gives²

$$k_{\text{res}} \approx -1.68 + 2.32i. \quad (4.28)$$

We illustrate our calculation in Fig. 4.4, where we plot the zero modes below and above the transition. Below the transition (for $L_y < L_c$), the solution is nondegenerate and symmetric, while above the transition (for $L_y > L_c$) the two zero modes are pushed towards the edges of the junction. The characteristic size of the region near the edge where the proximity correlations are localized are of the order 1 [from the solution (4.26)], i.e., ξ_H in the physical units.

²The Macdonald function $K_{3/4}(z)$ does not have zeros on the principal sheet of the Riemann surface, therefore the solution must have $\pi/2 < |\arg k| < \pi$. We also impose the condition $\Im k > 0$, for the mode decaying along the x direction. Finally, under these constraints, we select the root with the smallest imaginary part. Technically, the second sheet of the Riemann surface may be accessed with the relation $K_{3/4}(e^{i\pi} z) = e^{-3\pi i/4} K_{3/4}(z) - i\pi I_{3/4}(z)$.

Finally, we can verify that the limit $L_y \gg 1$ does not require imposing more conditions on L_x . Indeed, we find numerically from (4.20) that when $L_y \rightarrow \infty$ the difference between the imaginary part (decay rate) of the zero mode with slowest decay and the zero mode with the second slowest decay saturates to a finite value, approximately 2.4. Since this difference is given in units of ξ_H^{-1} , our long junction assumption $L_x \gg \xi_H$ is sufficient to ensure that we can safely restrict ourselves to the slowest zero mode.

4.5 Josephson current

The transition between the two types of behavior of the anomalous Green function, purely decaying and decaying with oscillations, may be observed in the critical current of the SNS junction in a magnetic field. Our result on the transition is consistent with the previous numerical works [95, 96], which indicate that the oscillations appear when the width of the normal region L_y becomes of the order of the magnetic length ξ_H . We show below that the oscillations of the critical current in the SNS system are governed by the same wave vector k as the oscillations of the anomalous Green function $F_\infty(x, y)$ in the SN system discussed in Sec. 4.4.

In the long-junction limit, the anomalous Green function is given by the expression (4.16), and, using the expression (4.11), one arrives at the sinusoidal current-phase relation [7],

$$J_{\text{tot}} = I_c \sin 2\chi, \quad (4.29)$$

where J_{tot} is the total Josephson current (integrated over the y and z directions).

In the “pure decay” regime ($L_y < L_c$), the asymptotic behavior of $F_\infty(x, y)$ is

$$F_\infty(x, y) = F_B \psi(y) e^{ikx} \quad (4.30)$$

with a purely imaginary k (see Fig. 4.3), and $\psi(y)$ proportional to the zero mode of the operator (4.19). This results in the exponential decay of the critical current as a function of L_x :

$$I_c = 8\pi e \nu_0 D T L_z \left(\sum_{n=0}^{\infty} F_B \right) \frac{1}{i} \left[\int_{-L_y/2}^{L_y/2} (k + 2\pi y) \psi^2(y) dy \right] e^{-|k|L_x}, \quad (4.31)$$

where L_z is the dimension of the junction along the z direction. Note that this expression is real [since $\psi(y) = \psi^*(-y)$ in this regime] and positive (one checks this numerically).

In the regime of “decaying oscillations” ($L_y > L_c$), the anomalous Green function $F_\infty(x, y)$ contains contributions from two zero modes,

$$F_\infty(x, y) = F_B \left[\psi(y) e^{ikx} + \psi^*(-y) e^{-ik^*x} \right] \quad (4.32)$$

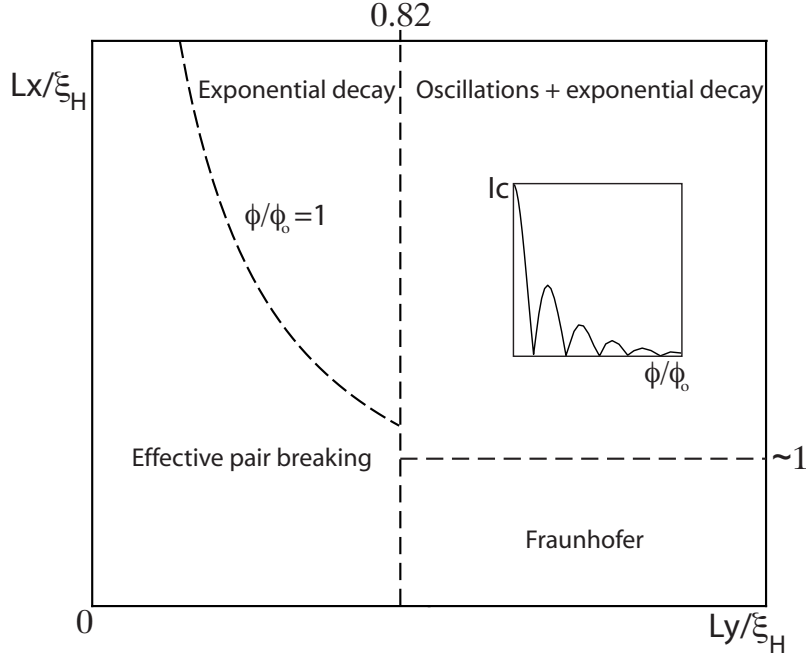


Figure 4.5: Phase diagram of the junction in the magnetic field. The left region corresponds to the pure decay regime while in the right one the critical current I_c exhibits interference patterns as a function of the flux of the field H .

[here $\psi(y) \neq \psi^*(-y)$ are the two zero modes of the operator (4.19)]. Integrating the critical current along the y direction, one finds

$$I_c = 8\pi e\nu_0 D T L_z \left(\sum_{n=0}^{\infty} F_B \right) \Im \left[\int_{-L_y/2}^{L_y/2} (k + 2\pi y) \psi^2(y) dy e^{ikL_x} \right], \quad (4.33)$$

so that $\Im k$ and $\Re k$ describe the rates of decay and oscillations of the critical current as a function of L_x , respectively. In Appendix E, we present the details of the derivation of (4.33). The derivation of (4.31) follows the same lines. Note that in the case of a wide junction, $L_y \gg \xi_H$, the localization of the superconducting pair correlations at the edge of the junction results in the localization of the superconducting current in the same region.

We sketch the phase diagram of the junction in Fig. 4.5 in the coordinates L_x and L_y . In experiments, however, one usually varies the external field for a given junction with fixed dimensions. In this setup, the easiest way to observe a transition between the two regimes is to study a junction with $L_x > L_y$ (theoretically, we assume $L_x \gg L_y$, but in practice L_x may be limited by the thermal length ξ_T and by the smallest measurable critical current). In this case, as the field H increases, one should be able to observe a crossover between the pure-decay regime and the decaying-oscillating regime as ξ_H crosses over L_y . At low fields

(for $\xi_H \gg L_y$), in the pure-decay regime, the field dependence of the critical current is

$$I_c = I_1 \frac{\phi}{\phi_0} \exp\left(-\frac{\pi}{\sqrt{3}} \frac{\phi}{\phi_0}\right) \quad (4.34)$$

where I_1 is of the order of the critical current in the absence of the field [and we have used the leading term in the asymptotics (4.22)]. This expression reproduces the existing result for a SNS junction with a finite depairing rate (4.24) [in our treatment, the approximation (4.16) implies assuming $\phi \gg \phi_0$] [100]

$$I_c = I_0 \frac{\frac{\pi}{\sqrt{3}} \frac{\phi}{\phi_0}}{\sinh\left(\frac{\pi}{\sqrt{3}} \frac{\phi}{\phi_0}\right)} \quad (4.35)$$

with I_0 the critical current in the absence of the field. Note that equation (4.35) is valid only for linearized Usadel equations while we will show in Sec. 4.6 that the domain of validity of the asymptotics (4.34) can be extended to non-linear situations. At high fields (for $\xi_H \ll L_y$), the critical current exhibits the decaying-oscillating behavior with

$$I_c = I_2 \frac{L_x}{L_y} \exp\left[-2.32 \frac{L_x}{\xi_H}\right] \sin\left[\frac{\pi\phi}{\phi_0} - 1.68 \frac{L_x}{\xi_H} + \varphi_0\right]. \quad (4.36)$$

Here I_2 is of the same order as I_1 and I_0 (the current in the absence of the external field), $\phi = HL_x L_y$ is the total flux through the junction, and φ_0 is a phase shift, which we do not compute here. Note that while both expressions (4.34) and (4.36) decay exponentially with increasing the field, the expression in the exponent of (4.34) is proportional to H , while that in the exponent of (4.36) only to \sqrt{H} .

If, however, one considers the current-field dependence for a contact with $L_x < L_y$, then one would observe a crossover from the Fraunhofer pattern (for $\xi_H \gg L_x$) [95, 96, 98]

$$I_c = I_0 \frac{\sin(\pi\phi/\phi_0)}{\pi\phi/\phi_0} \quad (4.37)$$

directly to the wide-junction regime (4.36), as the magnetic length ξ_H becomes shorter than L_x .

4.6 Applicability of the results

To simplify our discussion, we have considered in Sections 4.2–4.5 the linearized problem with rigid boundary conditions. However, our method is based on finding the zero modes of the operator (4.19) which describes the proximity effect in the middle of the junction. Therefore, our results remain valid for more general boundary conditions and for the non-linear case, as long as the junction is sufficiently long (so that the Green function $F_\infty(x, y)$ decays by a factor much larger than one by the middle of the junction). In this case, the

Usadel equation close to the middle of the junction can be linearized anyway, and our treatment of Sec. 4.4 can be performed in a similar way, albeit with more complicated boundary conditions. Therefore all the conclusions of Sections 4.4 and 4.5 about the different interference patterns of the critical current and about the transition value $L_c \approx 0.82\xi_H$ remain valid. The crucial condition for applicability of our method is thus that the junction is much longer than ξ_H [in the narrow-junction limit, we also need to assume that $\phi \gg \phi_0$ for applicability of our asymptotic formula (4.34)]. The only role of the boundary conditions and of the non-linearity of Usadel equations is the renormalization of the overall coefficients in the asymptotics (4.34) and (4.36).

Another approximation used in our calculation is the assumption of low temperature. As we have seen in the previous sections, the characteristic scale at which the anomalous Green function $F(x, y)$ varies is of the order ξ_H . Therefore, the assumption of low temperature [neglecting ω term in the Usadel equation (4.8)] implies $\xi_T \gg \xi_H$. Under this low-temperature assumption, the temperature enters only as small corrections to the calculations in the previous sections (including corrections to the zero-mode wave vector k).

We can now qualitatively discuss the high-temperature regime $\xi_T < \xi_H$. In this case, the decay of the anomalous Green function $F(x, y)$ along the x direction is determined mostly by ξ_T , rather than ξ_H , and, as a result, the critical current contains an exponential factor $\exp(-\kappa L_x)$ with $\kappa \approx \xi_T^{-1}$. However, one can still repeat much of the reasoning of Sec. 4.4 in the presence of the ω term. One then finds that in the limit $L_x \rightarrow \infty$, even at high temperature, one can still distinguish the two regimes of the purely decaying and oscillatory-decaying L_x dependence. The critical width L_c separating the two regimes is slightly decreased as compared to the low-temperature case: a dimensional estimate gives $L_c \propto \xi_H^{2/3} \xi_T^{1/3}$ at $\xi_T \ll \xi_H$. On the other hand, the same dimensional estimate indicates that the field contribution to the decay rate along the x direction is of the order $\xi_T^{1/3} \xi_H^{-4/3}$, which translates to a crossover from the purely Fraunhofer regime to the oscillatory-decaying regime at $L_x \sim \xi_H^{4/3} \xi_T^{-1/3}$, i.e., for slightly thicker junctions than at low temperatures.

4.7 Summary

To summarize, we consider a long diffusive SNS junction in an external magnetic field \mathbf{H} . We show that depending on the width of the junction relative to the magnetic length $\xi_H = \sqrt{\phi_0/H}$ two different regimes can be observed. For narrow junctions the anomalous Green function F decays monotonically along the junction while for wide junctions exponentially damped oscillations are present. We find that the transition between the two regimes occurs for a width $L_c \approx 0.82\xi_H$. Those different behaviors translate in a monotonic decay of the Josephson critical current (4.31) as a function of the magnetic flux through a narrow junction and in damped current oscillations for wide junctions. Finally, we show that for

wide links the current and the superconducting pair correlations are concentrated in a small region of size ξ_H close to the border of the junction.

The main finding of the present work [101], in comparison with previous studies of this problem, is the identification of the damped-oscillating phase for wide and long junctions. This phase resembles both the Fraunhofer regime (for wide and short junctions) and the damped phase (for narrow and long junctions). The period of oscillations is the same as in the Fraunhofer interference pattern, while the exponentially decaying factor resembles the damped phase.

Conceptually, the transition between the two asymptotic regimes for long junctions in our problem is similar to the transition between the two regimes in superconductor–ferromagnet–superconductor junctions with domains studied in Chapter 3 [42]. In both systems, the transition between the purely damped and damped-oscillating behavior is related to a bifurcation of the solution to the linearized Usadel equations.

Experimentally the limit of a long junction is accessible and has been the subject of recent experiments [98]. While the decaying regime has been observed, even though without a good quantitative agreement with the theory, the regime of decaying oscillations predicted here has not been reached, because the fields were not sufficiently high. In future experimental studies, it may be convenient to use junctions with the aspect ratio $L_x/L_y \sim 1$ to access this new damped-oscillating regime, in order to be able to use lower fields than for $L_x/L_y \gg 1$ junctions. In any case, an accurate analysis would be required to distinguish the decaying exponential regime predicted in our work from the distorted Fraunhofer pattern due to possible structural inhomogeneities of the critical current, as discussed in Ref. [47].

Chapter 5

Conclusion

The mere observation of transitions between the 0 and the π phase has constituted an important challenge to experimentalists. More than twenty years have passed between the first theoretical works suggesting the existence of SFS π junctions [3, 55] and their realization in experiments. After the pioneering works [51–54, 58, 60] which showed good qualitative agreement with the original theoretical predictions based on a quasi-one-dimensional model and a monodomain ferromagnetic interlayer, a better understanding of the actual magnetic structure of the ferromagnetic thin films is now necessary in order to progress towards the controlled realization of devices based on π junctions. Experimental results on the domain structure would also stimulate the interest in the long-range triplet component and challenge the existing theoretical predictions in this field of research [6].

Experimentally, a first insight into the presence of a domain structure can be given by the study of shifted Fraunhofer patterns. For a Josephson SFS junction with a monodomain ferromagnet, one expects a shift in the interference patterns by the net magnetization in the F layer, while in the presence of random domains the magnetization averages out and standard patterns are recovered [58]. The advantage of the method is to allow studying the ferromagnetic layer in the original SFS experimental setup. This might be important due to the possible [62] influence of the proximity effect on the domain structure. An important drawback is that no precise information on the size and form of the magnetic inhomogeneity is provided. The decoration method used in Ref. [61] offers a detailed image of the domain patterns. However, its spatial resolution is limited by the size of the decoration particles (in Ref. [61] the average size is of about ten nanometers). Higher resolutions are difficult to achieve since the saturation magnetization of the decoration particles decreases for small particles. The technique used in [61] is not sufficient to resolve magnetic inhomogeneities small enough to induce the effective spin-flip scattering expected from fits to the data. A rough estimate of the size of the magnetic inhomogeneity needed to get noticeable effects can be made from Eq. (3.31) (see also Refs. [20] and [41]) and yields domains smaller than

ten nanometers.

The theory of mesoscopic proximity structures has been developed via complementary use of analytical and numerical approaches. Numerical methods are useful in providing detailed fitting of experimental data or sometimes in giving a first insight into a phenomenon. Analytical approaches may give a better qualitative understanding of the physics by allowing to isolate the relevant parameters and may therefore help orienting experiments. The major part of the analytical works on hybrid structures uses the fact that quasiclassical formalism allows in many situations to reduce complicated inhomogeneous proximity systems to a simple one-dimensional problem with appropriate boundary conditions. However, as we have seen in Chapters 3 and 4, one needs sometimes to consider the physics beyond the quasi-one-dimensional geometry.

Appendix A

Collision integral in the presence of isotropic spin-flip scattering

We compute here the collision integral in the diffusive limit and in the presence of isotropic magnetic disorder (1.45). For simplicity, the derivation is done in the absence of the triplet component. The generalization to an arbitrary spin-structure of the Green function is straightforward.

We can write the collision integral (1.55) in terms of quasiclassical Green functions (1.53) (green functions integrated over $d\xi_p$ near the Fermi surface) using

$$\int \frac{d^3p}{(2\pi)^3} \check{G}(\mathbf{p}, \mathbf{p} - \mathbf{k}) = \hat{\tau}_3 \otimes \hat{\sigma}_0 \left(\nu_0 \pi i \int \frac{d\Omega_{\mathbf{p}}}{4\pi} \check{g}(\hat{\mathbf{p}}, \mathbf{k}) + \check{P} \int \frac{p^2 dp}{2\pi^2} \frac{1}{\xi_{\mathbf{p}}} \right). \quad (\text{A.1})$$

Here P represents the principal part of the integral for which only the normal state Green function gives a significant contribution ($\Delta \ll E_F$). The second term is proportional to the unit matrix in the Nambu \otimes spin space and can be incorporated into the chemical potential. Therefore, the self-energies in terms of the quasiclassical Green functions become

$$\Sigma_1(\hat{\mathbf{p}}, \mathbf{k}) = \frac{iv_F}{2} n_{imp} \int d\Omega_{\mathbf{p}_1} \sigma_1(\theta) g(\mathbf{p}_1, \mathbf{k}), \quad (\text{A.2})$$

and

$$\Sigma_2(\hat{\mathbf{p}}, \mathbf{k}) = \frac{iv_F}{2} n_{imp} \int d\Omega_{\mathbf{p}_1} \sigma_2(\theta) f(\mathbf{p}_1, \mathbf{k}), \quad (\text{A.3})$$

where we used the relation (1.41) between the scattering amplitudes $u_{1,2}$ (1.49), (1.50) and the corresponding cross sections $\sigma_{1,2}$ (Born approximation). Introducing

$$\sigma_{\mathbf{p}\mathbf{p}_1}^{sf} = \frac{1}{2} [\sigma_1(\theta) + \sigma_2(\theta)] \text{ and } \sigma_{\mathbf{p}\mathbf{p}_1} = \frac{1}{2} [\sigma_1(\theta) - \sigma_2(\theta)], \quad (\text{A.4})$$

we separate the matrix self-energy $\check{\Sigma}$ into a non-magnetic and a spin-flip part

$$\begin{aligned} \hat{\tau}_3 \otimes \hat{\sigma}_0 \check{\Sigma}(\hat{\mathbf{p}}, \mathbf{k}) &= \frac{iv_F}{2} n_{imp} \int d\Omega_{\mathbf{p}_1} \sigma_{\mathbf{p}\mathbf{p}_1}^{sf}(\theta) \tilde{g}(\mathbf{p}_1, \mathbf{k}) \\ &+ \frac{iv_F}{2} n_{imp} \int d\Omega_{\mathbf{p}_1} \sigma_{\mathbf{p}\mathbf{p}_1}(\theta) \check{\tau}_3 \tilde{g}(\mathbf{p}_1, \mathbf{k}) \check{\tau}_3. \end{aligned} \quad (\text{A.5})$$

We can also write the self-energies in terms of the scattering mean free times $\tau_{1,2}$ corresponding to the cross sections $\sigma_{1,2}$ following relation (1.43) and introduce the spin-flip time τ_s corresponding to σ^{sf}

$$\frac{2}{\tau_{sf}} = \frac{1}{\tau_1} + \frac{1}{\tau_2}. \quad (\text{A.6})$$

The collision integral \check{I} which we introduced in the Eilenberger equation (1.54) will therefore consist in two parts. To derive the contributions of the self-energies to the Usadel equation, we have to compute their average over the direction of the momentum \mathbf{p} . One can show (see for e.g. [14]) that the non-magnetic part vanishes after averaging over momentum direction. The spin-flip part of the collision integral does not vanish when averaged because \tilde{g} and $\check{\tau}_3 \tilde{g} \check{\tau}_3$ do not commute.

In the dirty limit, it is possible to expand the Green function in spherical harmonics. Using the expansion (1.61) to compute the collision integral and neglecting the second order terms in $\check{\mathbf{g}}$ (the vector part is expected to be smaller than the spherical part $\langle \check{g} \rangle$), we get for the spin-flip part of the collision integral averaged over the momentum direction

$$\begin{aligned} \langle \check{I}^s \rangle &= \left\langle \frac{iv_F}{2} n_{imp} \int \frac{d\Omega_p}{4\pi} \left[\int d\Omega_{p'} \sigma_{\mathbf{p},\mathbf{p}'}^{sf} \check{\tau}_3 \tilde{g} \check{\tau}_3, \tilde{g} \right] \right\rangle \\ &= \begin{pmatrix} 0 & \frac{1}{\tau_{sf}} \langle g \rangle \langle f \rangle \\ \frac{1}{\tau_{sf}} \langle g \rangle \langle f^\dagger \rangle & 0 \end{pmatrix}. \end{aligned} \quad (\text{A.7})$$

The non vanishing off-diagonal terms will introduce the effect of isotropic spin-flip scattering in the Usadel equation (1.62) (recall that we have considered the simple case where triplet correlations are absent).

Appendix B

Gap curve close to Γ_{sf}^c

In this appendix, we derive the asymptotic form of the minigap curve close to Γ_{sf}^c . We have seen previously that the minigap E_g is the largest energy compatible with equation (1.79). Introducing

$$\begin{aligned} z &= \sinh \beta + \alpha \\ z_1 &= \sinh \beta^1 + \alpha \\ \text{with } \alpha &:= \frac{\epsilon}{2\Gamma_{\text{sf}}}, \end{aligned}$$

we can rewrite equation (1.79) in the form

$$2\sqrt{\Gamma_{\text{sf}}} = \int_{\alpha}^{z_1} \frac{1}{\sqrt{z_1^2 - z^2}} \cdot \frac{1}{\sqrt{1 + (z - \alpha)^2}} dz. \quad (\text{B.1})$$

The integral in the r.h.s. is a function of z_1 and α , which we denote $Y(z_1, \alpha)$. To determine the minigap, we will find the maximum value of Y over z_1 for a given value of the parameter α .

The critical spin-flip scattering rate (1.80) can be obtained setting $\alpha = 0$ and maximizing (B.1). It turns out that $Y(z_1, \alpha)|_{\alpha=0}$ is largest for $z_1 = 0$. The next step is to go to finite energies and expand Y in α . We write

$$Y(z_1, \alpha) \approx Y(z_1, \alpha)|_{\alpha=0} + \frac{\partial Y(z_1, \alpha)}{\partial \alpha} \Big|_{\alpha=0} \alpha, \quad (\text{B.2})$$

where

$$\frac{\partial Y(z_1, \alpha)}{\partial \alpha} \Big|_{\alpha=0} = -\frac{1}{z_1} + \frac{z_1}{1 + z_1^2}. \quad (\text{B.3})$$

For a small α , the maximum of Y is expected to be close to the zero energy value $z_1 = 0$ and the second term $\sim O(z_1)$ can be neglected. The first term in the r.h.s. can be expanded

$$Y(z_1, \alpha)|_{\alpha=0} \approx \int_0^1 \frac{1}{\sqrt{1 - s^2}} \left[1 - \frac{(z_1 s)^2}{2} \right] ds. \quad (\text{B.4})$$

where $s = \frac{z}{z_1}$. Taking the derivative of Y over z_1 , using the expansion (B.2), we find that the maximum of Y is obtained for

$$\hat{z}_1 = \left(\frac{\alpha}{\sqrt{\Gamma_{\text{sf}}^c}} \right)^{1/3}. \quad (\text{B.5})$$

substituting back this result in (B.2) and using the definitions of $\alpha = \frac{\epsilon}{2\Gamma_{\text{sf}}}$ and $Y = 2\sqrt{\Gamma_{\text{sf}}}$ we obtain an expression for $E_g(\Gamma_{\text{sf}})$. Finally we write $\Gamma_{\text{sf}} = \Gamma_{\text{sf}}^c - \delta\Gamma_{\text{sf}}$ and expand in the small $\delta\Gamma_{\text{sf}}$ to get the asymptotic dependence (1.83).

Appendix C

Zero energy density of states for

$$\Gamma_{\text{sf}} > \Gamma_{\text{sf}}^{\text{c}}$$

For $\Gamma_{\text{sf}} > \Gamma_{\text{sf}}^{\text{c}}$ the DoS in the N-region is finite at any energy. In this domain the Usadel equation (1.74) at zero energy has a solution with θ real. Applying again the procedure of the first integral (1.78), but this time for a real θ , we get

$$\int_{\frac{\pi}{2}}^{\theta(x)} \frac{d\theta}{\sqrt{\cos^2 \theta^1 - \cos^2 \theta}} = -2\sqrt{\Gamma_{\text{sf}}} x. \quad (\text{C.1})$$

Inverting this elliptic integral, we can find a complete zero energy solution for equation (1.74). This solution involves the function $\text{dn}(u, k)$, which is one of the Jacobi elliptic functions, defined as inversions of the canonical forms of elliptic integrals (we follow the notations used in Refs. [28, 102])

$$\theta(x) = \arcsin \left[\frac{\sin \theta^1}{\text{dn}(2\sqrt{\Gamma_{\text{sf}}}(x-1), \cos \theta^1)} \right], \quad (\text{C.2})$$

where θ^1 can be determined imposing the rigid boundary condition (1.77) at $x = 0$

$$\sin \theta^1 = \text{dn} \left[-2\sqrt{\Gamma_{\text{sf}}}, \cos \theta^1 \right]. \quad (\text{C.3})$$

In the inset of Fig. C.1, we use relation (C.2) to represent the dependence on position of the DoS in the N-region for two different spin-flip rates. As expected the density of states increases when we move away from the interface. For large spin-flip scattering rates, the elliptic solution (C.2) saturates to the normal state bulk value $\theta(x) = 0$, everywhere except in a thin domain close to the SN interface (rigid boundary at $x = 0$).

Near the critical spin-flip rate, we found a square root dependence of the zero energy local DoS on Γ_{sf} . Expanding the integrand in (C.1) in the small $\cos \theta^1$, we obtain that for

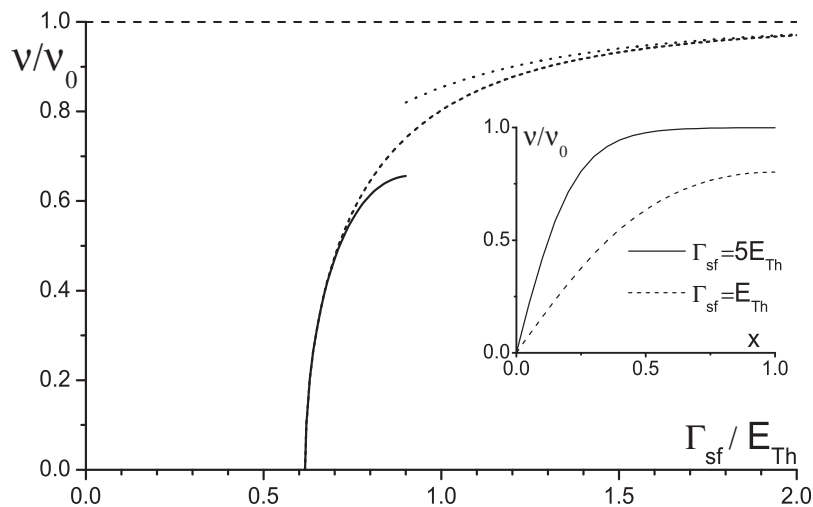


Figure C.1: Dependence of the zero energy local DoS, at the open boundary, on the spin-flip scattering rate: asymptotic expression near Γ_{sf}^c (solid line), complete elliptic solution (dashed line) saturating to the normal state bulk value ν_0 and its asymptotics at large Γ_{sf} (dots). The inset shows the dependence on position of the DoS for $\Gamma_{sf} = E_{Th}$ and $\Gamma_{sf} = 5 E_{Th}$.

$\Gamma_{sf} \rightarrow \Gamma_{sf}^c$ the density of states at the interface with vacuum is given by

$$\frac{\nu(\epsilon=0, x=1)}{\nu_0} = \sqrt{2} \left[\frac{\delta\Gamma_{sf}}{\Gamma_{sf}^c} \right]^{1/2} - \frac{11}{8\sqrt{2}} \left[\frac{\delta\Gamma_{sf}}{\Gamma_{sf}^c} \right]^{3/2} + \dots \quad (C.4)$$

In the limit of large spin-flip rates, when the density of states approaches the normal state one, the expansion [103] of the elliptic integral in (C.1) near $\cos\theta^1 = 1$ leads to an asymptotic expression for the DoS at the interface with vacuum

$$\frac{\nu(\epsilon=0, x=1)}{\nu_0} = 1 - 8e^{-4\sqrt{\Gamma_{sf}}} + \dots \quad (C.5)$$

In Fig. C.1, we compare the expressions (C.4) and (C.5) for the DoS at the open boundary with values obtained using the complete zero energy elliptic solution (C.2).

Appendix D

Solving the linearized Usadel equations

To solve the system of linear equations (2.12) and (2.13) with the 12 variables $A_{\pm,\perp}^j$ and $B_{\pm,\perp}^j$, it is convenient first to reduce the number of variables by resolving the continuity relations (2.13) in terms of the six variables

$$\begin{aligned}\beta_{\pm} &= B_{\pm}^1 \mp B_{\perp}^1 \tan \frac{\theta}{2} = B_{\pm}^2 \pm B_{\perp}^2 \tan \frac{\theta}{2} \\ \beta_{\perp} &= B_{\perp}^1 + \frac{B_{+}^1 - B_{-}^1}{2} \tan \frac{\theta}{2} = B_{\perp}^2 - \frac{B_{+}^2 - B_{-}^2}{2} \tan \frac{\theta}{2} \\ \alpha_{\pm} &= \lambda_{\pm} A_{\pm}^1 \mp \lambda_{\perp} A_{\perp}^1 \tan \frac{\theta}{2} = \lambda_{\pm} A_{\pm}^2 \pm \lambda_{\perp} A_{\perp}^2 \tan \frac{\theta}{2} \\ \alpha_{\perp} &= \lambda_{\perp} A_{\perp}^1 + \frac{\lambda_{+} A_{+}^1 - \lambda_{-} A_{-}^1}{2} \tan \frac{\theta}{2} = \lambda_{\perp} A_{\perp}^2 - \frac{\lambda_{+} A_{+}^2 - \lambda_{-} A_{-}^2}{2} \tan \frac{\theta}{2}.\end{aligned}$$

Solving now the set of 6 equations (2.12) produces the solution

$$\begin{aligned}\alpha_{\perp} &= \frac{2\Delta}{\omega} \lambda_{+} \lambda_{-} \lambda_{\perp} \cosh(\lambda_{\perp} d) \frac{p_{-}}{p_{+}^2 - p_{-}^2 + \tan^2 \frac{\theta}{2} (p_{+} q_{+} + p_{-} q_{-})} \tan \frac{\theta}{2} (1 + \tan^2 \frac{\theta}{2}) \cos \chi \\ \beta_{+} - \beta_{-} &= -\frac{4\Delta}{\omega} \lambda_{+} \lambda_{-} \sinh(\lambda_{\perp} d) \frac{p_{-}}{p_{+}^2 - p_{-}^2 + \tan^2 \frac{\theta}{2} (p_{+} q_{+} + p_{-} q_{-})} (1 + \tan^2 \frac{\theta}{2}) \cos \chi \\ \beta_{+} + \beta_{-} &= \frac{4\Delta}{\omega} \lambda_{+} \lambda_{-} \sinh(\lambda_{\perp} d) \frac{p_{+} + \tan^2 \frac{\theta}{2} q_{+}}{p_{+}^2 - p_{-}^2 + \tan^2 \frac{\theta}{2} (p_{+} q_{+} + p_{-} q_{-})} \cos \chi \\ \alpha_{+} - \alpha_{-} &= -\frac{4i\Delta}{\omega} \lambda_{+} \lambda_{-} \lambda_{\perp} \cosh(\lambda_{\perp} d) \frac{q_{-}}{q_{+}^2 - q_{-}^2 + \tan^2 \frac{\theta}{2} (p_{+} q_{+} + p_{-} q_{-})} (1 + \tan^2 \frac{\theta}{2}) \sin \chi \\ \alpha_{+} + \alpha_{-} &= -\frac{4i\Delta}{\omega} \lambda_{+} \lambda_{-} \lambda_{\perp} \cosh(\lambda_{\perp} d) \frac{q_{+} + \tan^2 \frac{\theta}{2} p_{+}}{q_{+}^2 - q_{-}^2 + \tan^2 \frac{\theta}{2} (p_{+} q_{+} + p_{-} q_{-})} \sin \chi \\ \beta_{\perp} &= \frac{2i\Delta}{\omega} \lambda_{+} \lambda_{-} \sinh(\lambda_{\perp} d) \frac{q_{-}}{q_{+}^2 - q_{-}^2 + \tan^2 \frac{\theta}{2} (p_{+} q_{+} + p_{-} q_{-})} \tan \frac{\theta}{2} (1 + \tan^2 \frac{\theta}{2}) \sin \chi,\end{aligned}$$

where

$$\begin{aligned} p_{\pm} &= \lambda_+ \lambda_- \sinh \lambda_{\perp} d (\cosh \lambda_+ d \pm \cosh \lambda_- d) \\ q_{\pm} &= \lambda_{\perp} \cosh \lambda_{\perp} d (\lambda_+ \sinh \lambda_- d \pm \lambda_- \sinh \lambda_+ d). \end{aligned}$$

In terms of the new variables, the supercurrent (2.16) becomes

$$\begin{aligned} I_J &= ie\nu_0 DS\pi T \sum_{\omega} \left[\frac{1}{4} (\alpha_+ + \alpha_-)(\chi)(\beta_+ + \beta_-)(-\chi) \right. \\ &\quad \left. + \frac{1}{4(1 + \tan^2 \frac{\theta}{2})} (\alpha_+ - \alpha_-)(\chi)(\beta_+ - \beta_-)(-\chi) + \frac{\alpha_{\perp}(\chi)\beta_{\perp}(-\chi)}{1 + \tan^2 \frac{\theta}{2}} \right] \\ &\quad - [\chi \leftrightarrow -\chi]. \end{aligned} \tag{D.1}$$

The resulting current-phase relation is sinusoidal with the critical current

$$\begin{aligned} I_c(\theta) &= 4I_0 \xi_h T^2 \sum_{\omega} \frac{(\lambda_+ \lambda_-)^2 \lambda_{\perp} \sinh 2\lambda_{\perp} d}{\omega^2} \\ &\quad \times \frac{(q_+ + p_+ \tan^2 \frac{\theta}{2})(p_+ + q_+ \tan^2 \frac{\theta}{2}) - (1 - \tan^4 \frac{\theta}{2})p_- q_-}{(p_+^2 - p_-^2 + \tan^2 \frac{\theta}{2}(p_+ q_+ + p_- q_-))(q_+^2 - q_-^2 + \tan^2 \frac{\theta}{2}(p_+ q_+ + p_- q_-))}. \end{aligned} \tag{D.2}$$

Eq. (D.2) can be used for numerical calculations of the critical current for an arbitrary relative orientation of the ferromagnetic exchange fields and for any value of their magnitude (e.g., for producing the plot in Fig. 2.5). In the body of the article, a simpler expression for the current is given in the high-exchange-field limit (Eq. (2.27)).

Appendix E

Josephson current for the SNS junction in a magnetic field

We derive here the expression for the total current (4.33) for $L_y > L_c$. We have seen in Sec. 4.4 that in the limit of a long junction, we can write the solution of the Usadel equation in the form

$$F(x, y) \approx F_\infty(x, y)e^{ix} + F_\infty(L_x - x, -y)e^{-ix} \quad (\text{E.1})$$

where for $L_y > 0.82$ the contributions of two zero modes need to be taken into account

$$F_\infty(x, y) = F_B \left[\psi_k(y)e^{ikx} + \psi_{-k^*}(y)e^{-ik^*x} \right] \quad (\text{E.2})$$

We can then compute the local current (4.11). Using the fact that the operation $k \leftrightarrow -k^*$ associated with the mirror operation $y \leftrightarrow -y$ corresponds to the complex conjugation in the zero-mode equation $A\psi_k = 0$ (with A given by (4.19)), we obtain the total current after integration along the y and z coordinates

$$I_c = 8\pi e\nu_0 DTL_z \left(\sum_{n=0}^{\infty} F_B \right) \Im \left[\int_{-L_y/2}^{L_y/2} (k + 2\pi y) \psi_k^2 dy e^{ikL_x} \right] + \int_{-L_y/2}^{L_y/2} \Re(\psi_k \psi_{-k^*}) \Im k e^{-\Im k L_x} + 2\pi y \Im(\psi_k \psi_{-k^*} e^{-\Im k L_x}) dy, \quad (\text{E.3})$$

We will prove now that the second term in (E.3) is always zero. Consider the integral

$$\int_{-L_y/2}^{L_y/2} \psi_{-k^*}(y) \psi_k''(y) - \psi_k(y) \psi_{-k^*}''(y) dy. \quad (\text{E.4})$$

By partial integration, it is easy to show that this integral is zero, recall that from (4.10)

$$\left[\psi_k'(y) \right]_{y=\pm L_y/2} = 0. \quad (\text{E.5})$$

The functions ψ_k are zero modes of the operator $A = \nabla_y^2 - (k + 2\pi y)^2$ we can thus write

$$\int_{-L_y/2}^{L_y/2} (k - k^*)\psi_{-k^*}(y)\psi_k(y) + 2\pi y\psi_{-k^*}(y)\psi_k(y)dy = 0. \quad (\text{E.6})$$

Using the fact that $\psi_{-k^*}(y) = \psi_k^*(-y)$ we get that the second term in (E.3) is zero and the final expression for the total current becomes (4.33)

$$I_c = 8\pi e\nu_0 D T L_z \left(\sum_{n=0}^{\infty} F_B \right) \Im \left[\int_{-L_y/2}^{L_y/2} (k + 2\pi y)\psi^2(y)dy e^{ikL_x} \right]. \quad (\text{E.7})$$

The derivation of the current (4.31) for $L_y < L_c$ follows similar lines, with a single purely imaginary wave vector k .

Bibliography

- [1] A. I. Buzdin, *Rev. Mod. Phys.* **77**, 935 (2005).
- [2] E. A. Demler, G. B. Arnold, and M. R. Beasley, *Phys. Rev. B* **55**, 15174 (1997).
- [3] L. N. Bulaevskii, V. V. Kuzii, and A. A. Sobyanin, *Pis'ma Zh. Eksp. Teor. Fiz.* **25**, 314 (1977), [*JETP Lett.* **25**, 290 (1977)].
- [4] P. G. De Gennes, *Rev. Mod. Phys.* **36**, 225 (1964).
- [5] J. Bardeen, L. N. Cooper, and J. R. Schrieffer, *Phys. Rev.* **108**, 1175 (1957).
- [6] F. S. Bergeret, A. F. Volkov, and K. B. Efetov, *Rev. Mod. Phys.* **77**, 1321 (2005).
- [7] A. A. Golubov, M. Y. Kupriyanov, and E. Il'ichev, *Rev. Mod. Phys.* **76**, 411 (2004).
- [8] P. Charlat, Ph.D. thesis, Université Joseph-Fourier - Grenoble I (1997).
- [9] J. Clarke and A. I. Braginski, eds., *The SQUID Handbook: Applications of SQUIDS and SQUID systems*, vol. II (Wiley-VCH, 2004).
- [10] I. Zutic, J. Fabian, and S. D. Sarma, *Rev. Mod. Phys.* **76**, 323 (2004).
- [11] L. B. Ioffe, V. B. Geshkenbein, M. V. Feigelman, A. L. Fauchere, and G. Blatter, *Nature* **398**, 679 (1999).
- [12] L. B. Ioffe, M. V. Feigel'man, A. Ioselevich, D. Ivanov, M. Troyer, and G. Blatter, *Nature* **415**, 503 (2002).
- [13] K. D. Usadel, *Phys. Rev. Lett.* **25**, 507 (1970).
- [14] N. Kopnin, *Theory of nonequilibrium superconductivity* (Oxford University Press, 2001).
- [15] P. W. Anderson, *J. Phys. Chem. Solids* **11**, 26 (1959).
- [16] A. F. Andreev, *Zh. Eksp. Teor. Fiz.* **46**, 1823 (1964), [*Sov. Phys. JETP* **19**, 1228 (1964)].

-
- [17] L. P. Gor'kov, Zh. Eksperim. i Teor. Fiz. **34**, 935 (1958), [Sov. Phys. JETP **7**, 505 (1958)].
- [18] P. G. De Gennes, *Superconductivity of Metals and Alloys* (W.A Benjamin. INC. New-York, 1966).
- [19] Y. Maeno, T. M. Rice, and M. Sigrist, Physics Today **54**, 42 (2001).
- [20] D. A. Ivanov and Y. V. Fominov, Phys. Rev. B **73**, 214524 (2006).
- [21] A. A. Abrikosov and L. P. Gor'kov, Zh. Eksp. Teor. Fiz. **39**, 1781 (1960), [Sov. Phys. JETP **12**, 1243 (1961)].
- [22] A. Abrikosov, L. Gor'kov, and I. Y. Dzyaloshinskii, *Quantum field theoretical methods in statistical physics* (Pergamon Press, 1965).
- [23] G. Eilenberger, Z. Phys. **214**, 195 (1968).
- [24] L. V. Keldysh, Zh. Eksp. Teor. Fiz. **47**, 1515 (1964), [Sov. Phys. JETP **20**, 1018 (1965)].
- [25] G. M. Eliashberg, Zh. Eksp. Teor. Fiz. **61**, 1254 (1971), [Sov. Phys. JETP **34**, 668 (1972)].
- [26] A. Zaitsev, Zh. Eksp. Teor. Fiz. **86**, 1742 (1984), [Sov. Phys. JETP **59**, 1015 (1984)].
- [27] M. Y. Kupriyanov and V. F. Lukichev, Zh. Eksp. Theor. Fiz. **94**, 139 (1988), [Sov. Phys. JETP **67**, 1163 (1988)].
- [28] A. Altland, B. D. Simons, and D. Taras-Semchuk, Adv. Phys. **49**, 321 (2000).
- [29] A. Millis, D. Rainer, and J. A. Sauls, Phys. Rev. B **38**, 4504 (1988).
- [30] J. Kopu, M. Eschrig, J. C. Cuevas, and M. Fogelström, Phys. Rev. B **69**, 094501 (2004).
- [31] M. Fogelström, Phys. Rev. B **62** (2000).
- [32] K. Maki, *Superconductivity*, vol. II (Marcel Dekker, Inc., 1966).
- [33] P. Fulde and R. A. Ferrell, Phys. Rev. **135**, A550 (1964).
- [34] A. I. Larkin and Y. N. Ovchinnikov, Zh. Eksp. Teor. Fiz. p. 1136 (1964), [Sov. Phys. JETP **20**, 762, 1965].
- [35] A. A. Golubov and M. Y. Kupriyanov, J. Low Temp. Phys. **70**, 83 (1988).
- [36] E. Scheer, W. Belzig, Y. Naveh, M. H. Devoret, D. Esteve, and C. Urbina, Phys. Rev. Lett. **86**, 284 (2001).

-
- [37] G. Rubio-Bollinger, C. delasHeras, E. Bascones, N. Agraït, F. Guinea, and S. Vieira, *Phys. Rev. B* **67**, 121407(R) (2003).
- [38] H. le Sueur, P. Joyez, H. Pothier, C. Urbina, and D. Esteve, *Phys. Rev. Lett.* **100**, 197002 (2008).
- [39] J. A. Melsen, P. W. Brouwer, K. M. Frahm, and C. W. J. Beenakker, *Europhys. Lett.* **35**, 7 (1996).
- [40] B. Crouzy, E. Bascones, and D. A. Ivanov, *Phys. Rev. B* **72**, 092501 (2005).
- [41] D. A. Ivanov, Y. V. Fominov, M. A. Skvortsov, and P. M. Ostrovsky, arXiv:0907.0113 (unpublished) (2009).
- [42] B. Crouzy, S. Tollis, and D. A. Ivanov, *Phys. Rev. B* **76**, 134502 (2007).
- [43] F. Zhou, P. Charlat, B. Spivak, and B. Pannetier, *J. Low Temp. Phys.* **110**, 841 (1998).
- [44] D. A. Ivanov, R. von Roten, and G. Blatter, *Phys. Rev. B* **66**, 052507 (2002).
- [45] P. M. Ostrovsky, M. A. Skvortsov, and M. V. Feigel'man, *Phys. Rev. Lett.* **87**, 027002 (2001).
- [46] B. D. Josephson, *Rev. Mod. Phys.* **36**, 216 (1964).
- [47] A. Barone and G. Paterno, *Physics and Applications of the Josephson Effect* (Wiley, New York, 1982).
- [48] E. Goldobin, D. Koelle, R. Kleiner, and A. Buzdin, *Phys. Rev. B* **76**, 224523 (2007).
- [49] T. Yamashita, K. Tanikawa, S. Takahashi, and S. Maekawa, *Phys. Rev. Lett.* **95**, 097001 (2005).
- [50] A. Bauer, J. Bentner, M. Aprili, M. L. D. Rocca, M. Reinwald, W. Wegscheider, and C. Strunk, *Phys. Rev. Lett.* **92**, 217001 (2004).
- [51] T. Kontos, M. Aprili, J. Lesueur, F. Genet, B. Stephanidis, and R. Boursier, *Phys. Rev. Lett.* **89**, 137007 (2002).
- [52] V. V. Ryazanov, V. A. Oboznov, A. Y. Rusanov, A. V. Veretennikov, A. A. Golubov, and J. Aarts, *Phys. Rev. Lett.* **86**, 2427 (2001).
- [53] V. V. Ryazanov, V. A. Oboznov, A. S. Prokofiev, V. V. Bolginov, and A. K. Feofanov, *J. Low Temp. Phys.* **136**, 385 (2004).
- [54] V. A. Oboznov, V. V. Bol'ginov, A. K. Feofanov, V. V. Ryazanov, and A. I. Buzdin, *Phys. Rev. Lett.* **96**, 197003 (2006).

-
- [55] A. I. Buzdin, L. N. Bulaevskii, and S. V. Panyukov, *Pis'ma Zh. Eksp. Teor. Fiz.* **35**, 147 (1982), [*JETP Lett.* **35**, 178 (1982)].
- [56] A. I. Buzdin and M. Y. Kupriyanov, *Pis'ma Zh. Eksp. Teor. Fiz.* **53**, 308 (1991), [*JETP Lett.* **53**, 321 (1991)].
- [57] M. Houzet, V. Vinokur, and F. Pistolesi, *Phys. Rev. B* **72**, 220506(R) (2005).
- [58] A. A. Bannykh, J. Pfeiffer, V. S. Stolyarov, I. E. Batov, V. V. Ryazanov, and M. Weides, *Phys. Rev. B* **79**, 054501 (2009).
- [59] J. W. A. Robinson, S. Piano, G. Burnell, C. Bell, and M. G. Blamire, *Phys. Rev. Lett.* **97**, 177003 (2006).
- [60] T. S. Khaire, W. P. Pratt, and N. O. Birge, *Phys. Rev. B* **79**, 094523 (2009).
- [61] I. S. Veshchunov, V. A. Oboznov, A. N. Rossolenko, A. S. Prokofiev, L. Y. Vinnikov, A. Y. Rusanov, and D. V. Matveev, *JETP Letters* **88**, 758 (2008).
- [62] M. Fauré and A. I. Buzdin, *Phys. Rev. Lett.* **94**, 187202 (2005).
- [63] F. S. Bergeret, A. F. Volkov, and K. B. Efetov, *Phys. Rev. B* **64**, 134506 (2001).
- [64] Y. M. Blanter and F. W. J. Hekking, *Phys. Rev. B* **69**, 024525 (2004).
- [65] V. N. Krivoruchko and E. A. Koshina, *Phys. Rev. B* **64**, 172511 (2001).
- [66] M. A. Khasawneh, J. W. P. Pratt, and N. O. Birge, *Phys. Rev. B* **80**, 020506 (2009).
- [67] F. S. Bergeret, A. F. Volkov, and K. B. Efetov, *Phys. Rev. Lett.* **86**, 3140 (2001).
- [68] E. A. Koshina and V. N. Krivoruchko, *Zh. Eksp. Teor. Fiz.* **71**, 182 (2000), [*JETP Lett.* **71**, 123 (2000)].
- [69] A. Buzdin and I. Baladie, *Phys. Rev. B* **67**, 184519 (2003).
- [70] M. Fauré, A. I. Buzdin, A. A. Golubov, and M. Y. Kupriyanov, *Phys. Rev. B* **73**, 064505 (2006).
- [71] I. B. Sperstad, J. Linder, and A. Sudbø, *Phys. Rev. B* **78**, 104509 (2008) **78**, 104509 (2008).
- [72] B. Crouzy, S. Tollis, and D. A. Ivanov, *Phys. Rev. B* **75**, 054503 (2007).
- [73] M. Houzet and A. I. Buzdin, *Phys. Rev. B* **76**, 060504(R) (2007).
- [74] J. C. Cuevas and M. Fogelström, *Phys. Rev. B* **64**, 104502 (2001).
- [75] M. Eschrig, J. Kopu, J. C. Cuevas, and G. Schön, *Phys. Rev. Lett.* **90**, 137003 (2003).

-
- [76] M. Weides, M. Kemmler, E. Goldobin, D. Koelle, R. Kleiner, H. Kohlstedt, and A. I. Buzdin, *Appl. Phys. Lett.* **89**, 122511 (2006).
- [77] S. Oh, Y. Kim, D. Youm, and M. Beasley, *Phys. Rev. B* **63**, 052501 (2000).
- [78] V. Shelukhin, A. Tsukernik, M. Karpovski, Y. Blum, K. B. Efetov, A. F. Volkov, T. Champel, M. Eschrig, T. Lofwander, G. Schön, et al., *Phys. Rev. B* **73**, 174506 (2006).
- [79] P. Koorevaar, Y. Suzuki, R. Coehoorn, and J. Aarts, *Phys. Rev. B* **49**, 441 (1994).
- [80] G. Verbanck, C. D. Potter, R. Schad, P. Belien, V. V. Moshchalkov, and Y. Bruynseraede, *Physica C* **235-240**, 3295 (1994).
- [81] L. N. Bulaevskii and E. M. Chudnovsky, *Phys. Rev. B* **63**, 012502 (2000).
- [82] E. B. Sonin, *Phys. Rev. B* **66**, 136501 (2002).
- [83] L. N. Bulaevskii, E. M. Chudnovsky, and M. Daumens, *Phys. Rev. B* **66**, 136502 (2002).
- [84] M. Daumens and Y. Ezzahri, *Phys. Lett. A* **306**, 344 (2003).
- [85] H. Sellier, C. Baraduc, F. Lefloch, and R. Calemczuk, *Phys. Rev. B* **68**, 054531 (2003).
- [86] Y. V. Fominov, A. F. Volkov, and K. B. Efetov, *Phys. Rev. B* **75**, 104509 (2007).
- [87] A. F. Volkov and A. Anishchanka, *Phys. Rev. B* **71**, 024501 (2005).
- [88] T. Champel, T. Lofwander, and M. Eschrig, *Phys. Rev. Lett.* **100**, 077003 (2008).
- [89] A. I. Buzdin, *Pis'ma Zh. Eksp. Teor. Fiz.* **42**, 283 (1985).
- [90] A. I. Buzdin and A. E. Koshelev, *Phys. Rev. B* **67**, 220504(R) (2003).
- [91] F. S. Bergeret, A. F. Volkov, and K. B. Efetov, *Phys. Rev. Lett.* **86**, 4096 (2001).
- [92] W. Belzig, C. Bruder, and G. Schön, *Phys. Rev. B* **54**, 9443 (1996).
- [93] P. M. Ostrovsky, Y. V. Fominov, and M. V. Feigel'man, *Phys. Rev. B* **74**, 104505 (2006).
- [94] M. S. Crosser, J. Huang, F. Pierre, P. Virtanen, T. T. Heikkilä, F. K. Wilhelm, and N. O. Birge, *Phys. Rev. B* **77**, 014528 (2008).
- [95] J. C. Cuevas and F. S. Bergeret, *Phys. Rev. Lett.* **99**, 217002 (2007).
- [96] F. S. Bergeret and J. C. Cuevas, *J. Low Temp. Phys.* **153**, 304 (2008).

- [97] G. Mohammadkhani, M. Zareyan, and Y. M. Blanter, *Phys. Rev. B* **77**, 014520 (2008).
- [98] L. Angers, F. Chiodi, G. Montambaux, M. Ferrier, S. Guéron, H. Bouchiat, and J. C. Cuevas, *Phys. Rev. B* **77**, 165408 (2008).
- [99] M. Abramowitz and I. A. Stegun, *Handbook of Mathematical Functions with Formulas, Graphs, and Mathematical Tables* (New York: Dover, 1972).
- [100] G. Montambaux, arXiv:0707.0411v1 (unpublished) (2007).
- [101] B. Crouzy and D. A. Ivanov, arXiv:0907.0632 (2009).
- [102] D. F. Lawden, *Elliptic Functions and Applications* (Springer, 1989).
- [103] B. C. Carlson and J. L. Gustafson, *SIAM J. Math. Anal.* **25**, 288 (1994).

Acknowledgements

First of all, I would like to thank Dmitri for accepting me in his group and suggesting my research topic. He managed to create a group with an excellent atmosphere between people. I really benefited from the contact with my colleagues Darius, George, Samuel and Sylvain. The visitors Sasha and Marina (with their kids), Bruce, Pavel, Misha and Yakov are also thanked for the interesting discussions, coffee breaks and climbing outings we shared.

The secretaries Leonor and Noemi have by their readiness to help and good mood contributed to make the institute a good place to work in. I want to thank the other members of the ITP, for their teaching when I was a student at the EPFL, support and for the time we spent together. I specially want to thank Davide with whom I shared my office for his pleasant company during most of my time at the institute and Valentina.

I enjoyed teaching and thank the students for this enriching experience.

I thank the thesis jury for accepting to review my work.

My family has supported me a lot during my studies. I thank my parents for financial and moral support. My grandparents and my sister Myriam have always been there to help and my grandmother has shown a lot of curiosity for my work. Noël and Denise are specially thanked for the last-minute invitations.

The outings in the mountains have contributed to make those years in Lausanne enjoyable. I thank Marco and Camille, Blanche, both Christophes (with a special mention for the camping on the Matterhorn in February), Daniel, Evi, Guenole, Laurent, Pierre, Roland, Tristan (who was always ready to help), Verena and all my friends from Club Montagne.

My roommates Mathias and François are thanked for their friendship and precious support.

Finally, I would like to thank Frederike for the happiness she brought in the last two years and for her support during the redaction of this manuscript.

Curriculum Vitae

Personal Information

Name	Crouzy Benoît
Date of birth	28.07.1980
Place of origin	Montana (VS) Switzerland
Nationality	Swiss and French
Address	Rue Général Guisan 29 3963 Montana Suisse benoit.crouzy@a3.epfl.ch

Education

1994-1999	Maturité type B (Latin), LCP Sion
2000-2005	Diploma in Physics, EPF Lausanne/ ETH Zürich
2005-2009	Doctoral studies in Physics, ITP EPF Lausanne

Languages

French	native
German	fluent
English	fluent

Teaching experience

Quantum Mechanics III & IV (2005-2006)

Quasiclassical approximation, scattering theory and path integral

Statistical Physics I & II (2006-2009)

Statistical mechanics of classical and quantum systems

Publications

- Magnetic interference patterns in a long SNS junction: analytical results
B. Crouzy, and D. A. Ivanov
arXiv:0907.0632 (submitted to PRB)
- Josephson current in a superconductor-ferromagnet-superconductor junction with in-plane ferromagnetic domains
B. Crouzy, S. Tollis, and D. A. Ivanov
Phys. Rev. B 76, 134502 (2007)
- Josephson current in a superconductor-ferromagnet junction with two noncollinear magnetic domains
B. Crouzy, S. Tollis, and D. A. Ivanov
Phys. Rev. B 75, 054503 (2007)
- Minigap in a superconductor-normal metal junction with paramagnetic impurities
B. Crouzy, E. Bascones, and D. A. Ivanov
Phys. Rev. B 72, 092501 (2005)